Probing Charge and Energy Transfer in Molecules by Multidimensional Stimulated Raman Spectroscopy with X ray Light
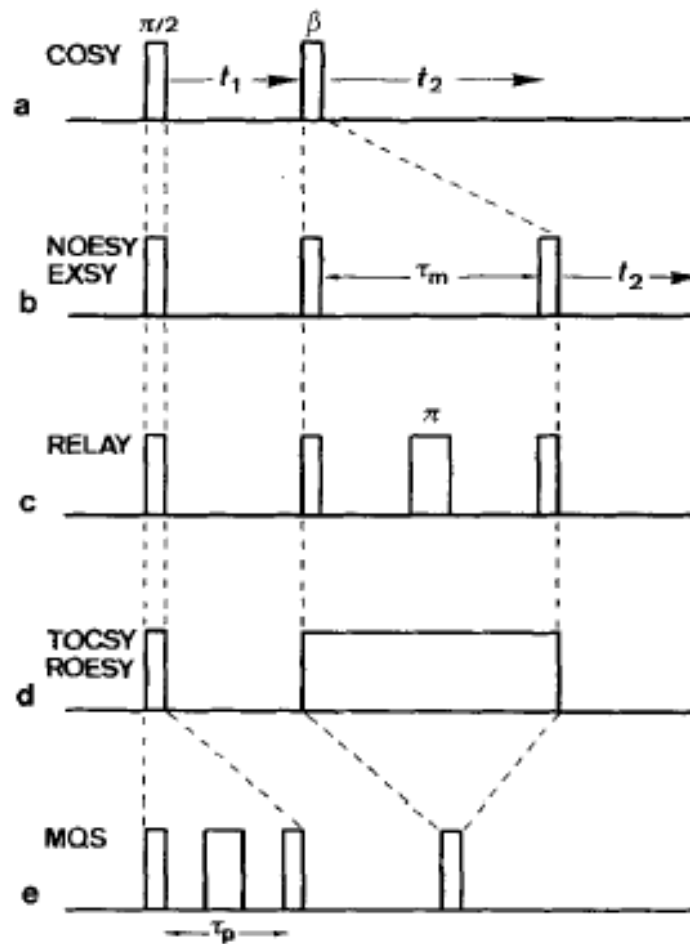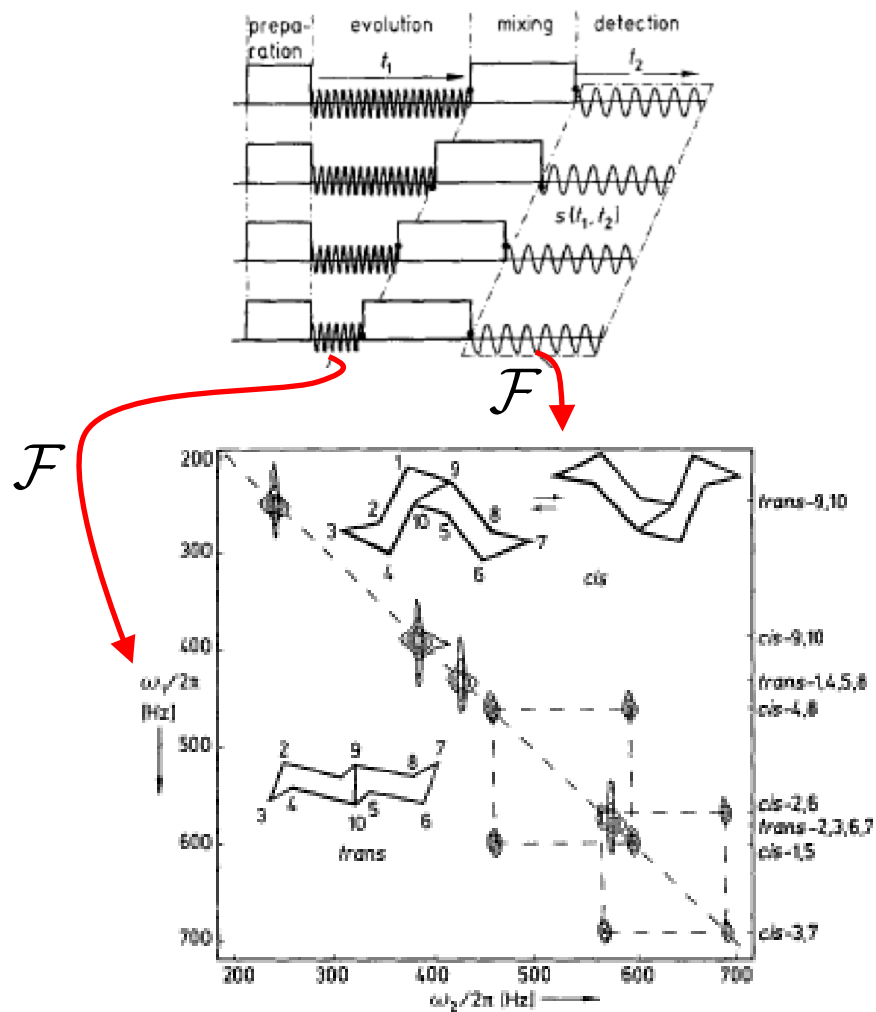

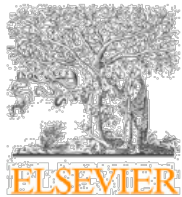Shaul Mukamel

University of California, Irvine

Nobel Symposium 158 on Free Electron Laser
Research ,Stockholm,June 17, 2015

2D NMR Spectroscopy

Nobel Prizes for NMR

Felix Bloch and Edward M. Purcell

Physics 1952

Discovery of NMR

Richard R. Ernst

Chemistry 1991

Development of 2D NMR

Kurt Wüthrich

Chemistry 2002

Development of NMR for determining structures of biomolecules in solution

Paul C. Lauterbur and Sir Peter Mansfield

Physiology or Medicine 2003

Discovery of MRI

Mortality and immortality: The Nobel Prize as an experiment into the effect of status upon longevity☆

Matthew D. Rablen [a,b,c], Andrew J. Oswald [a,b]

[a] University of Warwick, Coventry, United Kingdom
[b] Cornell University, United States
[c] University of Westminster, London, United Kingdom

ABSTRACT

It has been known for centuries that the rich and famous have longer lives than the poor and ordinary. Causality, however, remains trenchantly debated. The ideal experiment would be one in which extra status could somehow be dropped upon a sub-sample of individuals while those in a control group of comparable individuals received none. This paper attempts to formulate a test in that spirit. It collects 19th-century birth data on science Nobel Prize winners. Correcting for potential biases, we estimate that winning the Prize, compared to merely being nominated, is associated with between 1 and 2 years of extra longevity.
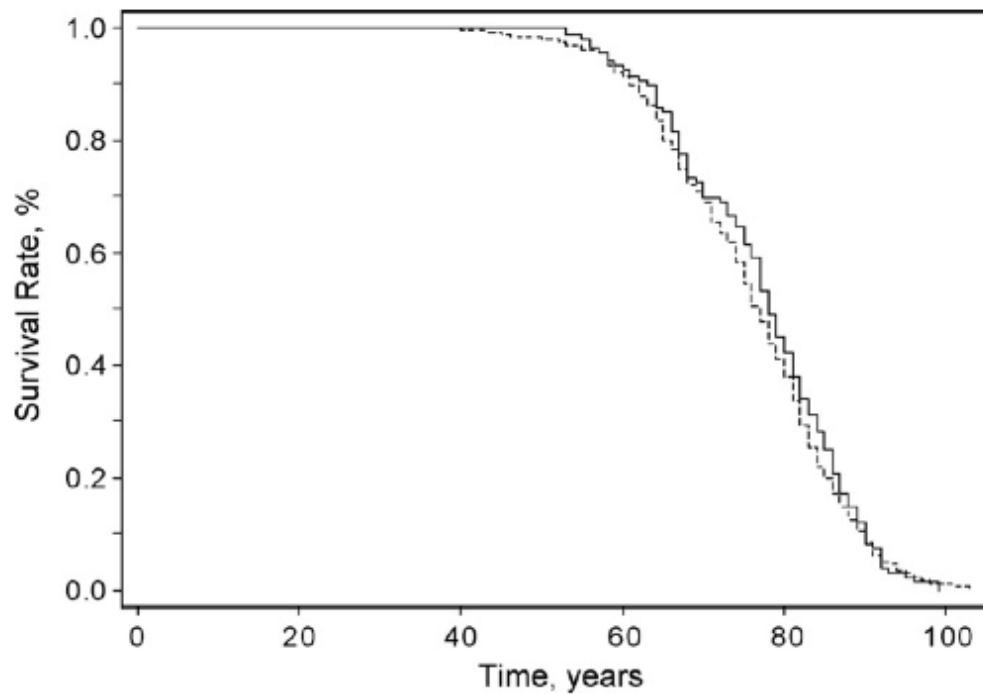
Fig. 1. Survival function for winners (solid line) and nominees (dashed line).

Table 2
Extra years of life from winning (a matching test)

	Window (years)	Matched winners (#)	Conditional test difference (years)	Unconditional test difference (years)
USA[a]	3	30	2.08	4.64
Germany[a]	3	38	1.30	2.45
EU[a]	5	102	0.69	1.36
All	3	135	0.33	1.38
All[a] (controls are only of winner's nationality)	13	125	0.99	–
Physics[a]	3	77	0.04	0.83
Chemistry[a]	5	79	1.35	2.75

[a] Each winner is matched only with controls from the same nationality, continent or scientific discipline, as specified.

Coherent Multidimensional Spectroscopy From NMR to X-rays

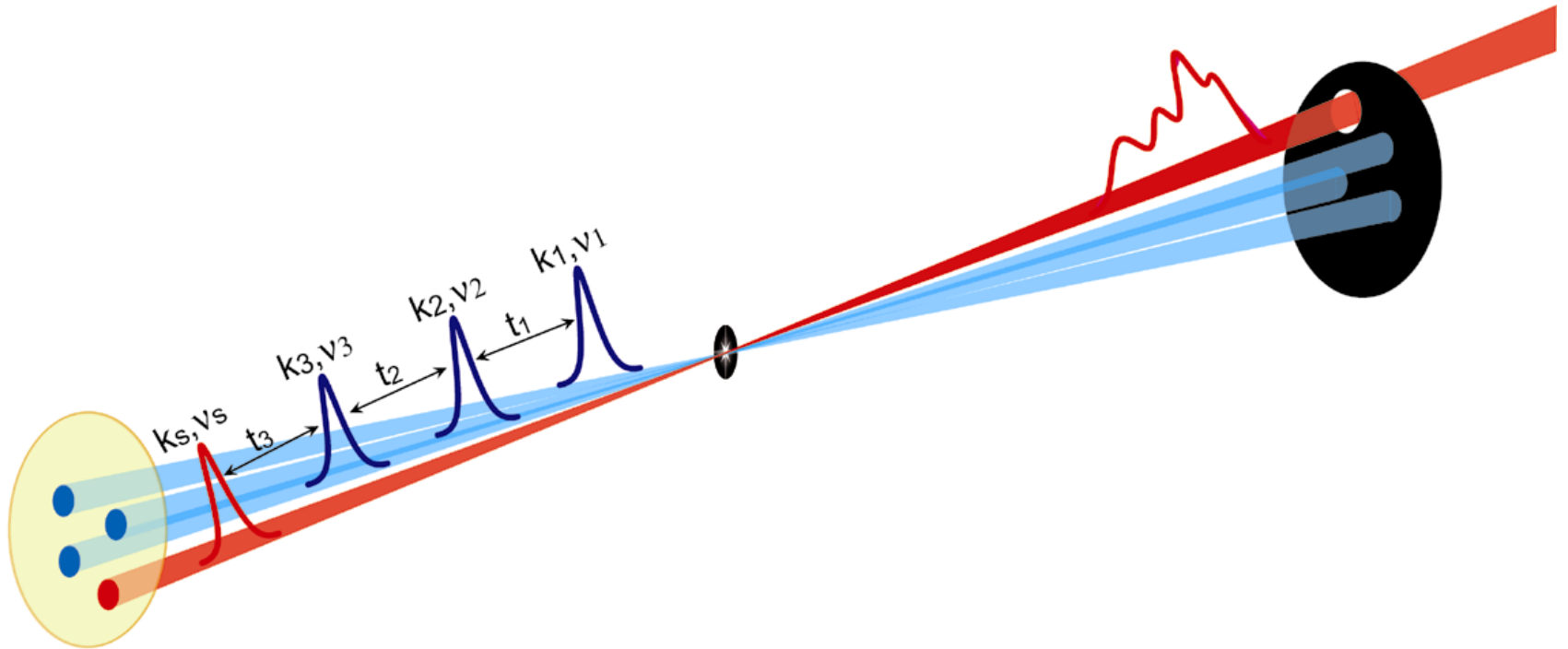## Coherent Multidimensional Optical Probes for Electron Correlations and Exciton Dynamics: From NMR to X-rays

SHAUL MUKAMEL,* DARIUS ABRAMAVICIUS, LIJUN YANG,
WEI ZHUANG,‡ IGOR V. SCHWEIGERT,¶ AND
DMITRI V. VORONINE§

Department of Chemistry, University of California,
Irvine, California

Heterodyne-Detected Four Wave Mixing

$$E(\boldsymbol{r}, \tau) = \sum_{j=1}^{4} \sum_{\nu} E_{j\nu}(\tau - \overline{\tau}_j) \exp[ik_j r - i\overline{\omega}_j(\tau - \overline{\tau}_j) - i\varphi_{j\nu}(\tau - \overline{\tau}_j)] + c.c.,$$

$$\boldsymbol{k}_s = \pm \boldsymbol{k}_1 \pm \boldsymbol{k}_2 \pm \boldsymbol{k}_3$$

Optical
multidimensional
coherent
SPECTROSCOPY

Steven T. Cundiff and Shaul Mukamel

Techniques developed decades ago for nuclear magnetic resonance and now adapted for the IR, visible, and UV regions of the spectrum are enabling new insights into chemical kinetics and solid-state physics.
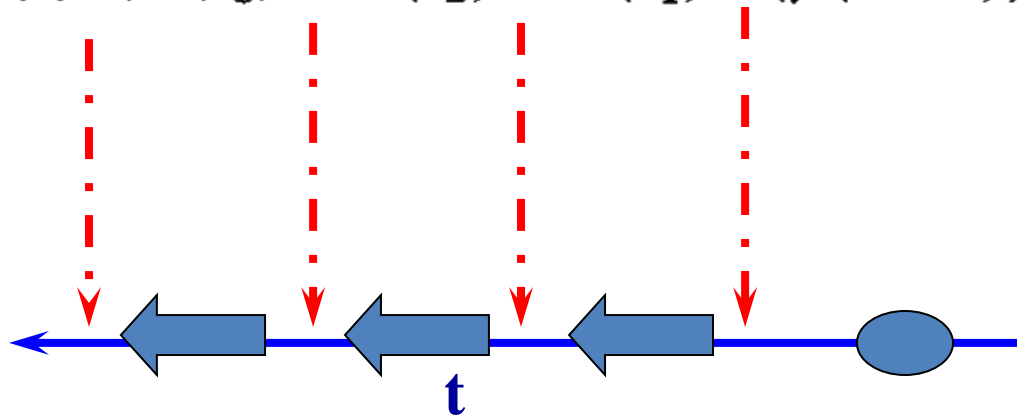
The Nonlinear Response Function

$$P(t) = Tr[V\rho(t)]$$

$$= P^{(1)}(t) + P^{(2)}(t) + P^{(3)}(t) + \cdots$$

$$P^{(3)}(t) = \int_0^\infty dt_3 \int_0^\infty dt_2 \int_0^\infty dt_1 S^{(3)}(t_3, t_2, t_1)$$

$$\times E(t - t_3)E(t - t_3 - t_2)E(t - t_3 - t_2 - t_1)$$

$$S^{(3)}(t_3, t_2, t_1) = \left(\frac{i}{\hbar}\right)^3 \langle\langle V|\mathcal{G}(t_3)\mathcal{V}\mathcal{G}(t_2)\mathcal{V}\mathcal{G}(t_1)\mathcal{V}|\rho(-\infty)\rangle\rangle$$
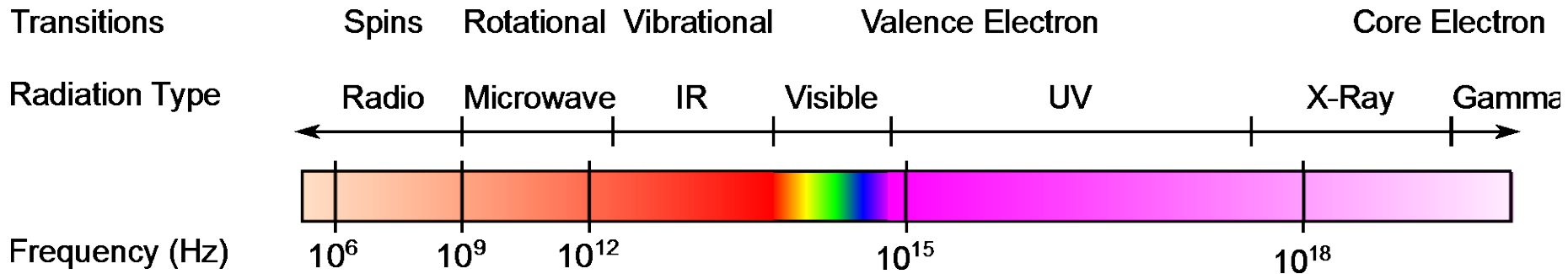
t

Double Fourier transform

$$S_I(\Omega_1, t_2, \Omega_3) = \int_0^\infty dt_3 \int_0^\infty dt_1 e^{i\Omega_1 t_1 + i\Omega_3 t_3} S(t_1, t_2, t_3)$$

$$S_{III}(t_1, \Omega_2, \Omega_3) = \int_0^\infty dt_3 \int_0^\infty dt_2 e^{i\Omega_2 t_2 + i\Omega_3 t_3} S(t_1, t_2, t_3)$$

- Useful for displaying structural and dynamical information
- Ultrafast (50 fs) time resolution
- Probe intra- and intermolecular interactions
- Spreading transitions in multiple dimensions
- Lineshapes reveal environmental fluctuations

Transitions		Spins	Rotational	Vibrational		Valence Electron		Core Electron

Radiation Type		Radio	Microwave	IR	Visible	UV	X-Ray	Gamma

Frequency (Hz) 10^6 10^9 10^{12} 10^{15} 10^{18}

Radio	NMR, atomistic structure, slow (millisecond) dynamics
Microwave	Rotational structure of molecules, Electron Spins EPR
Infrared	Protein structure and folding, picosecond kinetics, hydrogen bonding
	THz spectroscopy: Low frequency motion in liquids, intersuband transitions in semiconductors
Visible	Charge and energy transfer in photosynthetic complexes, solvation dynamics, femtosecond relaxation, quantum wells and dots
UV	Protein structure through backbone (FUV) and aromatic side chain (NUV) transitions, base stacking and photophysics in nucleic acids, DNA
X-Ray	Attosecond dynamics of core and valence electrons, atomistic structure
Gamma ray	Nuclear structure

Frenkel Exciton Hamiltonian

$$\hat{H}_0 = \sum_m \hbar \varepsilon_m \hat{B}_m^+ \hat{B}_m + \sum_{mn}^{m \neq n} \hbar J_{mn} \hat{B}_m^+ \hat{B}_n$$

$$+ \sum_{mnkl} \hbar U_{mnkl} \hat{B}_m^+ \hat{B}_n^+ \hat{B}_k \hat{B}_l$$

A simplified form

Resonant exciton coupling induced by transition charge interactions

$$\hat{H}_0 = \sum_m \hbar \varepsilon_m \hat{B}_m^+ \hat{B}_m + \sum_{mn}^{m \neq n} \hbar J_{mn} \hat{B}_m^+ \hat{B}_n + \frac{1}{2} \sum_m \hbar \Delta_m \hat{B}_m^{+2} \hat{B}_m^2$$

$$+ \frac{1}{2} \sum_{mn}^{m \neq n} \hbar \mathsf{K}_{mn} \hat{B}_m^+ \hat{B}_n^+ \hat{B}_m \hat{B}_n$$

Site energies

Off diagonal binding energy: induces double-exciton energy shifts from $\varepsilon_m + \varepsilon_n$

Diagonal exciton binding energy: induces double-exciton energy shift from $2\varepsilon_m$

$$\langle \Phi_{f_{mm}} | \hat{H}_0 | \Phi_{f_{mm}} \rangle = \hbar(2\varepsilon_m + \Delta_m)$$

$$\langle \Phi_{f_{mn}} | \hat{H}_0 | \Phi_{f_{mn}} \rangle = \hbar(\varepsilon_m + \varepsilon_n + \mathsf{K}_{mn})$$

The relevant exciton space
for third-order measurements
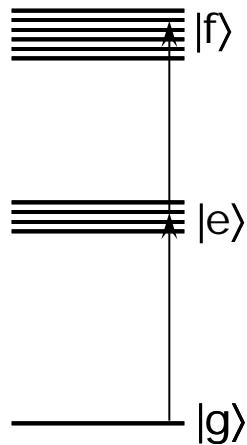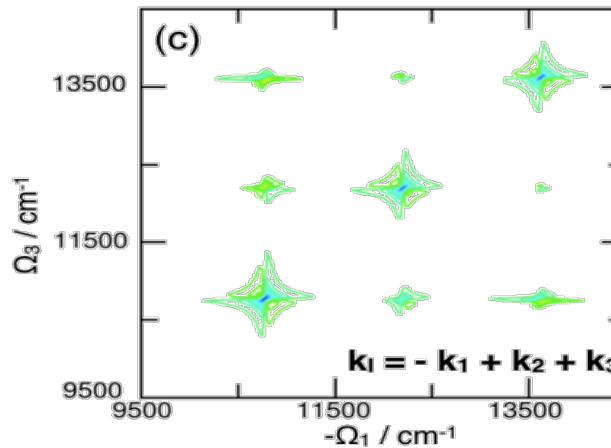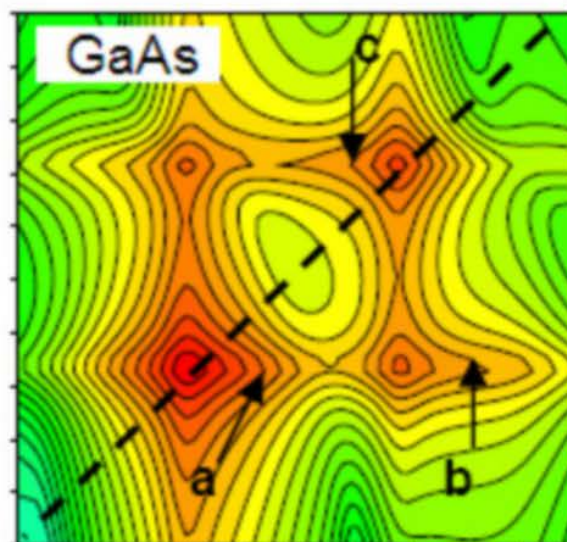

The exciton level scheme
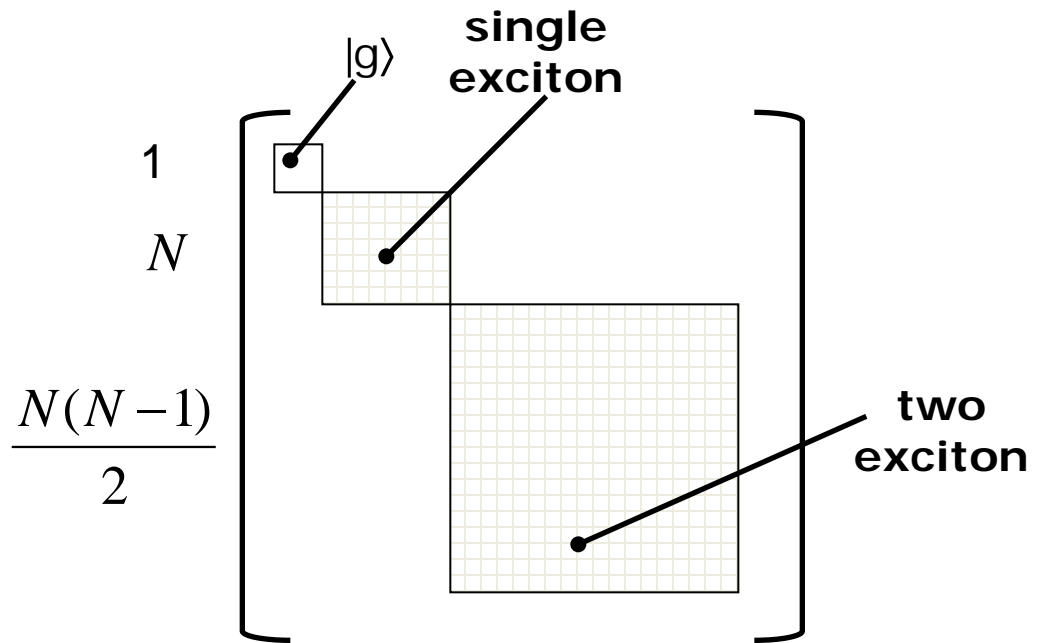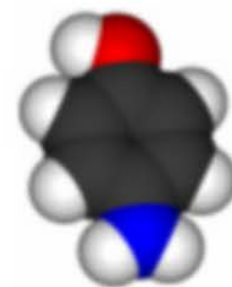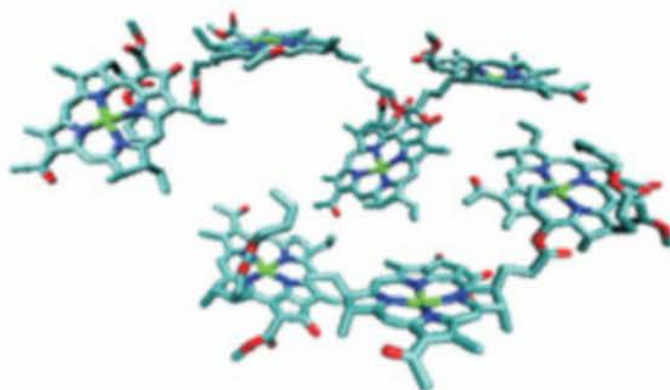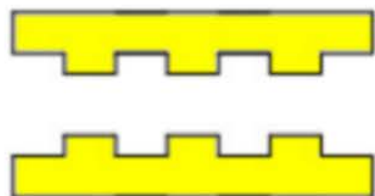
Block-diagonal Hamiltonian matrix

Linear Absorption
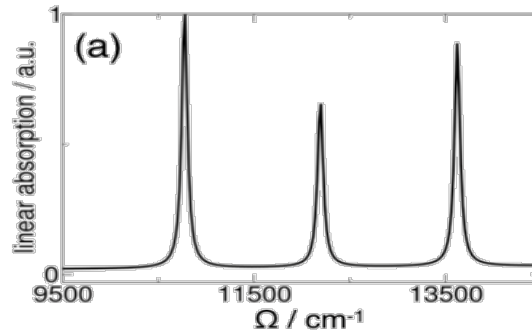
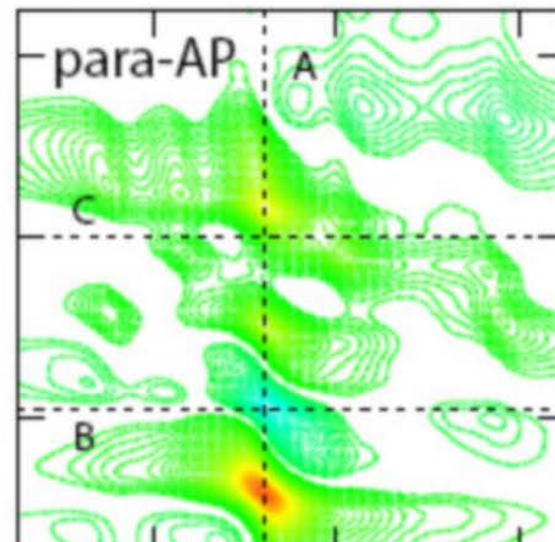Photon Echo of Uncoupled Chromophores
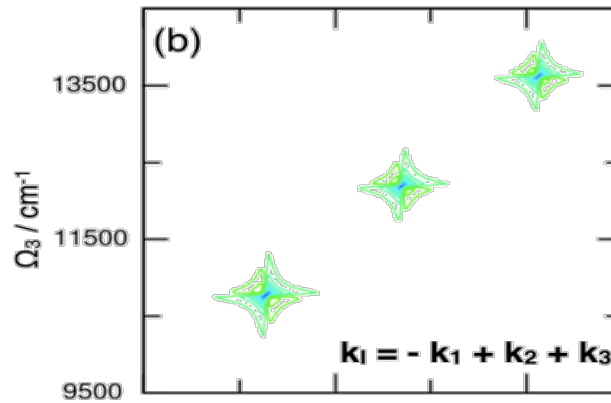
Photon Echo of Coupled Chromophores

Cross peaks reveal distinct signatures of intermolecular couplings

(a)

linear absorption / a.u.

Ω / cm^{-1}

(b)

Ω_3 / cm^{-1}

$k_I = - k_1 + k_2 + k_3$

(c)

Ω_3 / cm^{-1}

$k_I = - k_1 + k_2 + k_3$

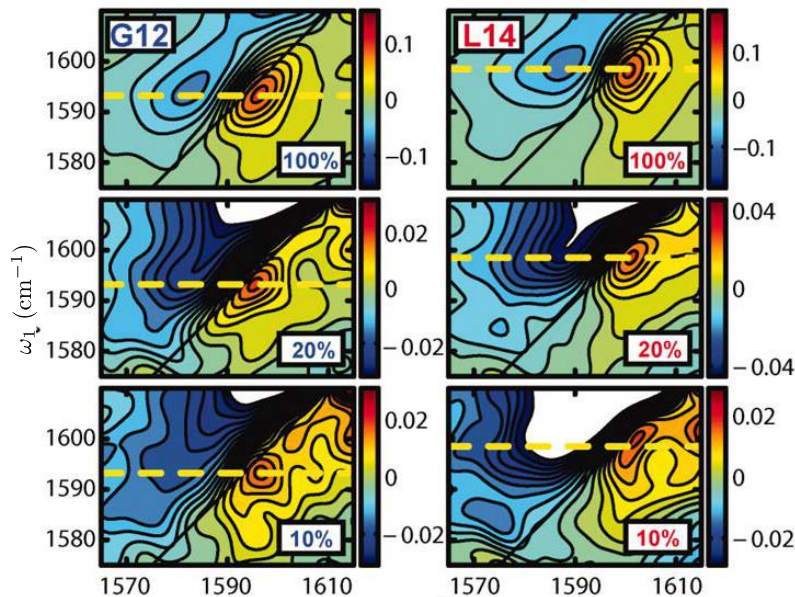$-\Omega_1$ / cm^{-1}

Wannier excitons
(meV)
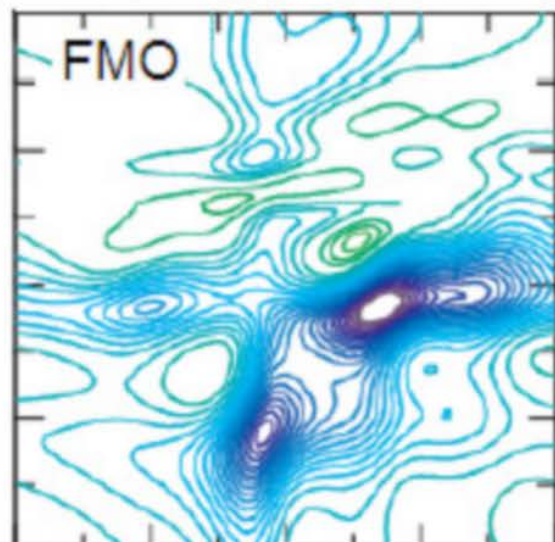
Frenkel excitons
(0.1 eV)
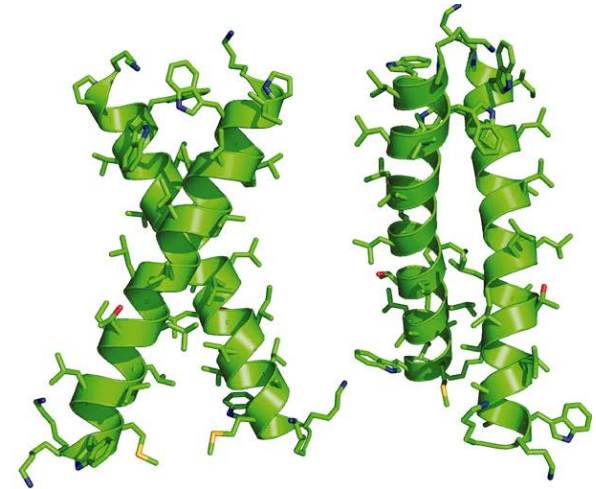
Core excitons
(eV)

# Protein structure determination using 2DIR

Structure of 30-residue homodimeric transmembrane dimer solved using 2DIR

Residue level constraints obtained using $^{13}C={}^{18}O$ site-specific isotope labeling

A. Remorino, I.V. Korendovych, Y. Wu, W.F. DeGrado, and R. Hochstrasser, *Science* **332**, 1206-1209 (2011).
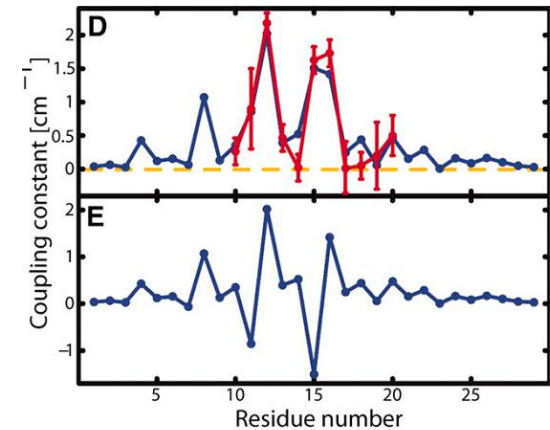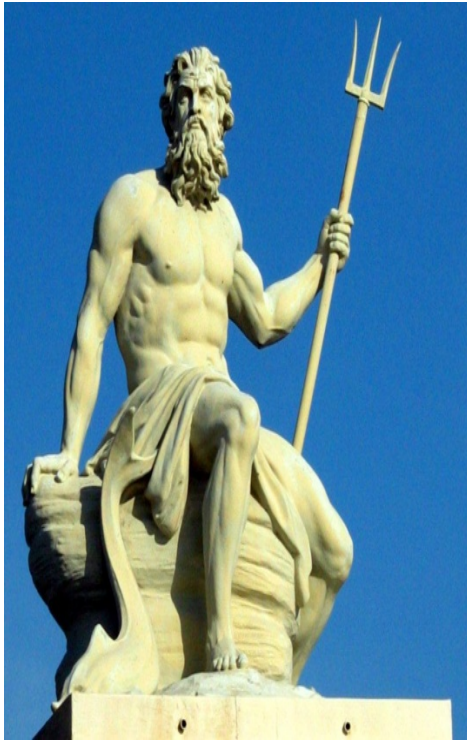
parallel pathways of energy transfer with femtosecond temporal resolution

energy transfer pathways in light-harvesting complex of plants LHC2
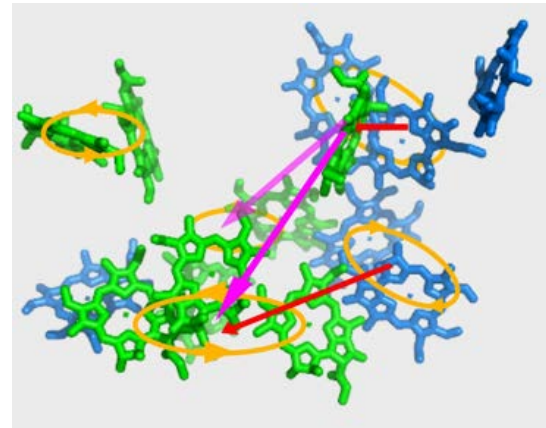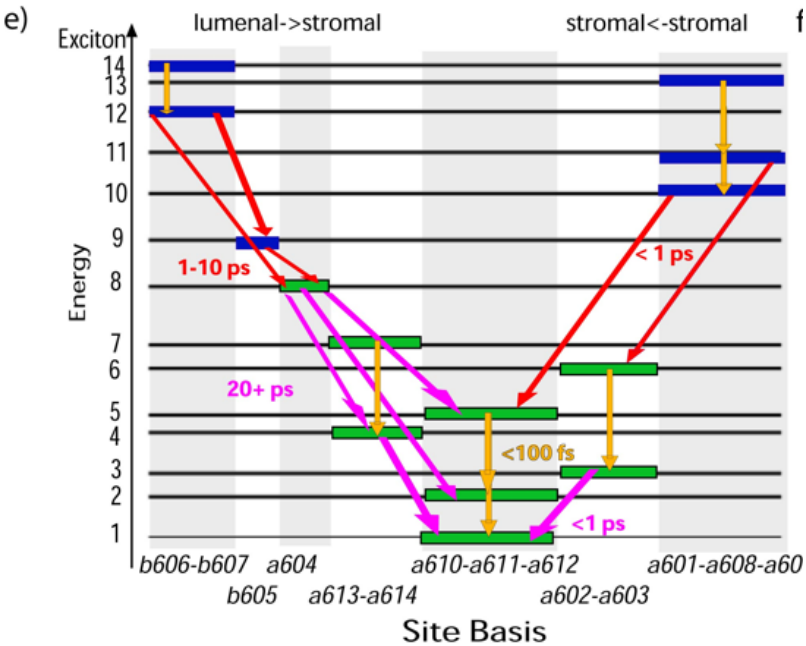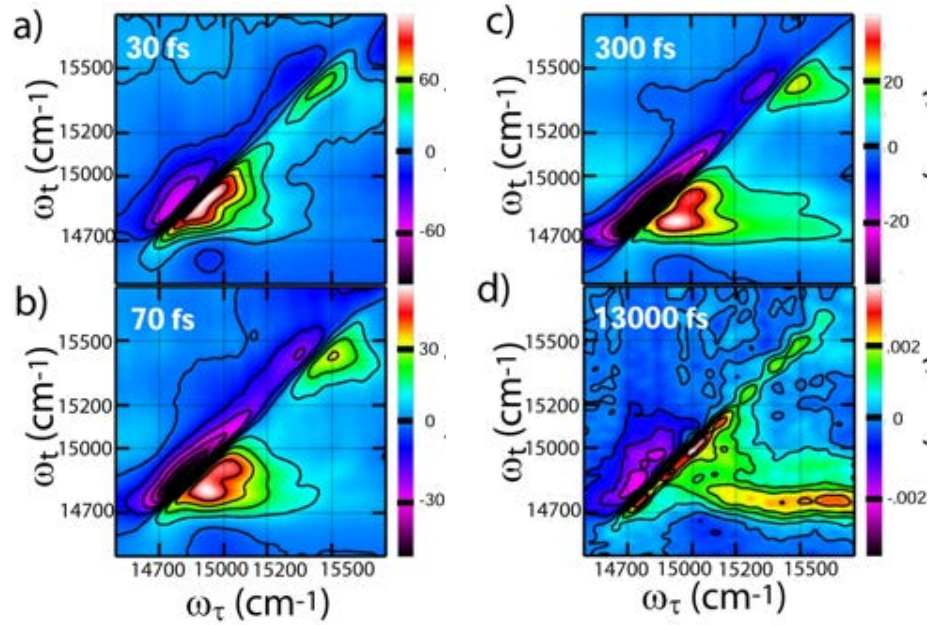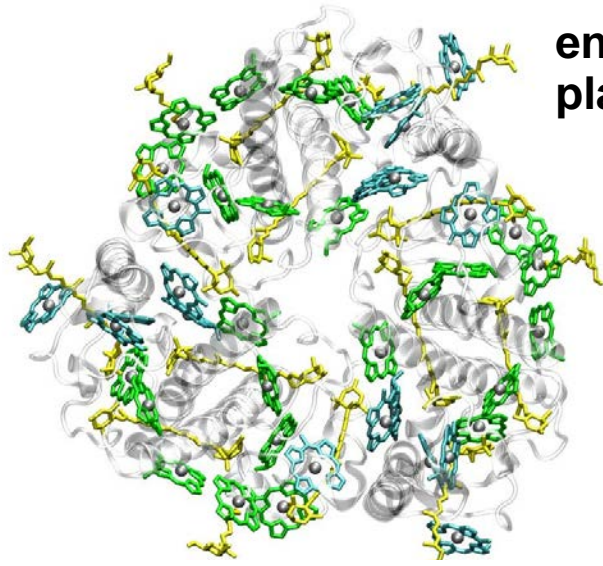
Wavefunction

$$\frac{d\psi_j}{dt} = -\frac{i}{\hbar} \sum_m H_{jm} \psi_m$$

N-component state vector

$$|\psi\rangle = \sum_j \psi_j |j\rangle$$

Density Matrix

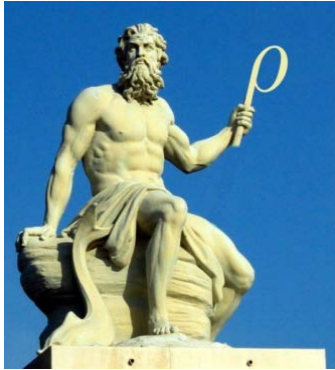$$\frac{d\rho_{jk}}{dt} = -\frac{i}{\hbar} \sum_{m,n} \mathcal{L}_{jk,mn} \rho_{mn}$$

$$\mathcal{L}_{jk,mn} = H_{jm}\delta_{kn} - H_{kn}^*\delta_{jm}$$

N²-component state vector

$$|\rho\rangle\rangle = \sum_{j,k} \rho_{jk} |jk\rangle\rangle$$

The Nonlinear Response to a classical field

Quantum pathways correspond to n field-matter interactions with *m+1* interactions from left and *n-m* interactions from right
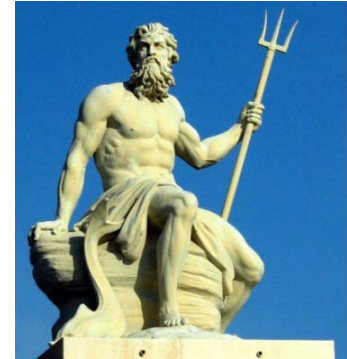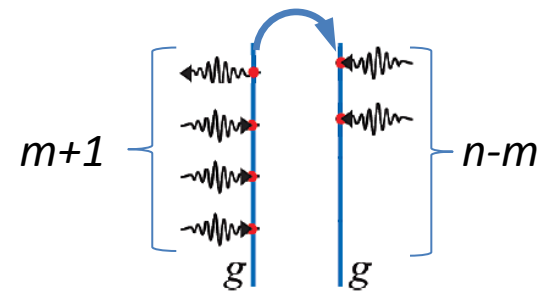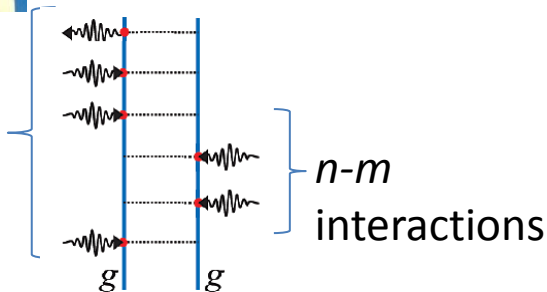
$$\mathbf{S^{(n)}(t)} = \mathrm{Tr}[\mathbf{V}\rho(\mathbf{t})] \qquad \mathbf{S^{(n)}(t)} = \langle\mathbf{\Psi(t)}|\mathbf{V}|\mathbf{\Psi(t)}\rangle$$

2^n Ladder Diagrams n+1 Loop Diagrams

m+1 interactions   *n-m* interactions

m+1   *n-m*

- Move forward in time
- Density matrix ~N^2 space
- Can eliminate bath (reduced description)
- Keep track of complete time ordering (more terms)

- Move forward and backward in time
- Wave function ~N space
- Must include all degrees of freedom
- Partial time ordering (fewer terms)

Ladder Diagram Rules

1. The diagrams represent all possible interaction configurations
2. Time propagates from bottom – up.
3. Wave-vectors pointing *right* mark + , left - k $\mathbf{k}$
4. Wave-vectors, pointing *into* diagram: *absorption*
5. Wave-vectors, pointing *out of* diagram: *emission*
6. Intervals between interactions: t_3, t_2, t_1
7. The state of the density matrix at any time is given by labels on vertical bars.
8. The initial and final states must be *populations.*
9. The response function is a product of density matrix propagations in each interval.
10. The amplitude of the pathway is an ordered product of transition dipoles for each interaction.
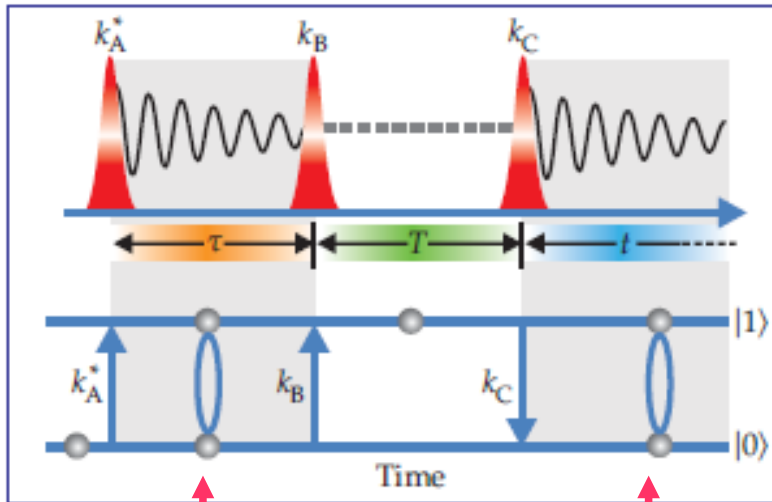11. Odd number of interactions on the right "brings" "-" overall sign.
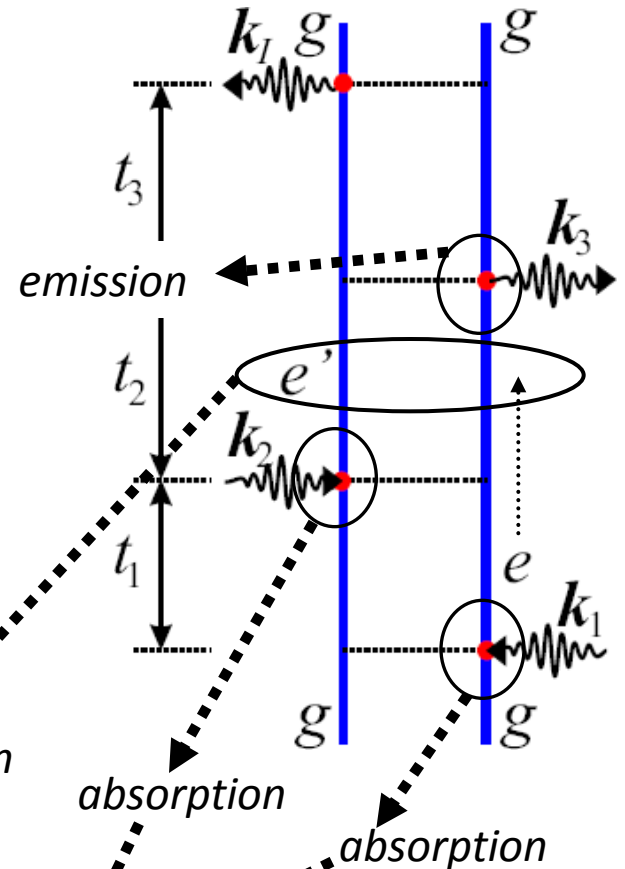
$$R_i(t_3,t_2,t_1) = \left(\frac{i}{\hbar}\right)^3 \theta(t_1)\theta(t_2)\theta(t_3)\sum_{ee'} \mu_{ge'}\mu_{eg}\mu_{e'g}\mu_{ge}$$

$$\times \exp(-i\omega_{ge}t_1 - i\omega_{e'e}t_2 - i\omega_{e'g}t_3 - \gamma_{ge}t_1 - \gamma_{e'e}t_2 - \gamma_{e'g}t_3)$$
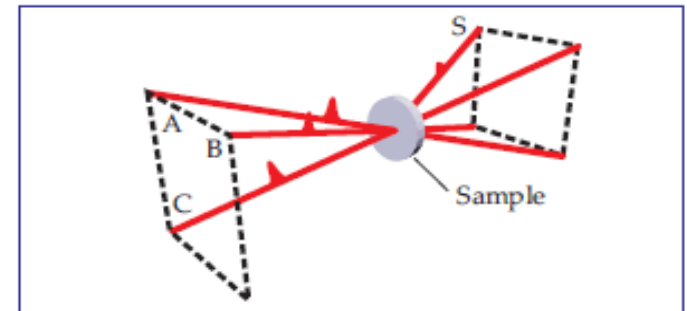
Optical 2D spectroscopy

2D spectrum:

Signal (τ,t) $\longrightarrow$ Fourier transform

$\mathbf{k}_s = -\mathbf{k}_A + \mathbf{k}_B + \mathbf{k}_C$

excited state
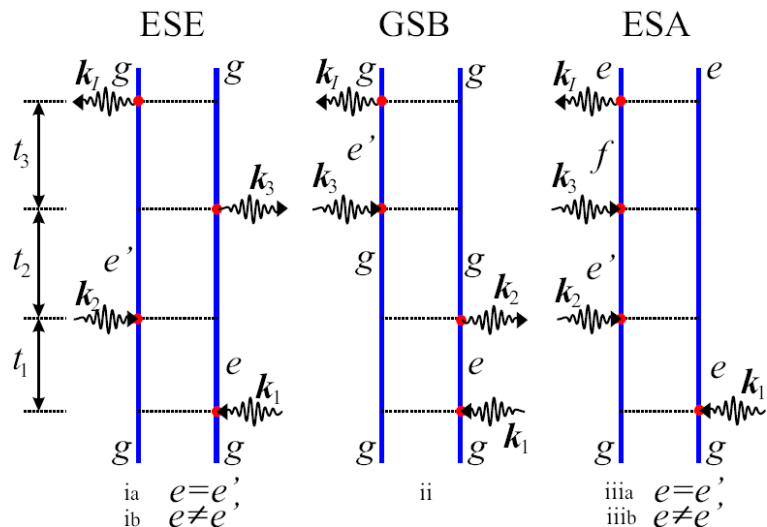
ground state

Coherent superposition

Rephasing spectrum:
conjugate pulse arrives 1st

Nonrephasing spectrum:
conjugate pulse arrives 2nd

Feynman diagrams for various multidimensional signals
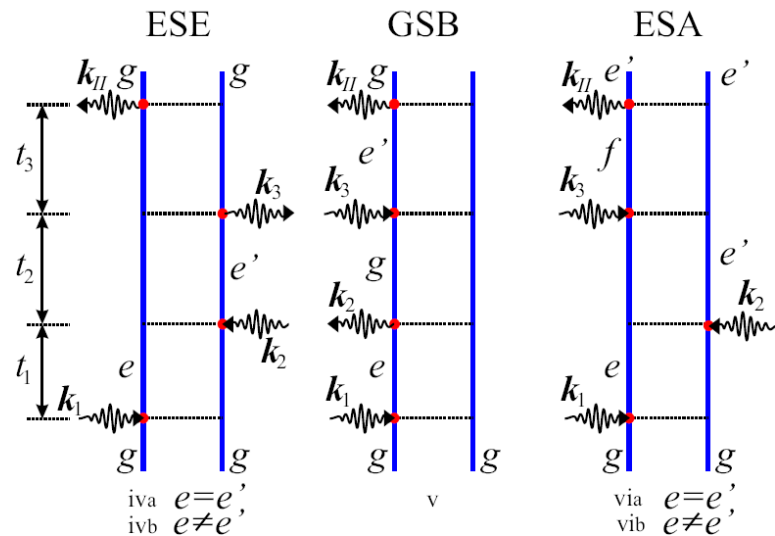
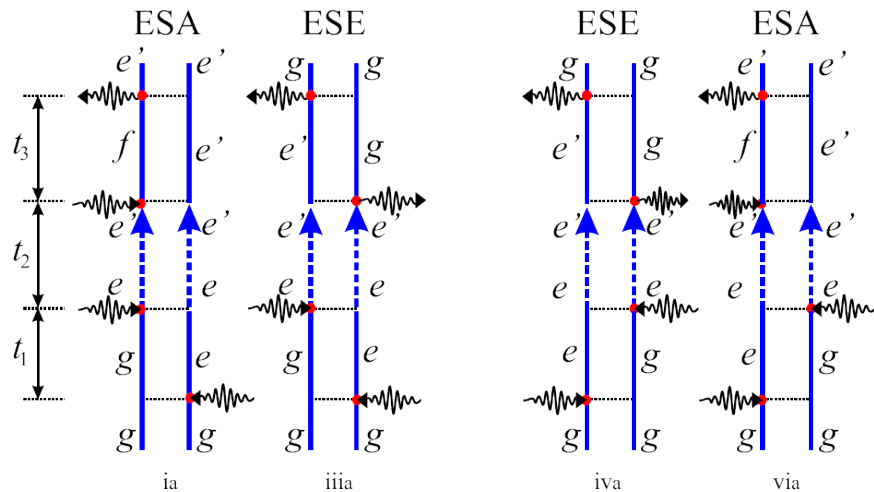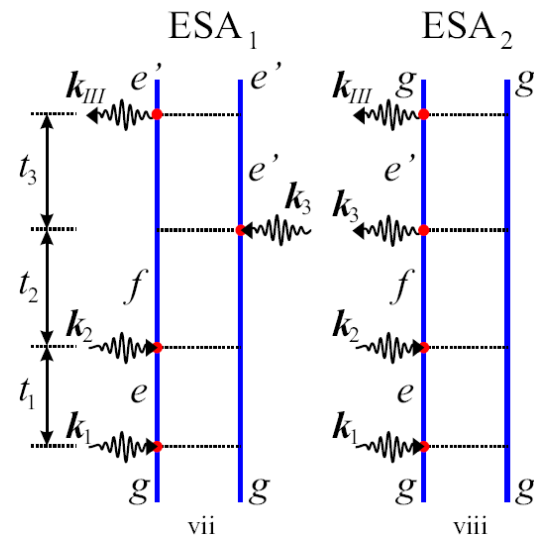# Multidimensional X-ray Four-wave Mixing Signals

## Coherent Ultrafast Core-Hole Correlation Spectroscopy: X-Ray Analogues of Multidimensional NMR

Igor V. Schweigert and Shaul Mukamel

Department of Chemistry, University of California, Irvine, California 92697-2025, USA

- We propose two-dimensional x-ray coherent correlation spectroscopy for the study of interactions between core-electron and valence transitions. This technique may find experimental applications in the future when very high intensity x-ray sources become available. Spectra obtained by varying two delay periods between pulses show off-diagonal crosspeaks induced by coupling of core transitions of two different types. Calculations of the N1s and O1s signals of aminophenol isomers illustrate how novel information about many-body effects in electronic structure and excitations of molecules can be extracted from these spectra.

Simulated 2DXCS signal of para-aminophenol
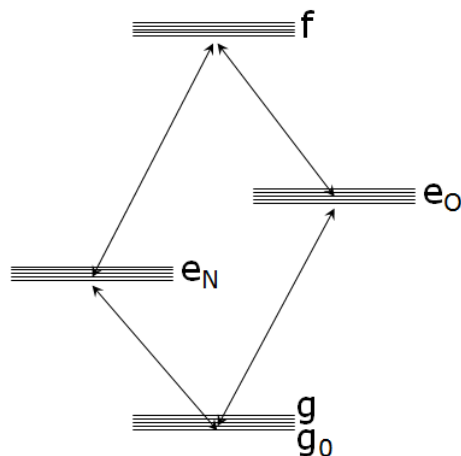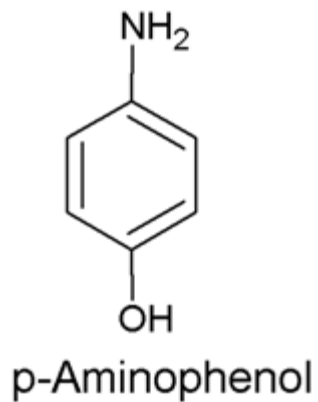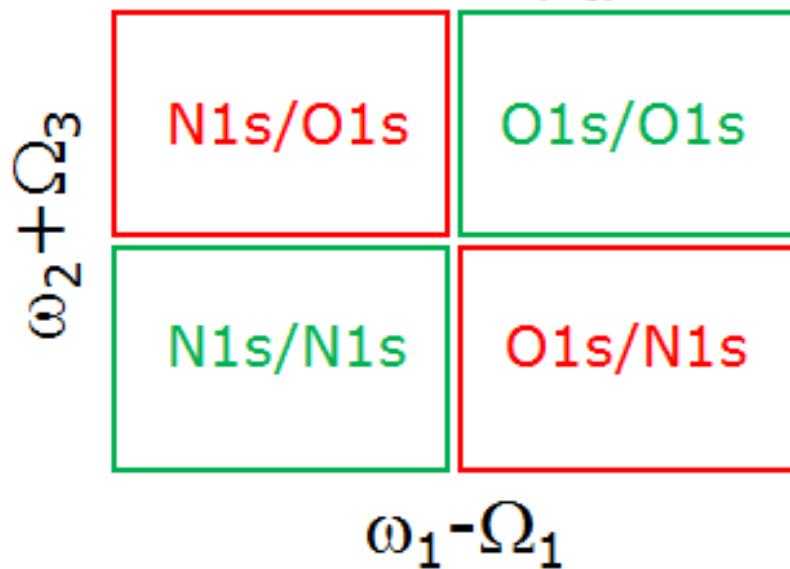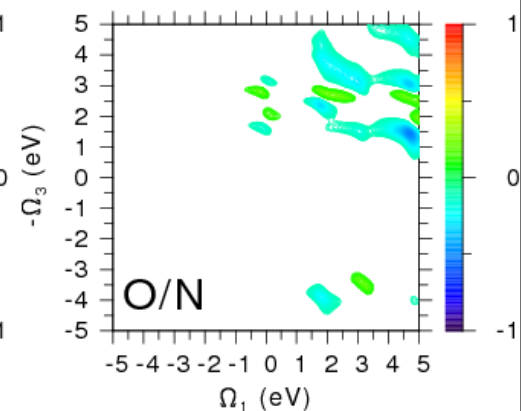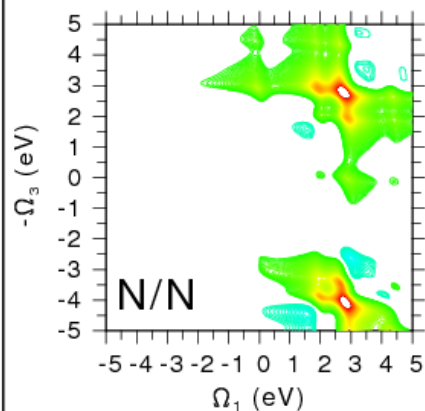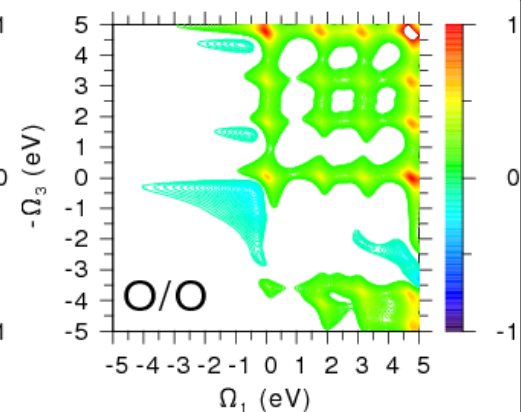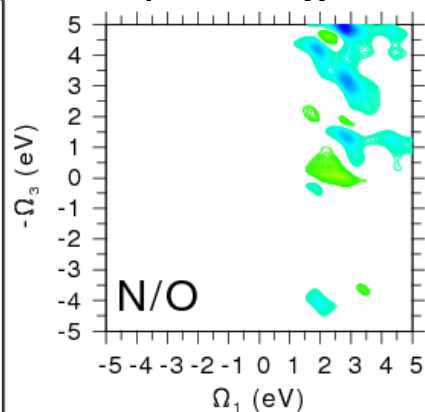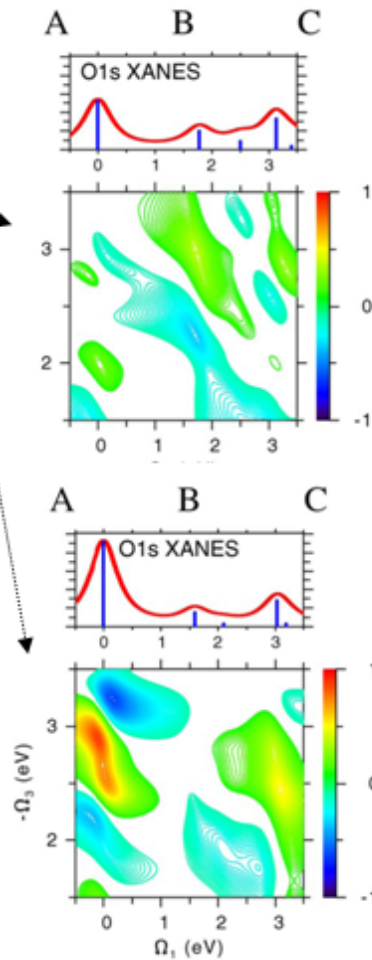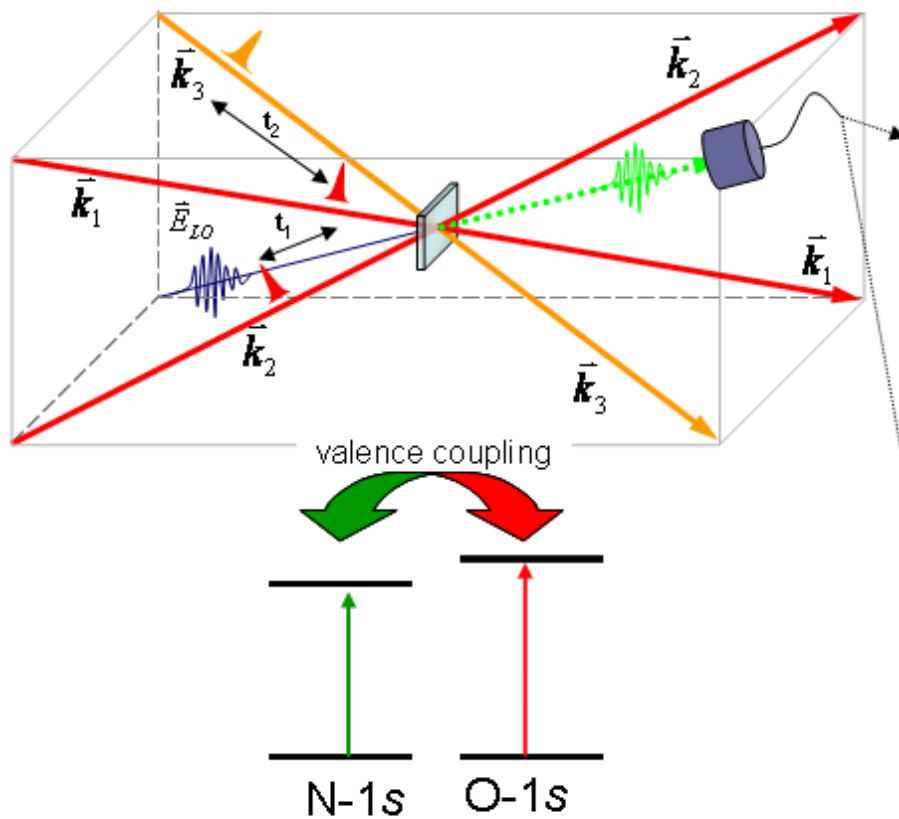
Left: Proposed four-wave mixing of ultrashort x-ray pulses resonant with the O-1*s* and N-1*s* levels; **Middle**: theoretically predicted two-dimensional spectra the lower of which exhibits the coupling of excitations on the oxygen with those of the nitrogen in para and ortho-aminophenol molecules at right [from S. Mukamel].

2D O1s/N1s photon echo signal (t2=0) of p- and o-aminophenol
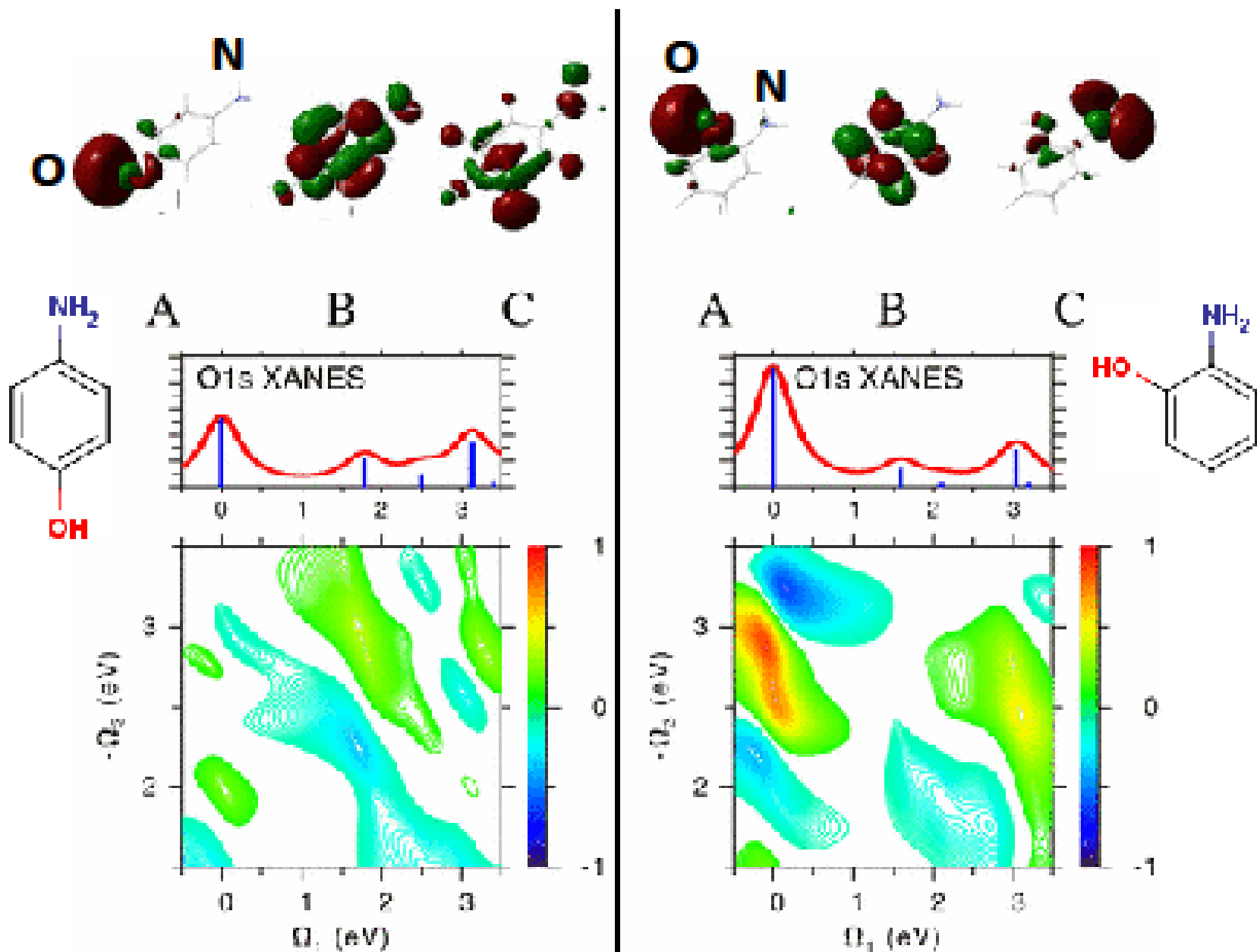
Exciton Quasiparticles in Multidimensional Spectroscopy of Aggregates

- 2D spectroscopy

Double-quantum coherence

$$k_{III} = +k_1 + k_2 - k_3$$

Coherent state $|f><g|$

photon echo

$$k_I = -k_1 + k_2 + k_3$$

Coherent states $|g><g|$ or $|'e><e|$
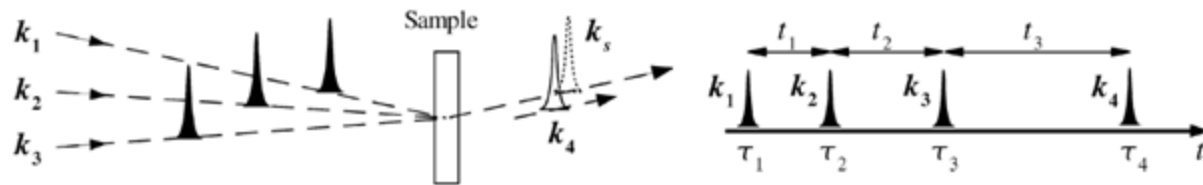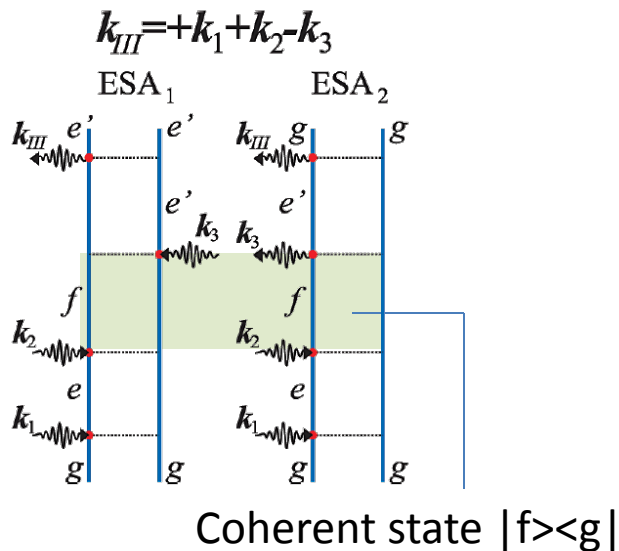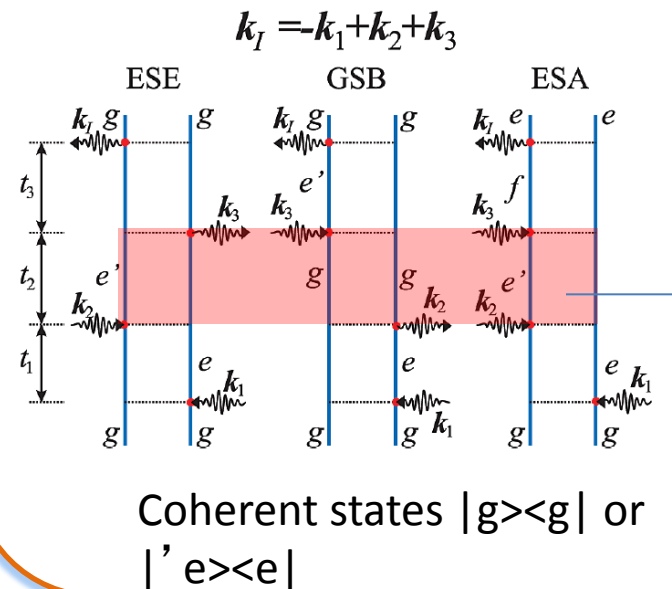
Double-Quantum-Coherence Technique

$$k_{III} = +k_1 + k_2 - k_3$$
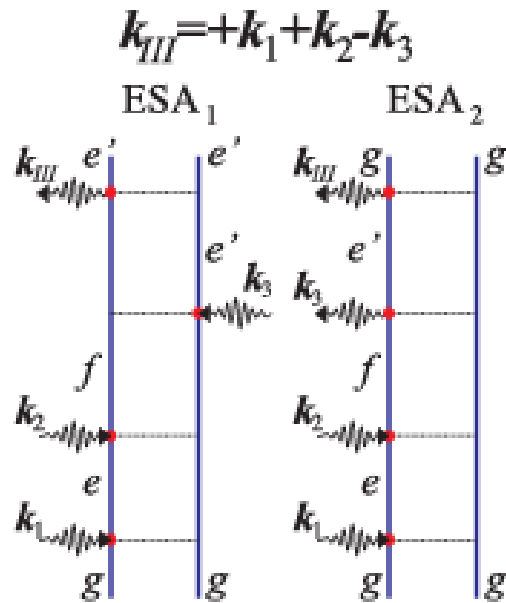
no entanglement

$$|f\rangle$$

each state

composed of $|e\rangle$

2 states

$$|f\rangle = |e_1\rangle|e_2\rangle$$

- double quantum coherence
- projection of $|f\rangle$ states

strongly entangled states $|f\rangle$

each state projects

into all single excitons

$$|f\rangle = \sum_{i,j} |e_i\rangle|e_j\rangle$$
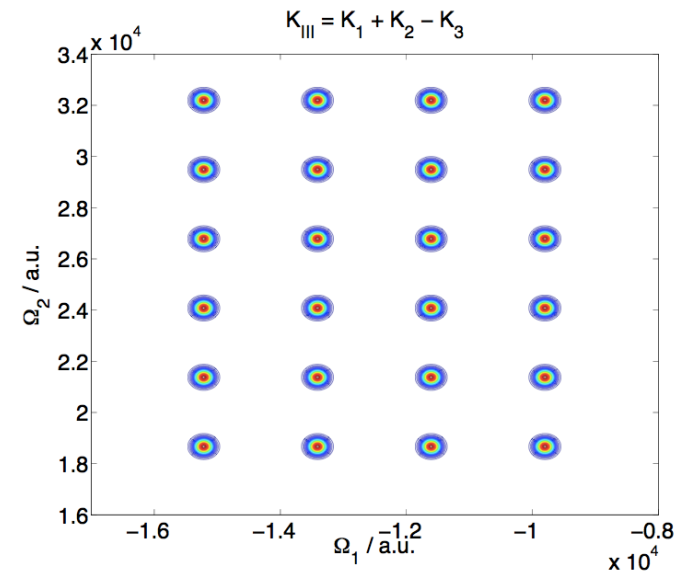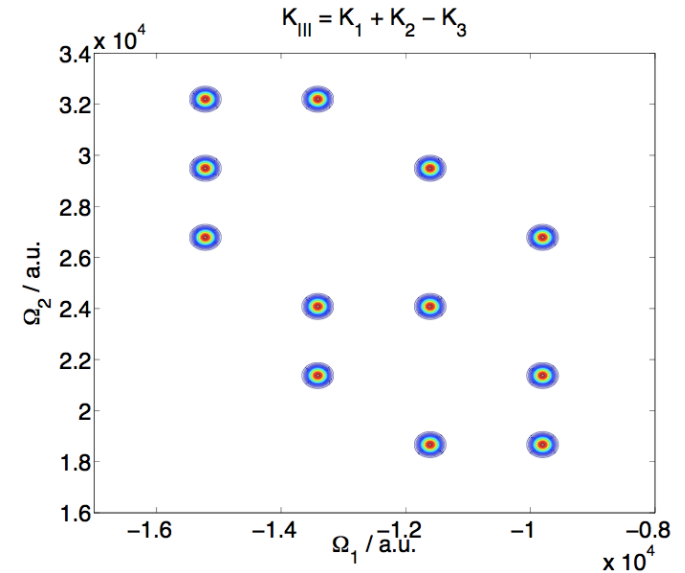
DQC Signal

$$S_{\text{III;A}} = \sum_{fe'e} \frac{(\mu_{ge'}^{\nu_4}\varepsilon_s^*(\omega_s - \omega_{e'g}))(\mu_{e'f}^{\nu_3}\varepsilon_3^*(\omega_3 - \omega_{fe'}))(\mu_{fe}^{\nu_2}\varepsilon_2(\omega_2 - \omega_{fe}))(\mu_{eg}^{\nu_1}\varepsilon_1(\omega_1 - \omega_{eg}))}{(\Omega_3 - \omega_{e'g} + i\gamma_{e'g})(\Omega_2 - \omega_{fg} + i\gamma_{fg})(\Omega_1 - \omega_{eg} + i\gamma_{eg})}$$

$$S_{\text{III;B}} = -\sum_{fe'e} \frac{(\mu_{e'f}^{\nu_4}\varepsilon_s^*(\omega_s - \omega_{fe'}))(\mu_{ge'}^{\nu_3}\varepsilon_3^*(\omega_3 - \omega_{e'g}))(\mu_{fe}^{\nu_2}\varepsilon_2(\omega_2 - \omega_{fe}))(\mu_{eg}^{\nu_1}\varepsilon_1(\omega_1 - \omega_{eg}))}{(\Omega_3 - \omega_{fe'} + i\gamma_{fe'})(\Omega_2 - \omega_{fg} + i\gamma_{fg})(\Omega_1 - \omega_{eg} + i\gamma_{eg})}$$

$$S_{\text{III}} = S_{\text{III;A}} + S_{\text{III;B}}$$
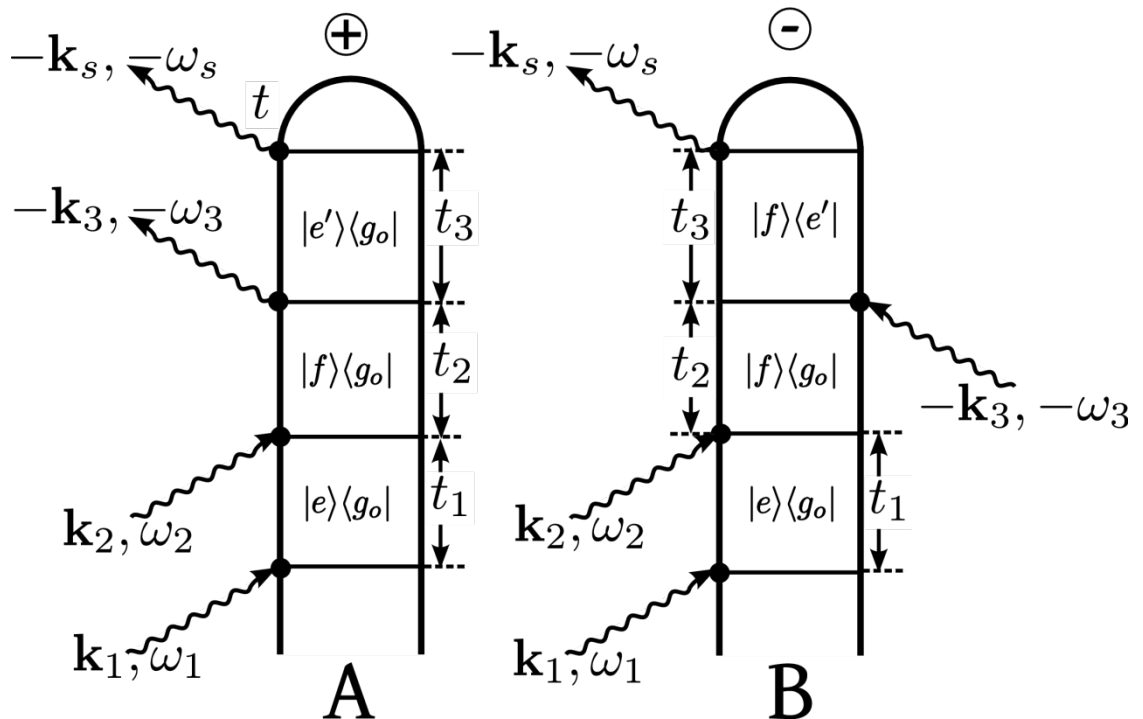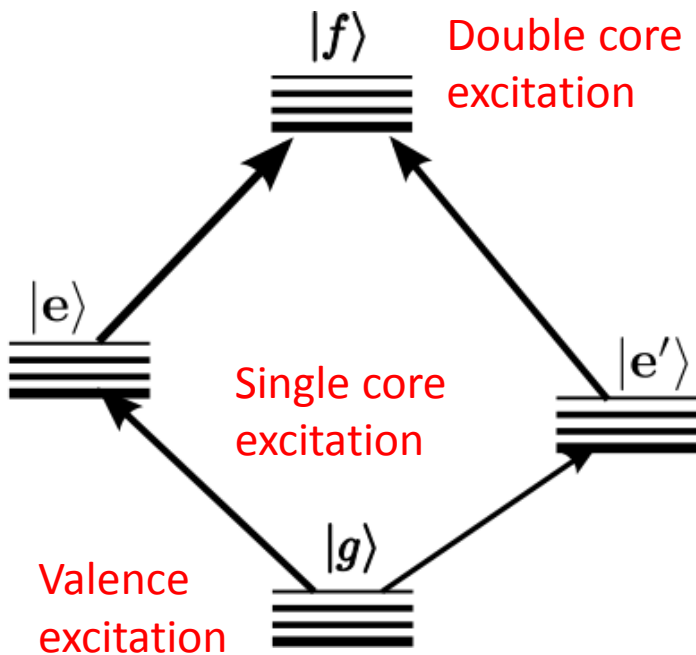
XCH+REW-TDDFT for Double Core-excitations of Formamide

formamide
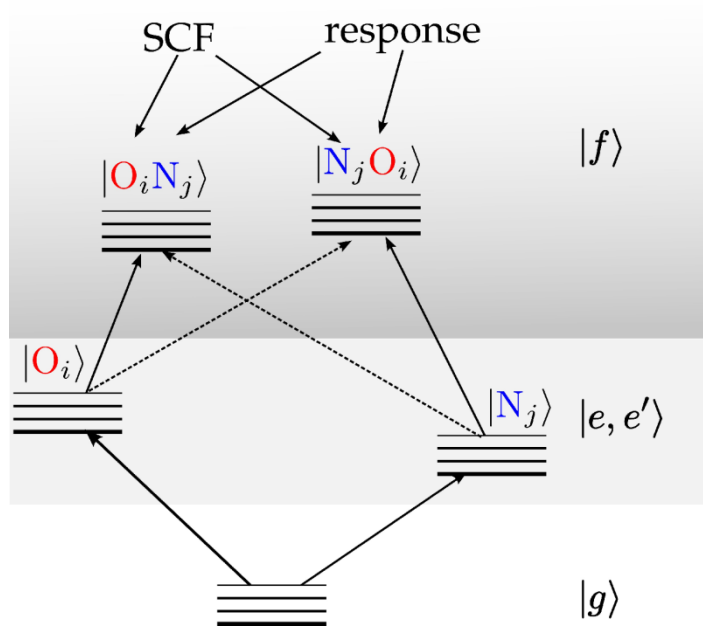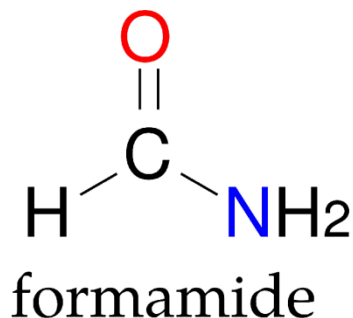
1. SCF calculation provides a reference state with a single core hole and an excited electron (excited core hole approximation, XCH).

2. This reference state is used to run a REW-TDDFT calculation to get the second core-excitation.

Y. Zhang, , D. Healion, J. D. Biggs, and S. Mukamel, *J. Chem. Phys.* **138**, 144303 (2013).

DQC Signal in Formamide

$S_{\mathrm{III}}(t_3 = 5 \text{ fs}, \; \Omega_2, \; \Omega_1)$

ONNO signal with XXXX polarization configuration.

Diagonal features imply weak correlation between single and double excitations.
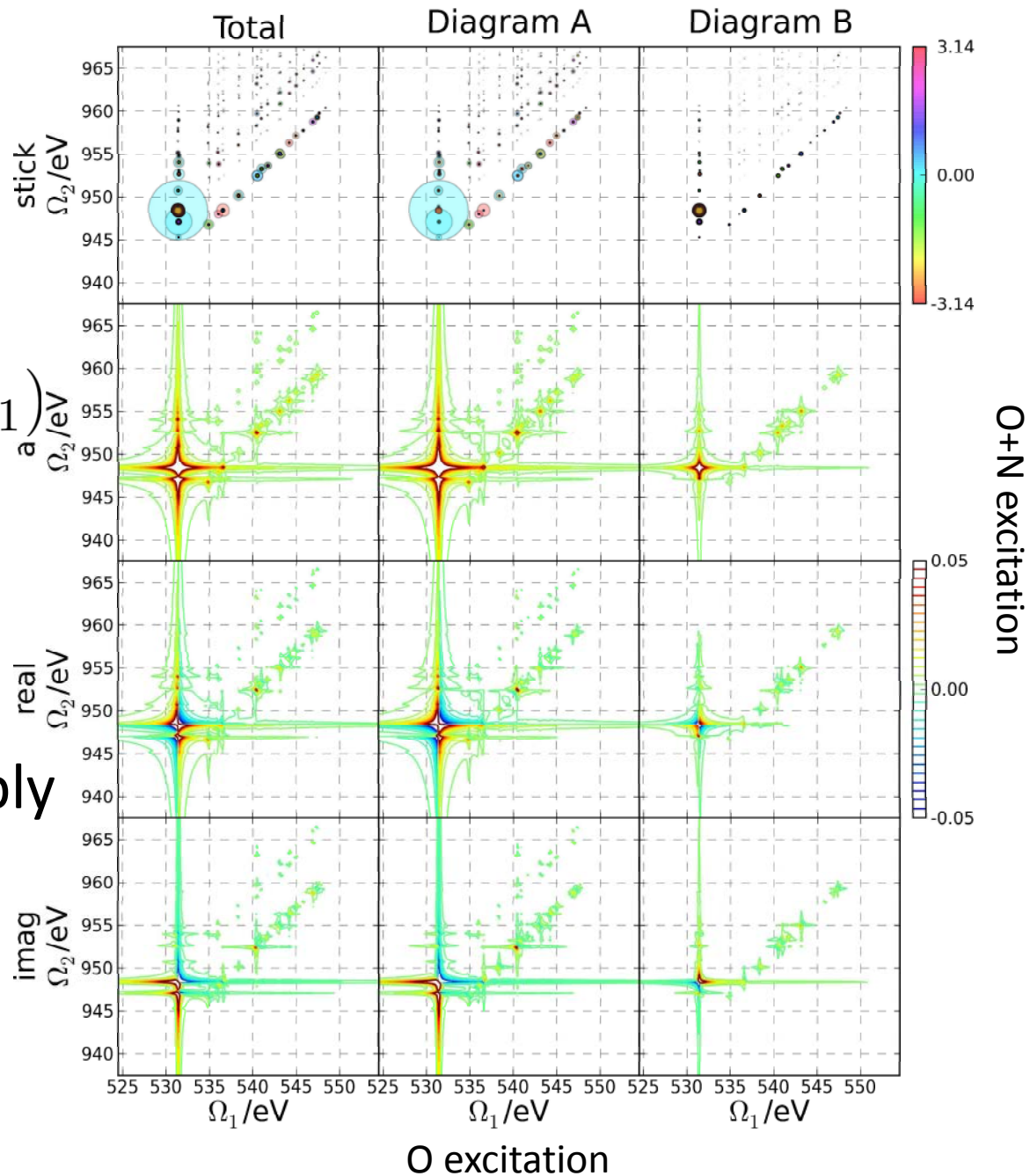
k$_I$ and k$_{III}$ of an uncoupled system
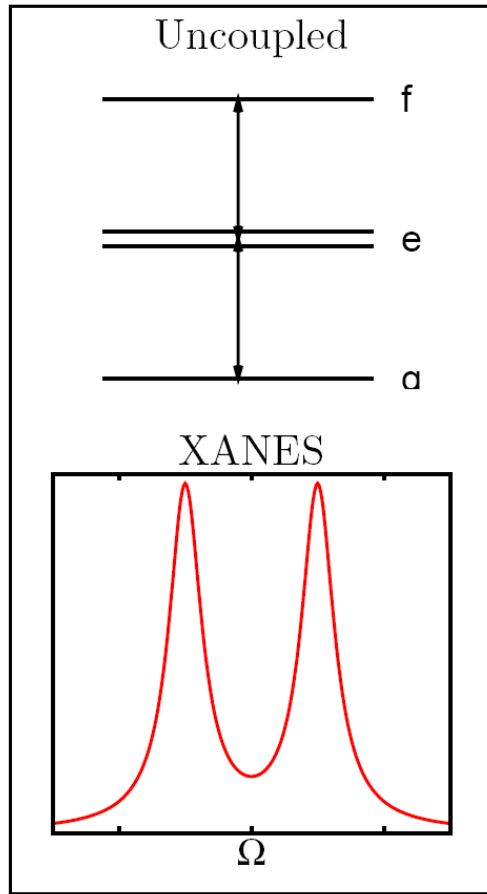
opposite signs
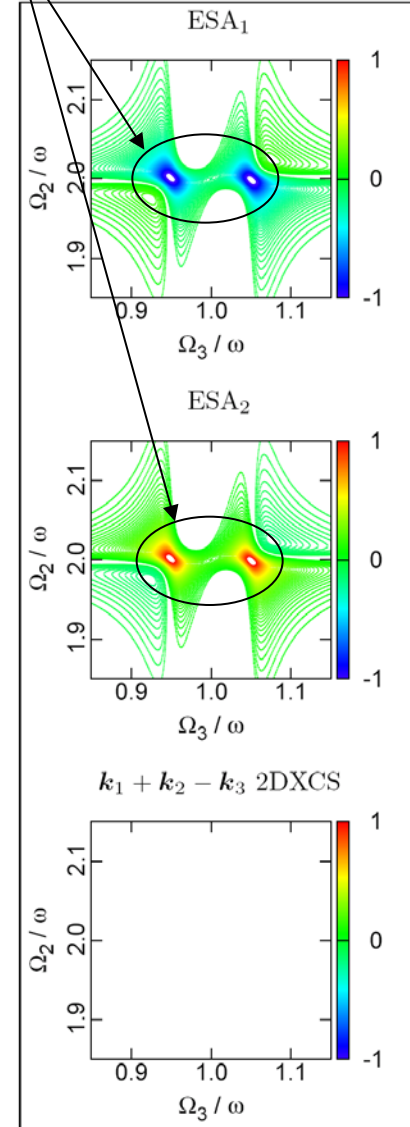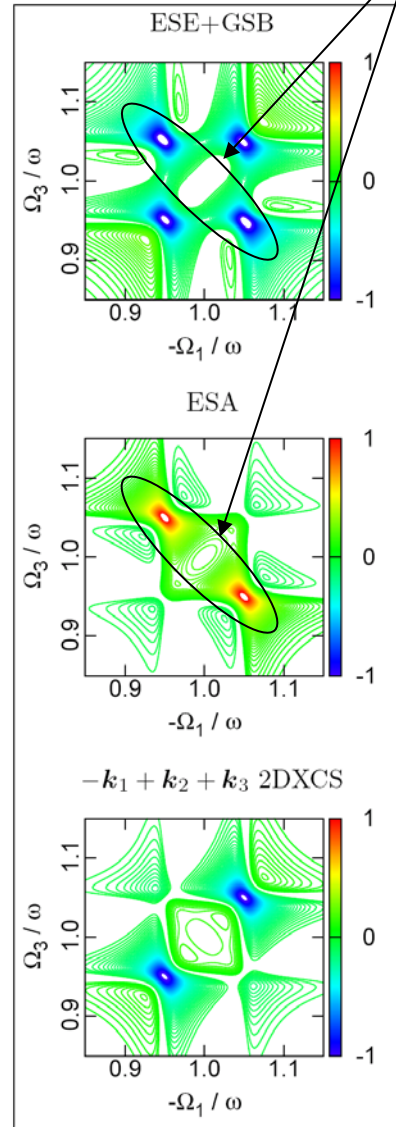
off diagonal peaks in photon echo cancel exactly

…as does the k$_{III}$ signal.

Coherent Stimulated X-ray Raman Spectroscopy

Coherent X-Ray Raman Spectroscopy: A Nonlinear Local Probe for Electronic Excitations

Satoshi Tanaka[1,3] and Shaul Mukamel[1,2]

[1]Department of Chemistry, University of Rochester, Rochester New York, 14627
[2]Department of Physics and Astronomy, University of Rochester, Rochester New York, 14627
[3]College of Integrated Arts and Sciences, Osaka Prefecture University, Sakai 599-8531, Japan
(Received 27 November 2001; published 9 July 2002)

- Nonlinear x-ray four-wave mixing experiments are becoming feasible due to rapid advances in high harmonic generation and synchrotron radiation coherent x-ray sources. By tuning the difference of two x-ray frequencies across the valence excitations, it is possible to probe the entire manifold of molecular electronic excitations. We show that the wave vector and frequency profiles of this x-ray analogue of coherent Raman spectroscopy provide an excellent real-space probe that carries most valuable structural and dynamical information, not available from spontaneous Raman techniques.

Vibrational Raman
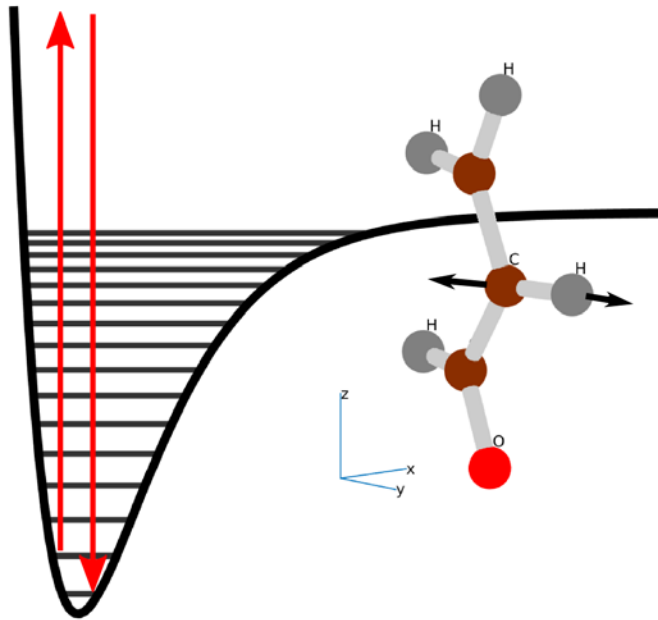
- Vib. transitions

- Optical frequencies

- **femto**seconds

X-Ray Raman

$|c\rangle$ core hole states

$|b\rangle$

valence states

$|a\rangle$
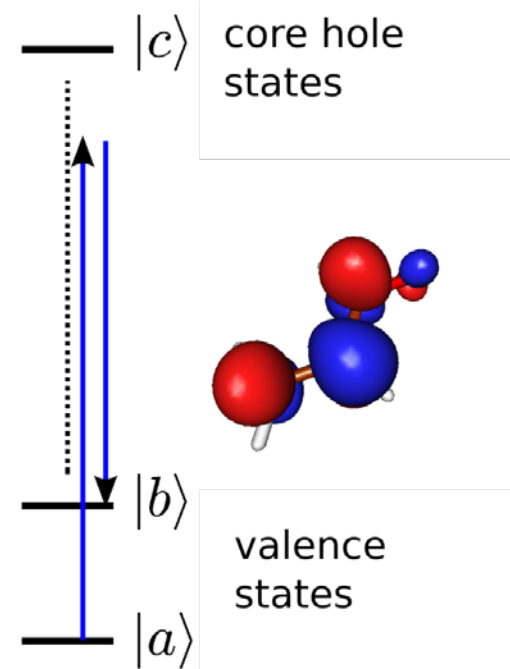
- Electronic transitions

- XUV/X-Ray

- **atto**seconds

UV/Vis   X-ray

	UV/Vis	X-ray
Pulse Duration:	~10fs	~100as
Energies:	1-10eV	+100eV
Dynamics probed:	nuclear wavepackets on different valence PESs.	probes valence excitations with different core occupations
Decay Mechanisms:	Fluorescence, IVR	Fluorescence, Auger
Slow, Low Frequency System:	vibrations / IR	valence electrons / UV-VIS
Fast, High Frequency System:	valence electrons /UV-VIS	core-electrons / X-ray
Absorption	Infrared	XANES
Direct Probe of slow system:	Infrared	UV-Vis
Impulsive Excitation	Raman	RIXS
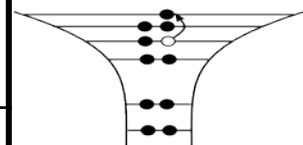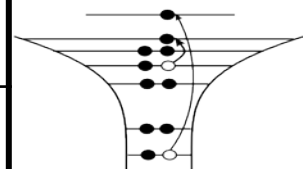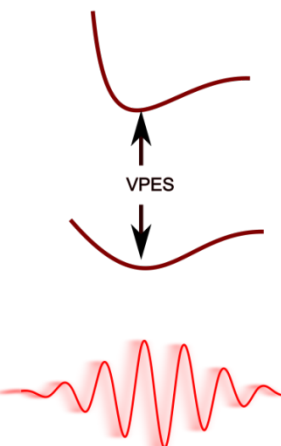
Molecular vibrations   **Valence Electrons**

Conventional Raman

$$\alpha = \alpha_0 + \sum_i \frac{\partial \alpha}{\partial Q_i} Q_i + \sum_{ij} \frac{1}{2} \frac{\partial^2 \alpha}{\partial Q_i \partial Q_j} Q_i Q_j + \ldots$$

$$Q_i = \sqrt{\frac{\hbar}{2 m_i \omega_i}} \left(a_i{}^\dagger + a_i \right)$$

Boson creation and annihilation operators for vibrations

X-Ray Raman (RIXS)

$$\alpha = \alpha_0 + \sum_{i,j} K_{ij} c_i^\dagger c_j + \sum_{i,j,r,s} K_{ijrs} c_i^\dagger c_j c_r^\dagger c_s + \ldots$$

$$c_i^\dagger (c_j)$$

Fermi creation (annihilation) operators of valence orbitals

Multidimensional X-Ray Raman Spectroscopy

One Dimensional	Two Dimensional	Three Dimensional
Integrated two-pulse Stimulated X-Ray Raman Scattering (I2P-SXRS)	Dispersed two-pulse SXRS	Frequency-Dispersed three-pulse SXRS
	Integrated three-pulse SXRS	Heterodyne-detected four-wave mixing

Two-pulse

k_1 k_2

Three-pulse

k_1 k_2 k_3

Four-pulse

k_1 k_2 k_3 k_4
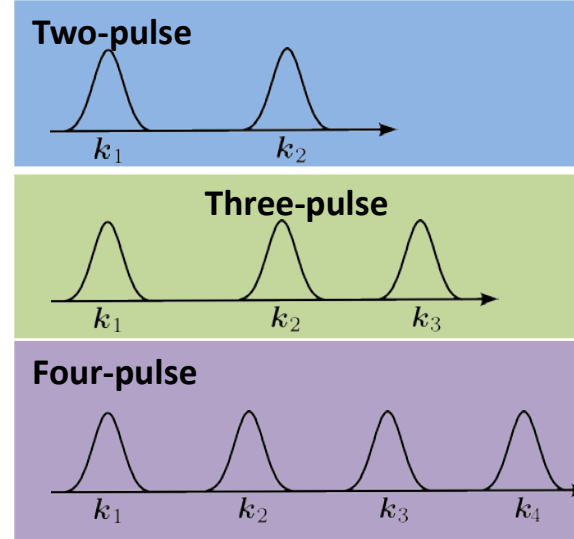
Simulated experiments on the nitrogen K-edge of cysteine. Lower dimensional signals are projections of higher dimensional signals.

Heterodyne-detected Four-wave mixing

Integrated SXRS

Dispersed SXRS

Integrated 2-Pulse Stimulated X-ray Raman

k_1 k_2

$\leftarrow \tau \rightarrow$
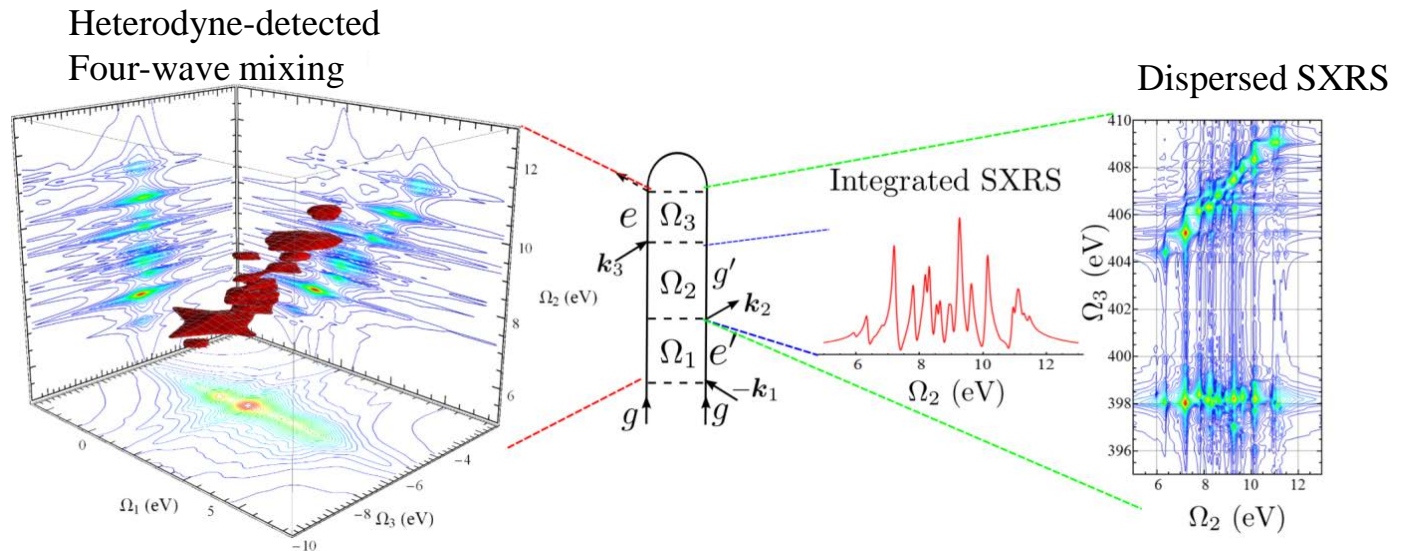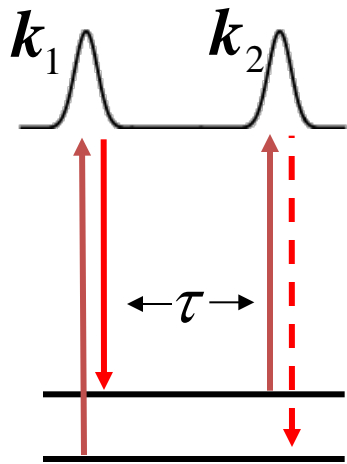
- The signal is measured by scanning the interpulse delay rather than the detection frequency

- The observation window is controlled by the pulse bandwidths

Keith Nelson *et al.* α-perylene (1991)

Diffraction Efficiency

X10

Time (psec)

Fourier Transform

Frequency (cm⁻¹)

Frequency (THz)
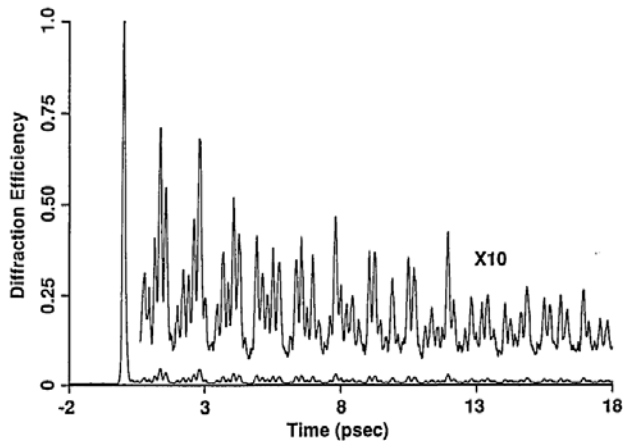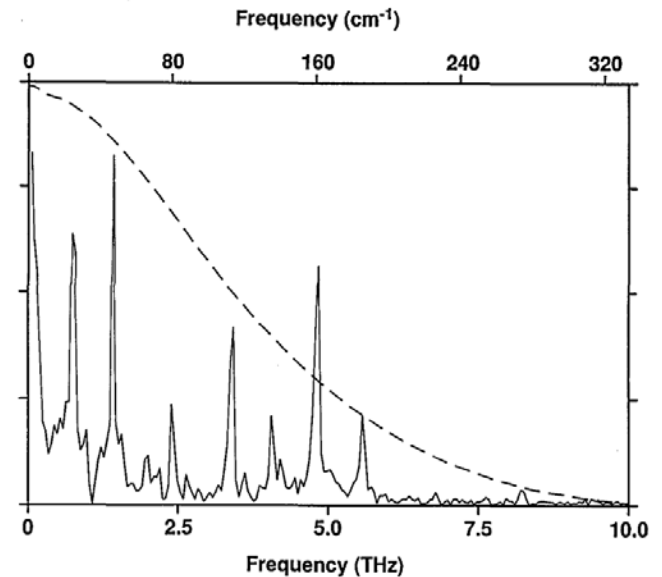
Fig. 3. Single-pulse ISRS data recorded from α-perylene with $T < 10$ K and with all pulses linearly polarized parallel to the b crystallographic axis. The femtosecond excitation pulses drive several phonon modes whose combined response yields a characteristic beating pattern. The spike at $t = 0$ is a purely electronic response of the crystal to the excitation pulses.

Fig. 4. Solid curve: Fourier transform of the scattering data shown in Fig. 3. The electronic scattering peak at $t = 0$ in the time-domain data was suppressed before the Fourier transform was performed. Dashed curve: Fourier transform of the electronic scattering peak, representing the instrumental response function.

Multidimensional X-Ray Raman Spectroscopy

- Stimulated X-Ray Raman
  - Integrated pump-probe 1D
  - Two-Dimensional X-ray Raman 2D
  - Frequency-resolved pump-probe 2D
  - k_{III} photon echo 3D
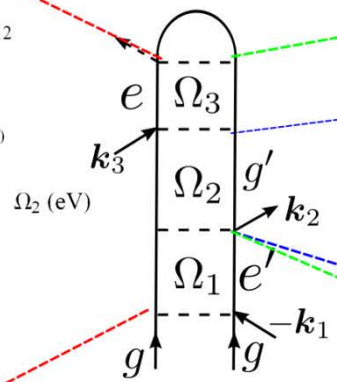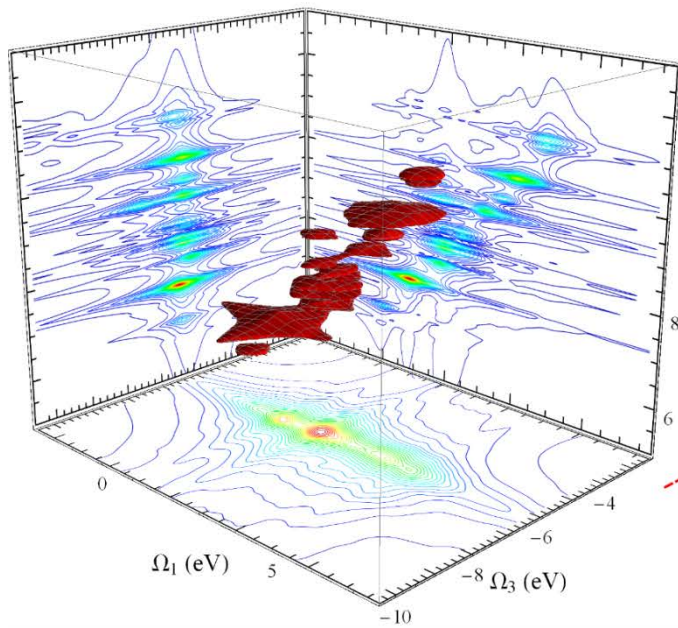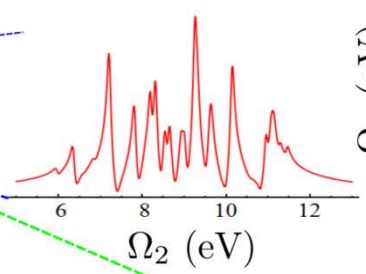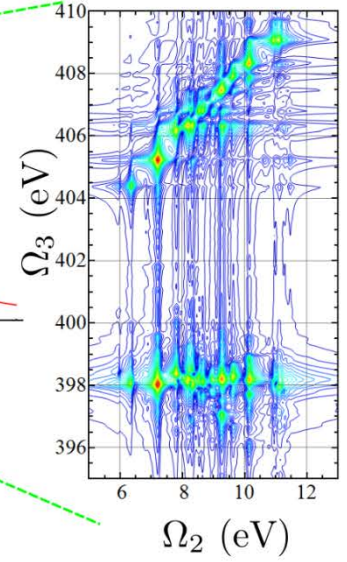
2-Pulse Stimulated X-ray Raman

1D-SXRS

detector
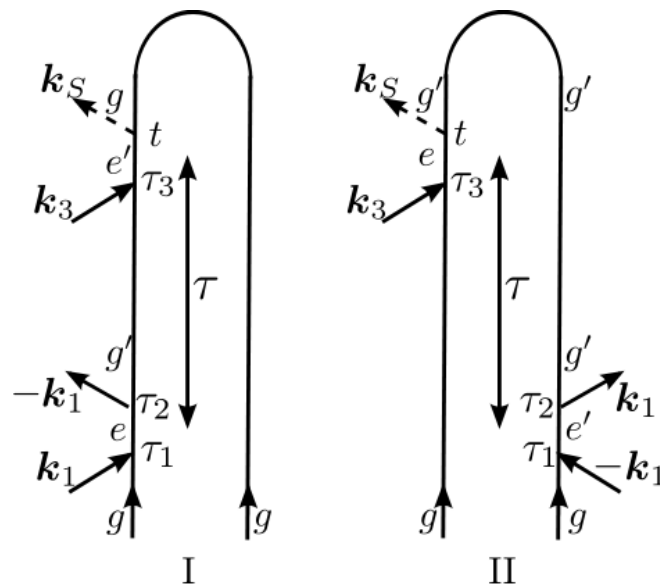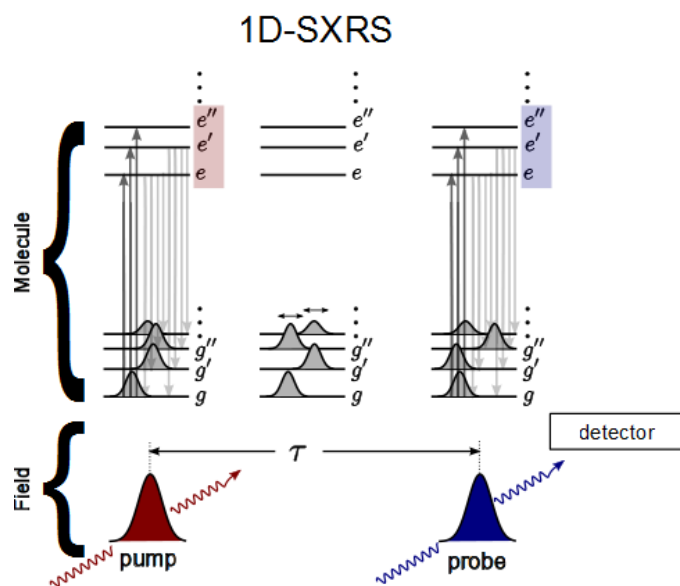
The system interacts twice with the pump and twice with the probe. No phase control is required.

The resonannt pump creates a wavepacket of valence-excited states which then evolves for a time τ before the arrival of the probe pulse.
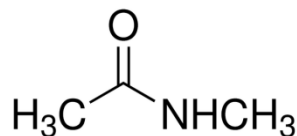
N-Methylacetamide (NMA)
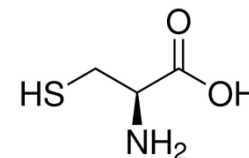
L-Cysteine

Impulsive Time-Domain Stimulated Raman Spectroscopy (1D)
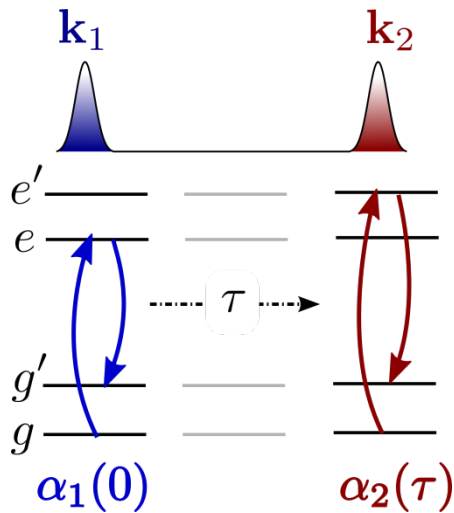
A common picture for X-rays and vibrations

$$\langle \alpha_2(\tau)\alpha_1(0)\rangle \qquad \langle \alpha_1^\dagger(0)\alpha_2(\tau)\rangle$$
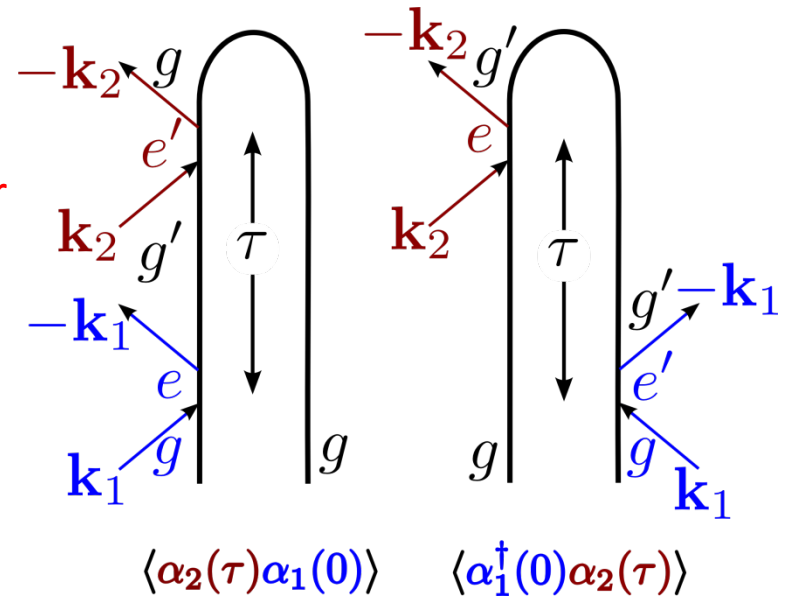
signal generated using broadband (femtosecond or attosecond) laser pulses, monitored in the time domain

The resonannt pump creates a wavepacket of valence-excited states which then evolves for a time τ before the arrival of the probe pulse.

The system interacts twice with the pump and twice with the probe. No phase control is required.

The effective polarizability depends on the pulse envelopes.

$$\alpha_{j;g'g} = \frac{1}{2\pi} \sum_e V_{g'e} V_{eg} \int d\omega \frac{\varepsilon_j^*(\omega)\varepsilon_j(\omega - \omega_{ge})}{\omega_j + \omega - \omega_{eg'} + i\epsilon}$$

One-Color and Two-Color 1D-SXRS of trans-NMA

Tuning the X-ray pulse to be resonant with different core-edge transitions
Probes delocalized valence excitations perturbed by the selected localized core hole.
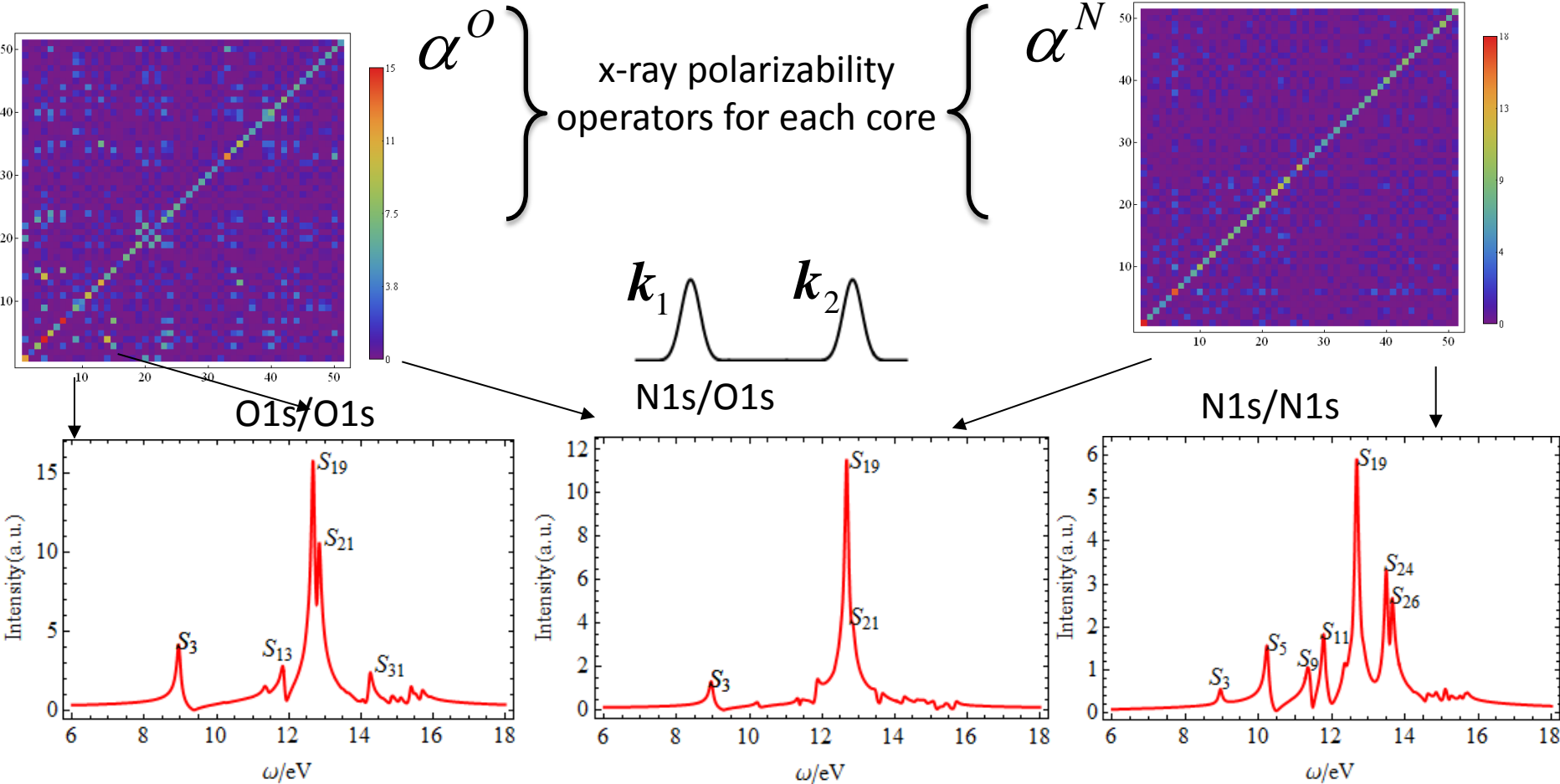
Two Dimensional Stimulated X-ray Raman Spectroscopy (2D-SXRS)
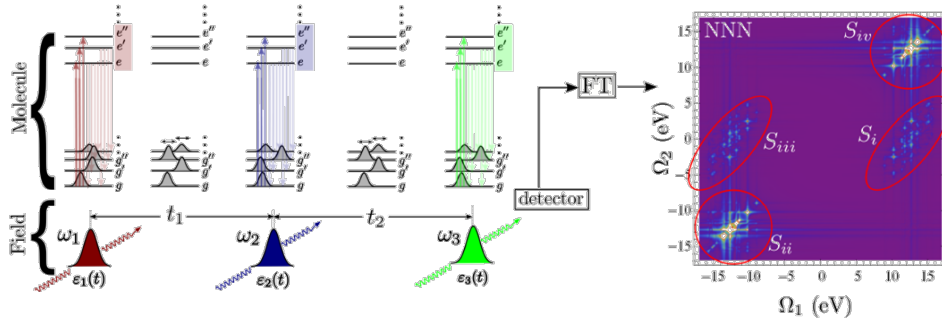
The two-pulse technique is extended by adding another pulse. Now two pulses create and then modify the valence-excited wavepacket that is then detected by the probe. As before, both integrated and dispersed detection are possible.

This signal is dependent on the matrix elements of the polarizability between different valence-excited states.

Ω_2 and Ω_4 are the delay times between the pulses, and both correspond to valence-excited states. Ω_5 is the dispersed frequency and reveals core-excited levels.
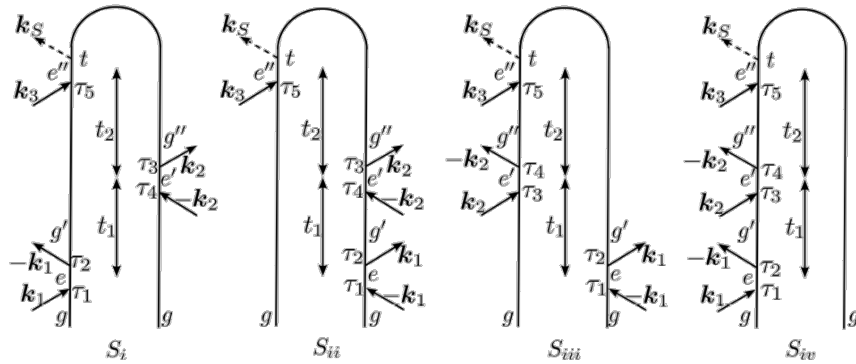
$$S_{I3P-SXRS}(\Omega_2, \Omega_4) = \sum_{g',g''} \frac{i\alpha_{1;g'g}}{\Omega_2 - \omega_{g'g} + i\Gamma_{g'}} \left(\frac{\alpha^\dagger_{2;gg''}\alpha''_{3;g''g'}}{\Omega_4 - \omega_{g'g''} + i\Gamma_{g'}} - \frac{\alpha''_{3;gg''}\alpha_{2;g''g'}}{\Omega_4 - \omega_{g''g} + i\Gamma_{g''}} \right).$$

$$S_{D3P-SXRS}(\Omega_2, \Omega_4, \Omega_5) =$$

$$\sum_{e,g',g''} \frac{i\alpha_{1;g'g}\alpha^\dagger_{2;g,g''}(\bar{\alpha}_{3;g''g'}(\Omega_5) - \bar{\alpha}^\dagger_{3;g''g'}(\Omega_5))}{(\Omega_2 - \omega_{g'g} + i\Gamma_{g'})(\Omega_4 - \omega_{g'g''} + i\Gamma_{g'})} - \frac{i\alpha_{1;g'g}\alpha_{2;g'',g'}(\bar{\alpha}_{3;gg''}(\Omega_5) - \bar{\alpha}^\dagger_{3;gg''}(\Omega_5))}{(\Omega_2 - \omega_{g'g} + i\Gamma_{g'})(\Omega_4 - \omega_{g''g} + i\Gamma_{g''})}$$

x-ray pulse polarizations are all-parallel (VVV)

NNN   NNO   NON   NOO

Ω_2 (eV)

×1.   ×4.3   ×2.3   ×6.6

Ω_1 (eV)
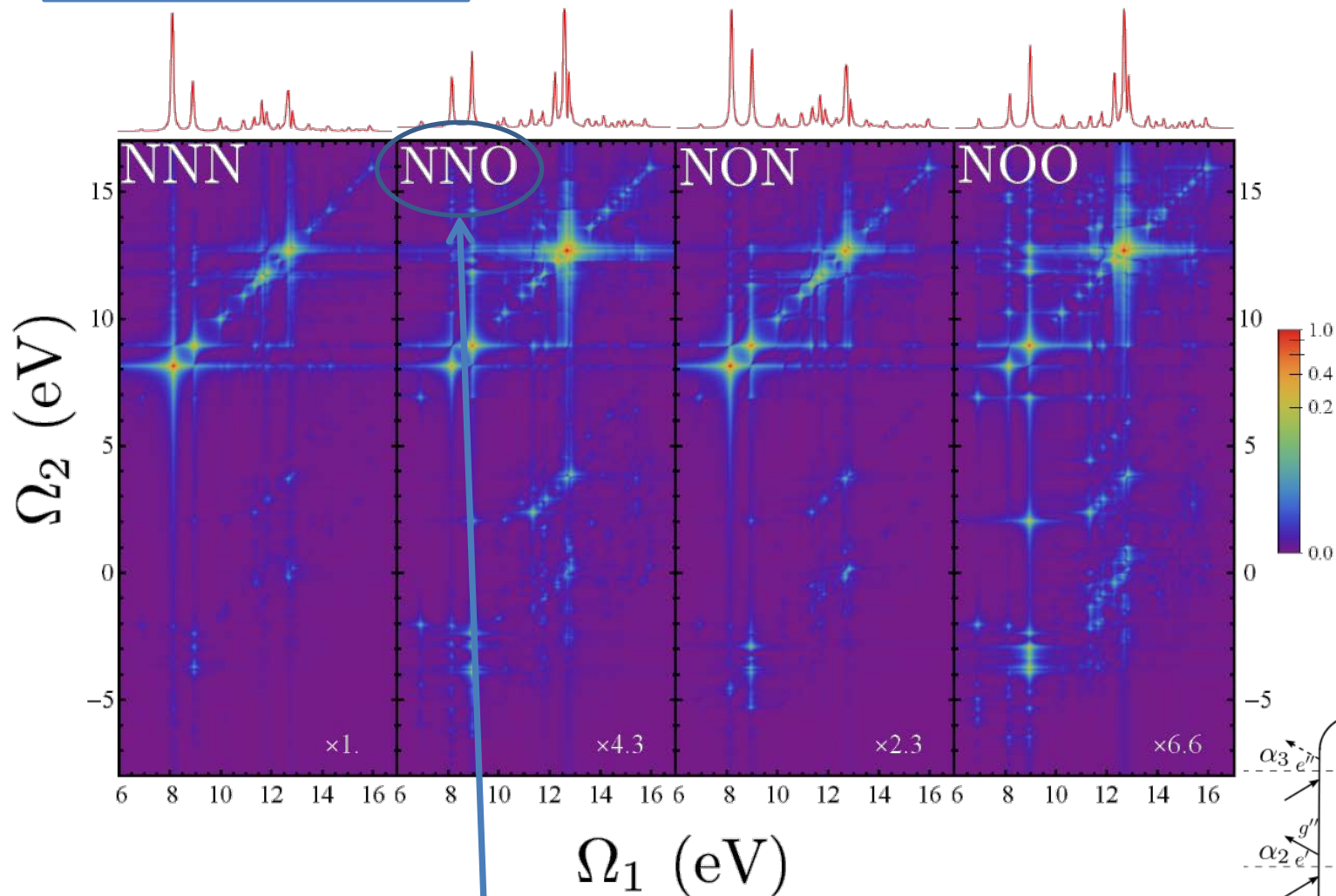
pulses1 and 2 tuned to Nitrogen K-edge, pulse 3 to Oxygen K-edge
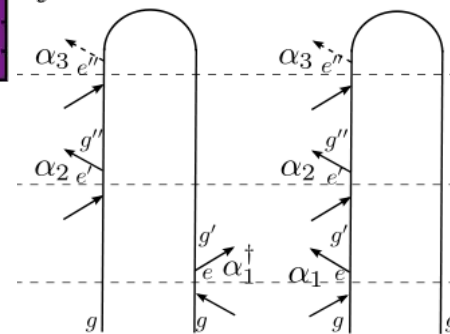
Integrated and dispersed 3-pulse SXRS from cysteine
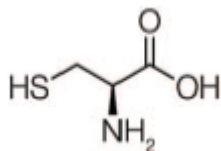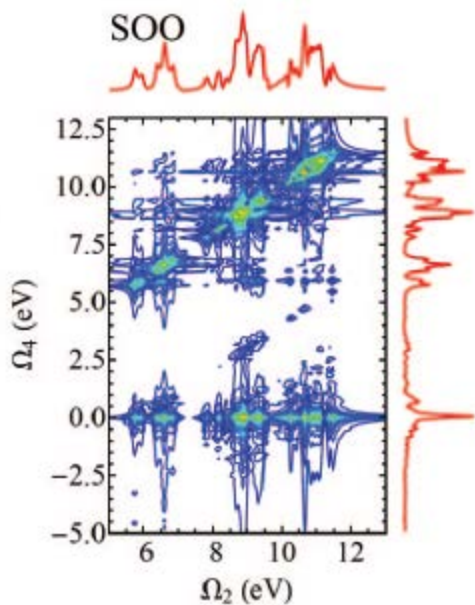
By integrating over the dispersed frequency Ω_5 we recover the integrated signal.
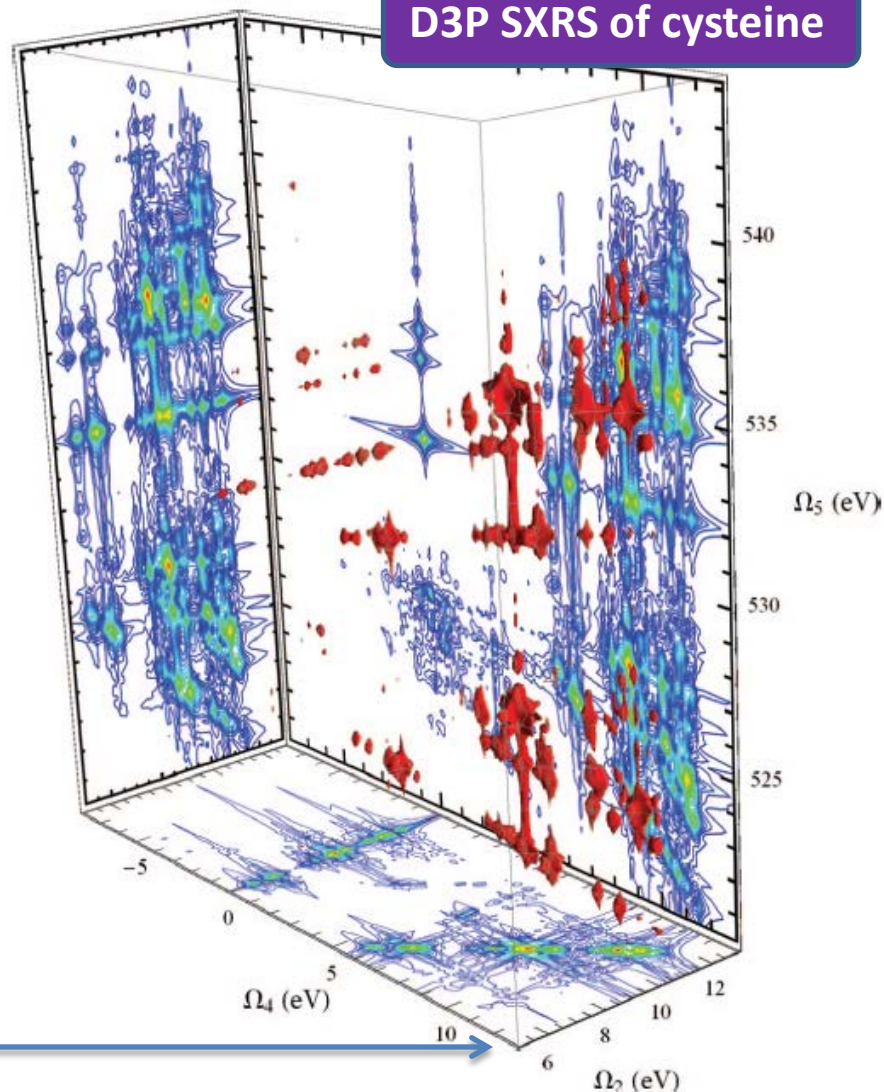
$$S_{I3P-SXRS}(\Omega_2, \Omega_4) = \int d\Omega_5 S_{D3P-SXRS}(\Omega_2, \Omega_4, \Omega_5).$$

Energy Transfer in Porphyrin Heterodimers

Core-excited states calculated using restricted excitation window time-dependent density functional theory (**REW-TDDFT**), which allows for the efficient calculation of core-excited states, and valence-excited states using a common theoretical framework.

Zinc monomer

Nickel monomer

UV Absorption

X-ray Raman probes valence-excitations, but through a core-excited intermediate. The same states show up in the UV/visible absorption spectrum, but with vastly different amplitudes.

K-edge XANES

L-edge XANES

Ni1s

Ni2p

Zn1s

Zn2p
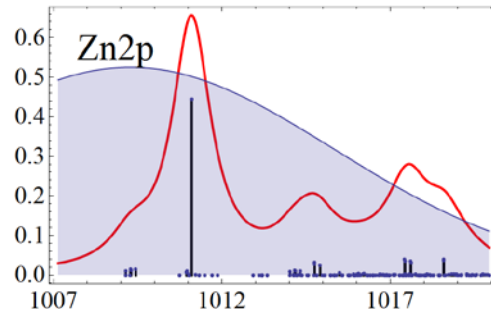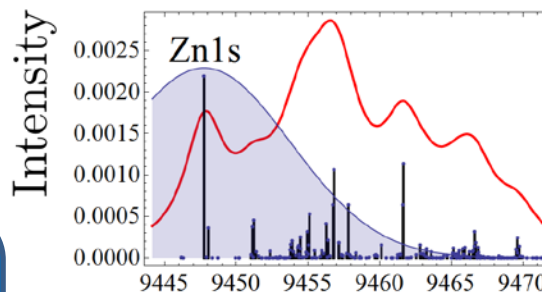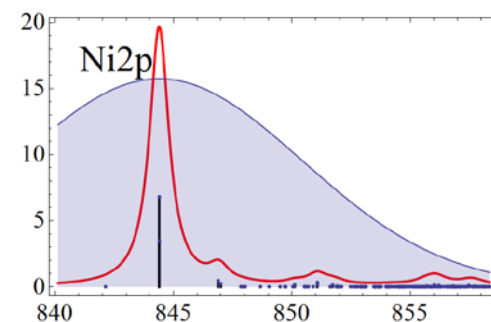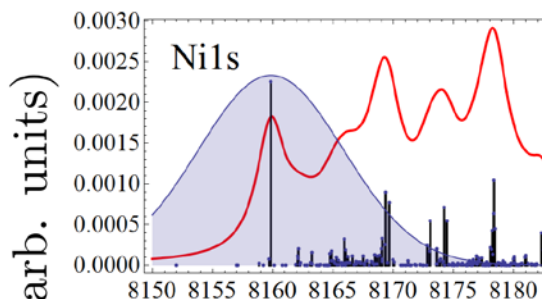
Pulse power spectra shown in blue
FWHM of 166 as (10.9 eV)

Integrated 2-Pulse Stimulated X-ray Raman

The pump pulse creates a valence wavepacket by scattering off a manifold of core-excited states within the pulse bandwidth

This superposition of valence-excited states then evolves during the interpulse delays

The probe pulse then returns the system to the ground state by scattering off of core-excited states. In a two-color setup, these core-excited states are different than those accessed by the pump
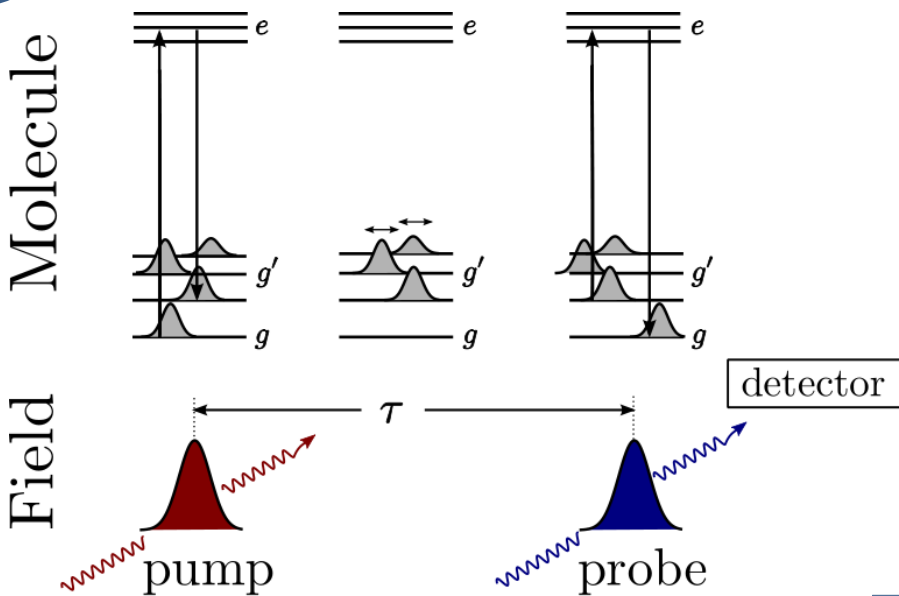
choose long delays: core-ionized states are off-resonance

Biggs, Zhang, Healion, and Mukamel; J. Chem. Phys. **136**, 174117 (2012)

Integrated 2-Pulse Stimulated X-ray Raman – cont'd

Time Domain:

$$\mathbb{S}_{SXRS}(\tau) = 2\Im\langle \bar{\alpha}_2''(\tau)\bar{\alpha}_1(0)\rangle$$

Frequency Domain:

$$\mathbb{S}_{SXRS}(\Omega) = \sum_{g'} \frac{\bar{\alpha}_{2;gg'}''\bar{\alpha}_{1;g'g}}{\Omega - \omega_{g'g} + i\Gamma_{g'}}$$

The signal is determined by the effective isotropic polarizability, which is averaged over the finite bandwidth of the excitation pulses.

Real part of the polarizability – responsible for off-resonance Raman scattering.

Imaginary part of the polarizability – goes to zero off resonance.

$$\bar{\alpha}_j = \bar{\alpha}' + i\bar{\alpha}''$$

polarizbility for the jth ultrafast pulse

$$= \sum_{e,g',g''} |g'\rangle \frac{\boldsymbol{\mu}_{g'e}\cdot\boldsymbol{\mu}_{eg''}}{2\pi} \int_{-\infty}^{\infty} d\omega \frac{\mathcal{E}_j^*(\omega)\,\mathcal{E}_j(\omega + \omega_{g'g''})}{\omega + \omega_j - \omega_{eg'} + i\Gamma_e} \langle g''|$$

$\overline{\overline{\overline{}}}\ e$

$\overline{\overline{\overline{}}}\ g'$

$\underline{\quad}\ g$

Since the I2P-SXRS signal is defined as the change in the integrated intensity of the probe pulse, the probe must be on resonance. Therefore the signal only depends on the imaginary part of the probe polarizability.

One-color SXRS: Pump and Probe at same edge

One color SXRS from porphyrin dimer

$$S_{I2P-SXRS} = -\Im\langle\psi_W|\psi_D(\tau)\rangle$$

time-independent window created by probe

time-dependent doorway created by pump

One-color SXRS measures the autocorrelation of the doorway. Only the Zn2p/Zn2p signal exhibits strong low-frequency oscillations indicative of energy transfer. Other on-color signals show only exponential decay.

Zinc metal: K-edge, L-edge
Nickel metal: K-edge, L-edge

Time Domain   **Frequency Domain**

Ni1s/Ni1s $\times 1.93 \times 10^8$

Ni2p/Ni2p $\times$ 1.

Zn1s/Zn1s $\times 1.86 \times 10^8$

Zn2p/Zn2p $\times 3.47 \times 10^3$

Intensity (arb. units)

τ (fs) Ω (eV)
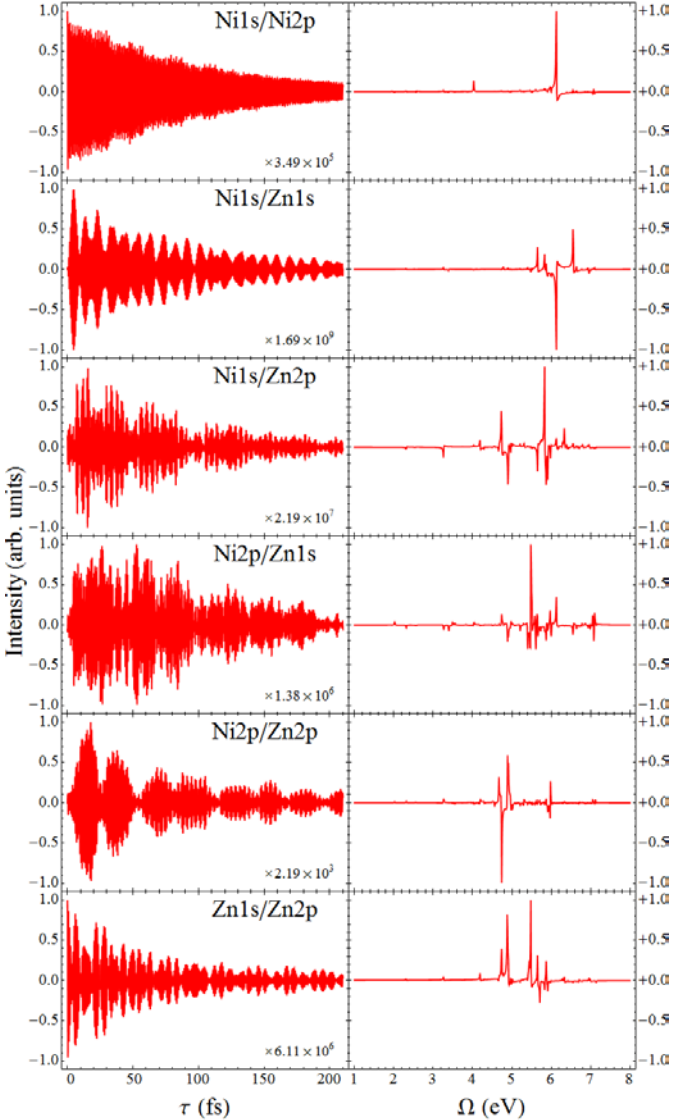
Two-color signals vanish when the two core electrons are not coupled to the same valence manifold. For the porphyrin dimer, a nonzero signal is evidence of energy or charge transfer.

Switching the order in which the two pulses arrive results in nearly identical signals.
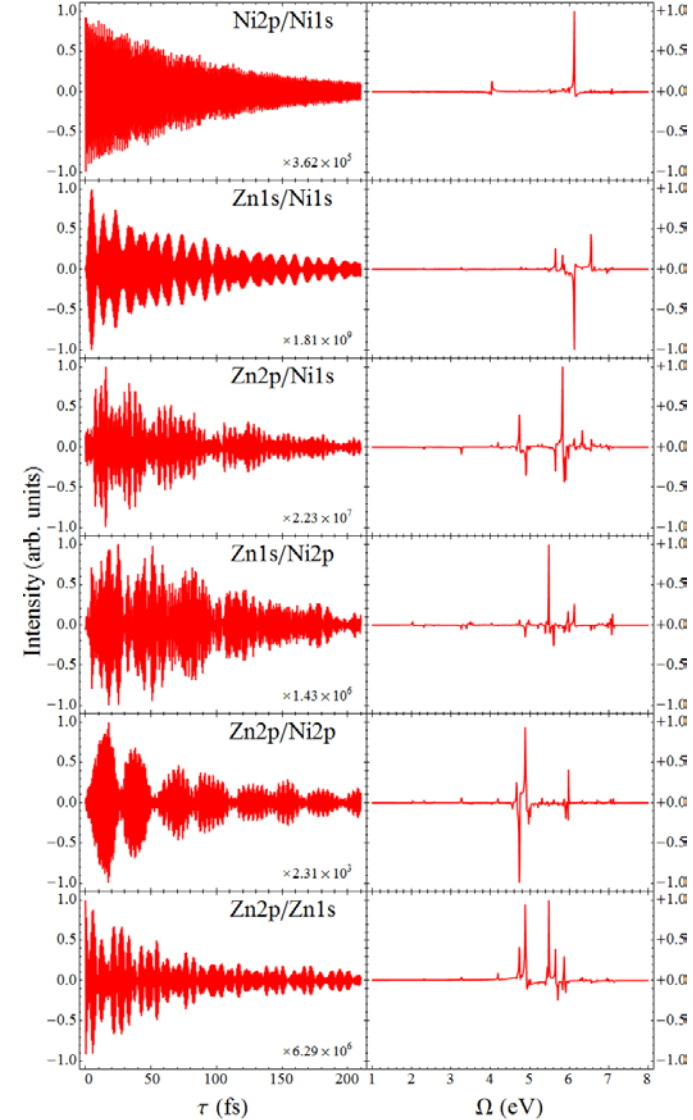
Time-reversal symmetry in 2-color SXRS

Time Ordered Signals

Difference Signals
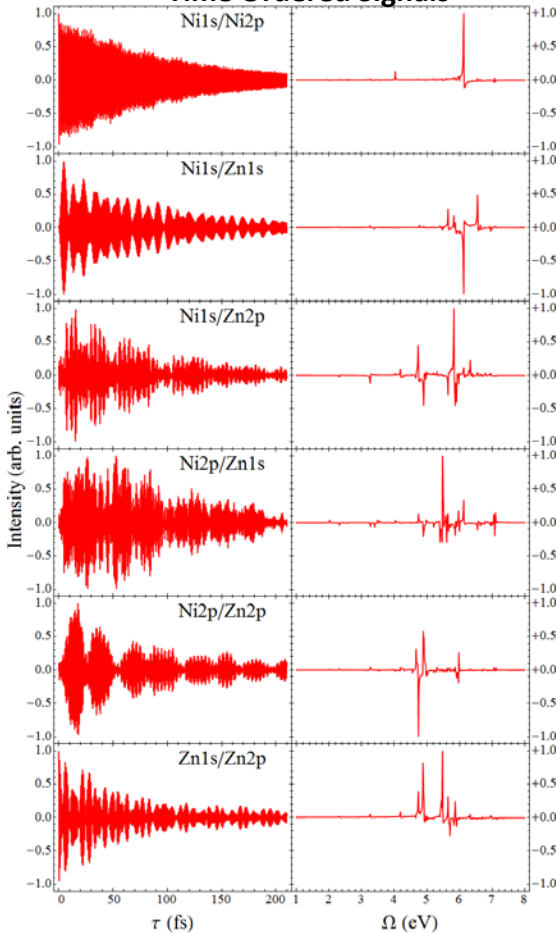
In the time domain, the difference signals (in purple) resemble the time-ordered signals (in red). In the frequency domain, the difference signals report upon the interference between the real and imaginary polarizabilities for the two different core edges considered.
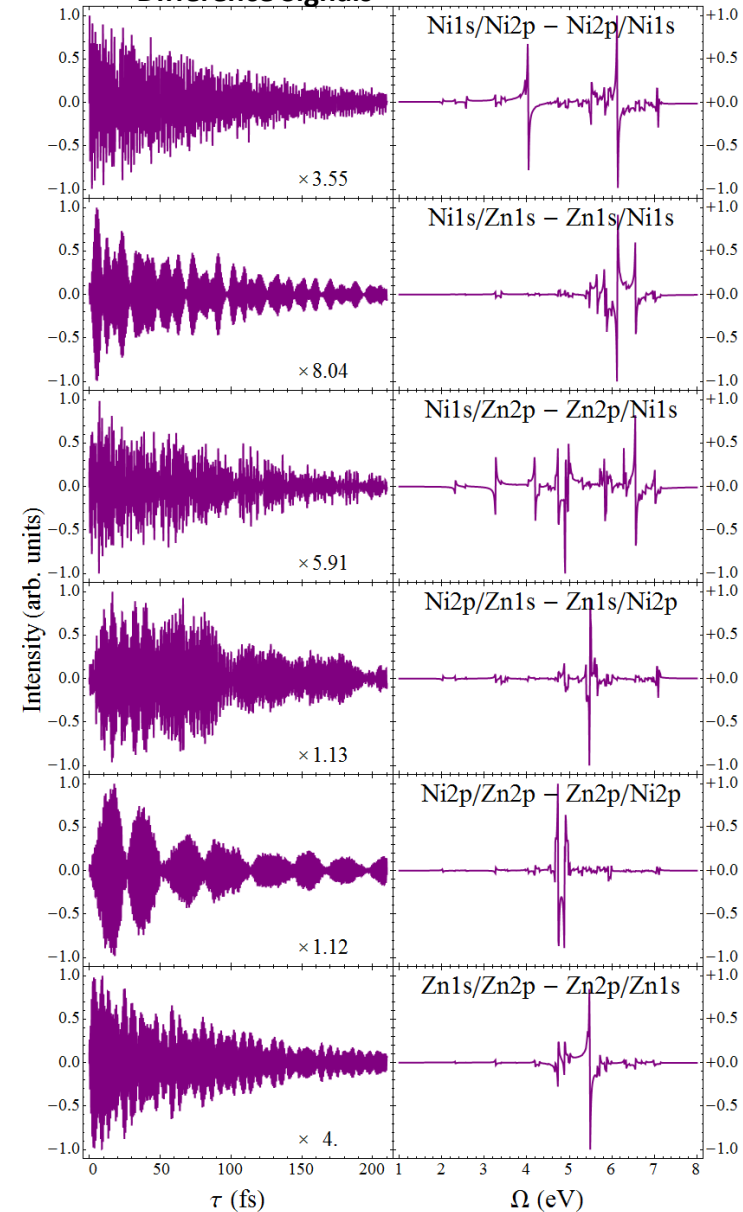
$$\mathbb{S}_{\text{Diff}}(\tau) \equiv \mathbb{S}_{SXRS}(\tau) - \mathbb{S}_{SXRS}(-\tau)$$

$$\mathbb{S}_{\text{Diff}}(\Omega) = \sum_{g'} \frac{\left(\bar{\alpha}''_{2;gg'} \bar{\alpha}'_{1;g'g} - \bar{\alpha}''_{1;gg'} \bar{\alpha}'_{2;g'g} \right)}{\Omega - \omega_{g'g} + i\Gamma_{g'}}$$

Natural Orbitals Decomposition

Interaction with the pump creates the doorway, a wavepacket of valence excited states

$$|\psi_D(\tau)\rangle = \sum_{g'} \alpha_{1;g'g_o} e^{-i\epsilon_{g'}\tau} |g'\rangle = \hat{K}(\tau)|g\rangle$$

The time-dependent operator $K(\tau)$ acts upon the ground state to create the doorway.

$$|g'\rangle = \sum_{ai} C^{g'}_{ai} c^\dagger_a c_i |g\rangle$$

$$\hat{K}(\tau) = \sum_{g,ai} \alpha_{1;g'g_o} C^{g'}_{ai} c^\dagger_a c_i e^{-i\epsilon_{g'}\tau}$$

Valence excitations written in MO basis

A singular value decomposition of provides the most compact representation of the doorway in the space of single excitations.

$c^\dagger_a$ creation operator for virtual orbital a

$$K(\tau) = V(\tau)W(\tau)U^\dagger(\tau)$$

c_i annihilation operator for occupied orbital i

$$|\psi_D(\tau)\rangle = \sum_\xi w_\xi(\tau) c^\dagger_\xi(\tau) d_\xi(\tau) |g\rangle$$

The participation ratio R^{-1} is a useful measure of the degree to which the electron and hole are entangled. When the state is described by a single electron-hole pair, they are not entangled at all and $R^{-1}=1$. Higher values indicate greater entanglement.

Through a rotation of the MO basis, a new set of natural orbitals is achieved which minimizes the number of electron-hole pairs needed to describe the state.

$$c^\dagger_\xi(\tau) = \sum_a V_{a,\xi}(\tau) c^\dagger_a$$

$$d_\xi(\tau) = \sum_i U^*_{i,\xi}(\tau) c_i$$

$$R^{-1}(\tau) = \frac{1}{\sum_\xi w^4_\xi(\tau)}$$

$$\sum_\xi w^2_\xi(\tau) = 1$$

Natural Transition Orbitals for Valence Eigenstates
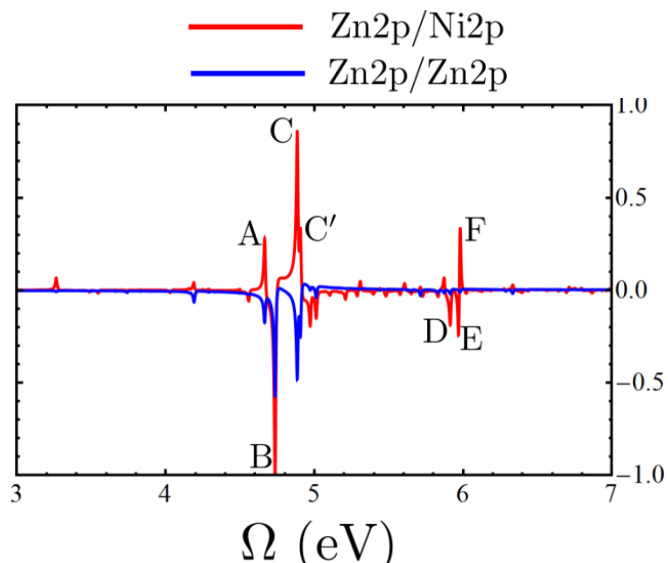
The eigenstates which show up in the Fourier-Transform spectra are delocalized valence states.

Table 1. Frequencies, participation ratios, and integrated electron and hole densities for the states corresponding to the major peaks in the right panel of Fig. 3.

Peak	Ω	R^{-1}	hole density		electron density	
			Ni monomer	Zn monomer	Ni monomer	Zn monomer
A	4.67	1.57	0.41	0.59	0.38	0.62
B	4.74	2.45	0.37	0.63	0.29	0.71
C	4.89	4.48	0.34	0.66	0.40	0.60
C′	4.91	3.42	0.57	0.43	0.46	0.54
D	5.91	4.51	0.45	0.55	0.44	0.56
E	5.97	1.39	0.92	0.08	0.99	0.01
F	5.98	3.82	0.60	0.40	0.84	0.16
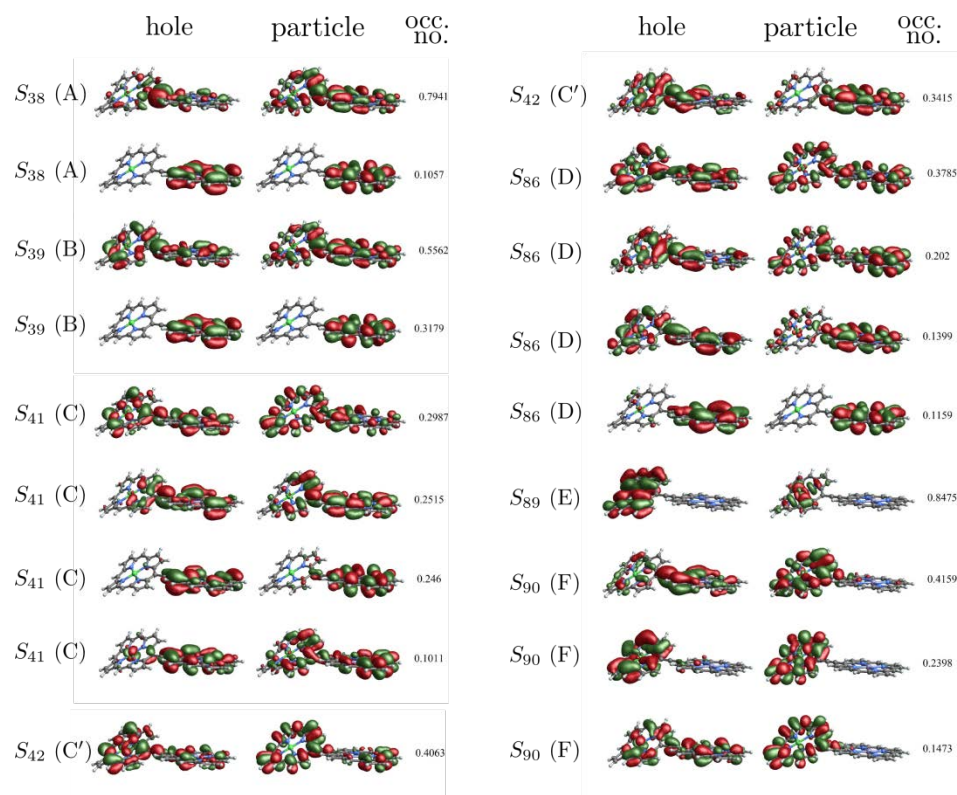
Natural transition orbitals provide the most compact representation of these states. Orbital rotations which result from a singular-value decomposition of the transition density matrices in the space of single excitations

Time-dependent Natural Orbitals for Valence Wavepackets

Zn2p/Zn2p Signal –Time Domain
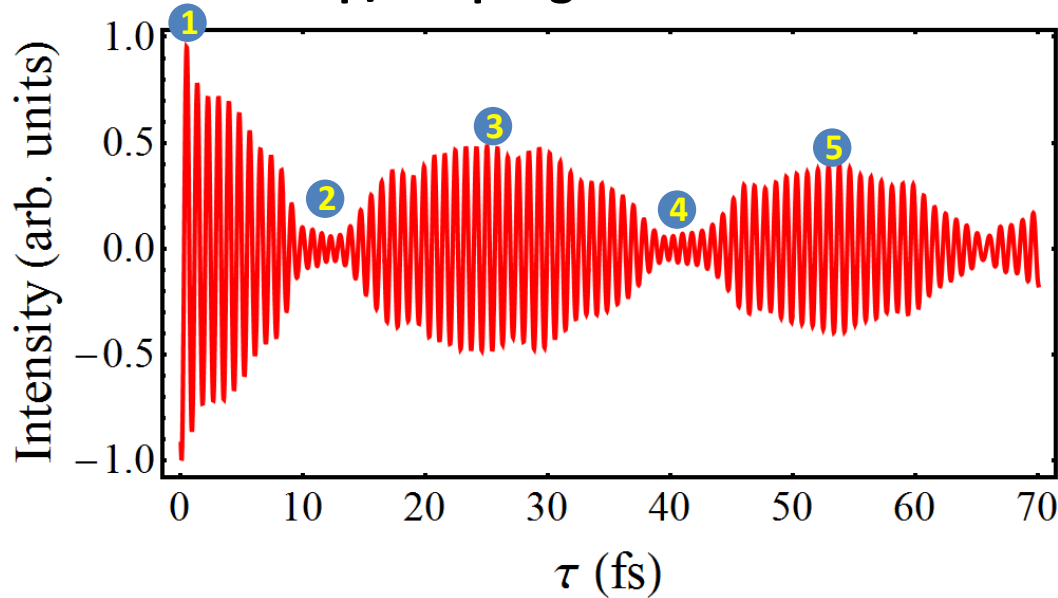
The superposition of delocalized electronic eigenstates resulting from Raman excitation is localized in space. Maxima and minima in this signal correspond to times when the excitation is on the zinc and nickel monomers, respectively.
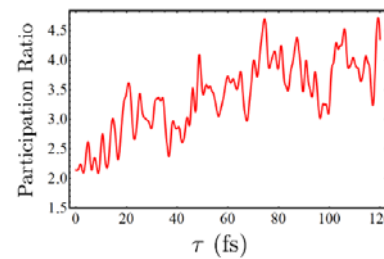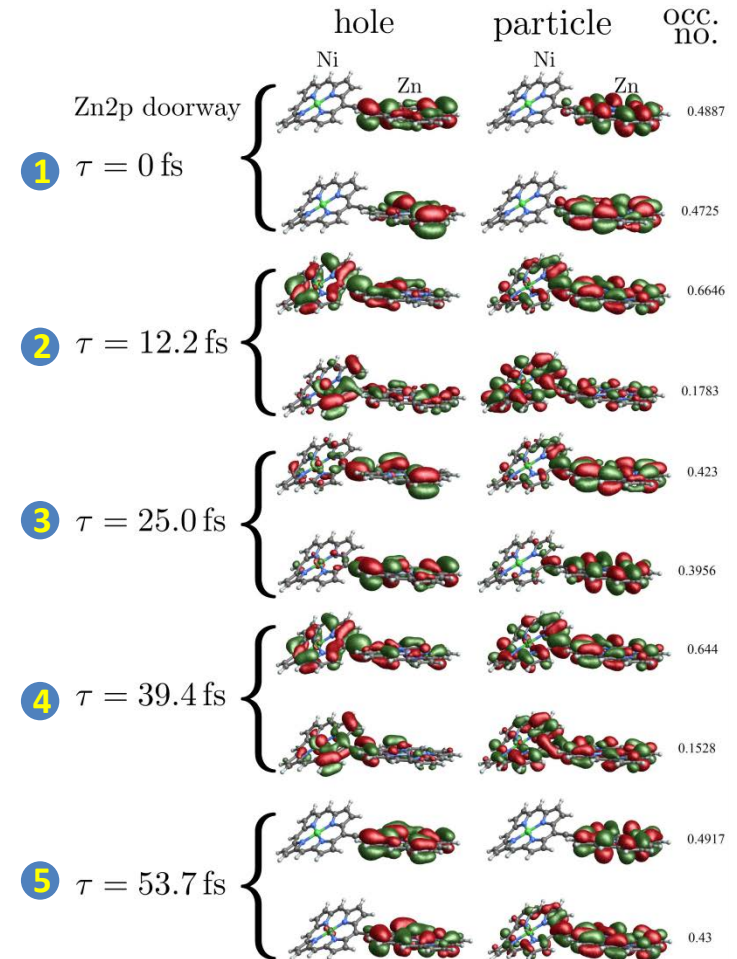
The electron-hole pairs comprising the wavepacket become increasingly entangled following excitation

Charge density vs. signal

There is a correspondence between the nonequilibrium charge density and the spectroscopic signal. The electron and hole densities move across monomers together, indicating energy transfer rather than charge transfer.
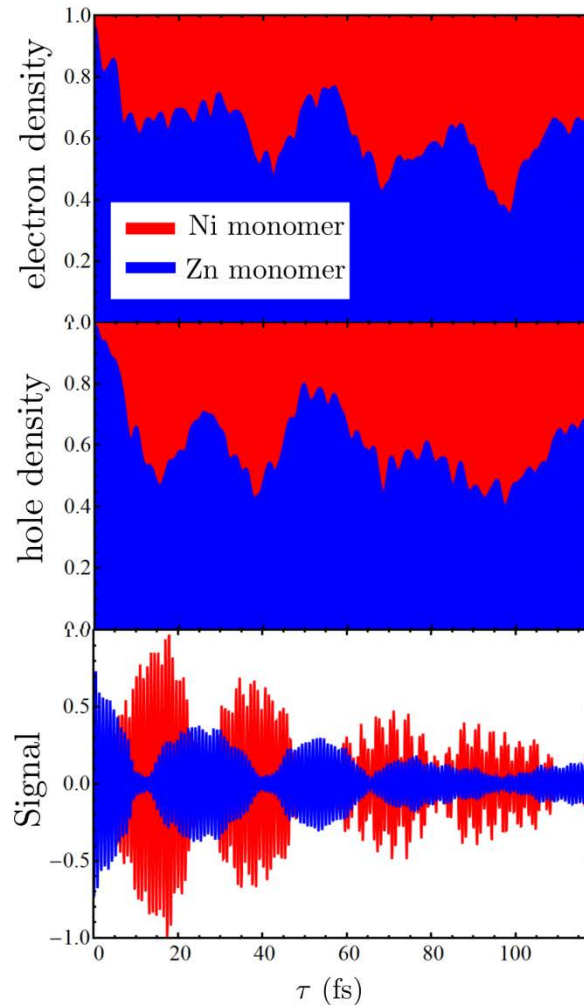
Zn2p Raman Wavepacket Densities
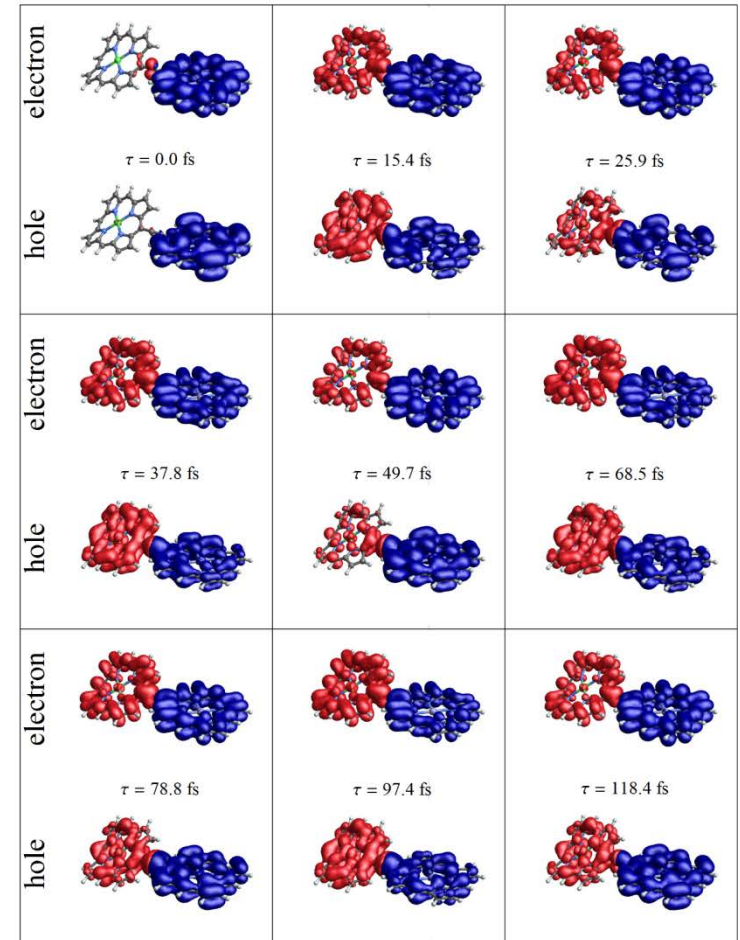
Animation – short simulation
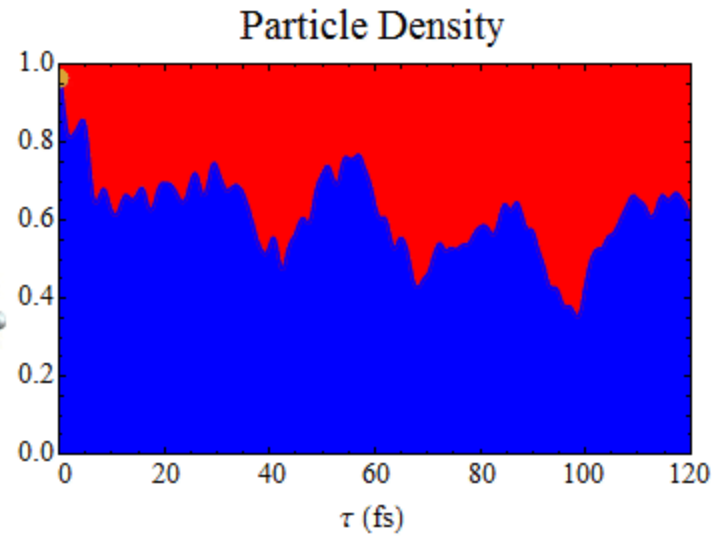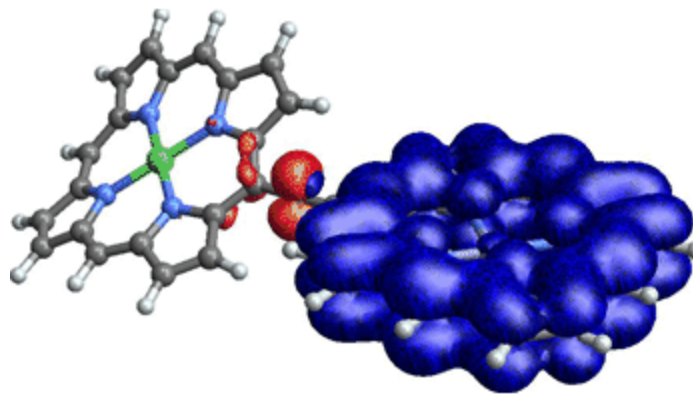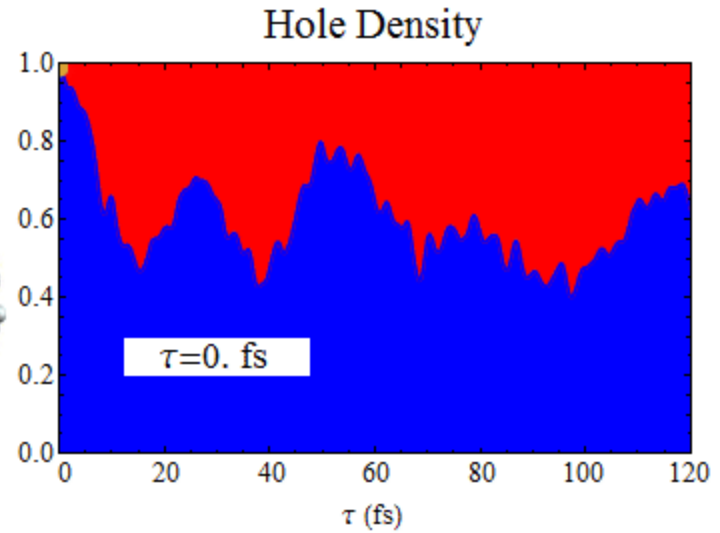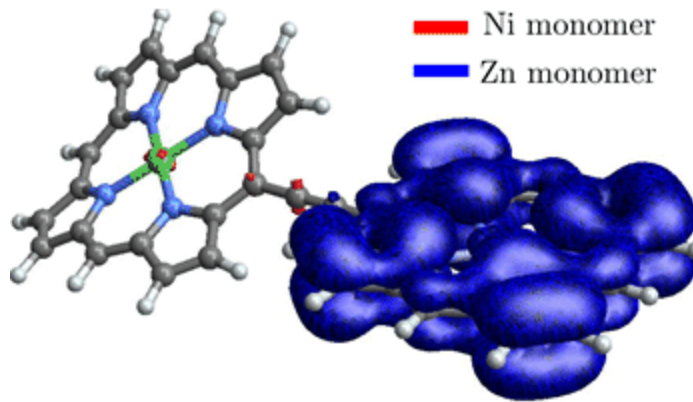
Long Range Electron Transfer in Rhenium-modified Azurin
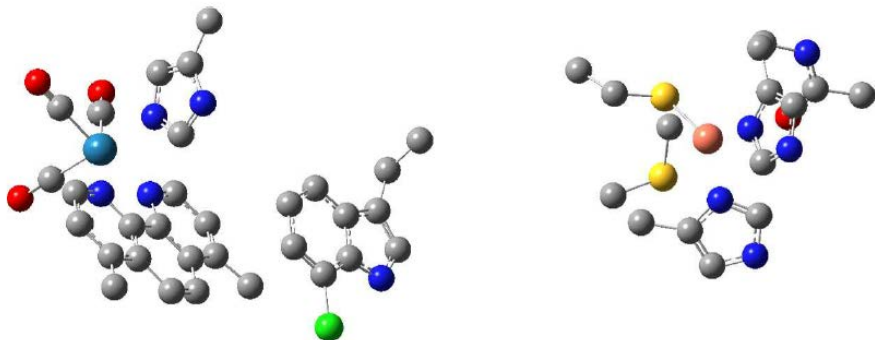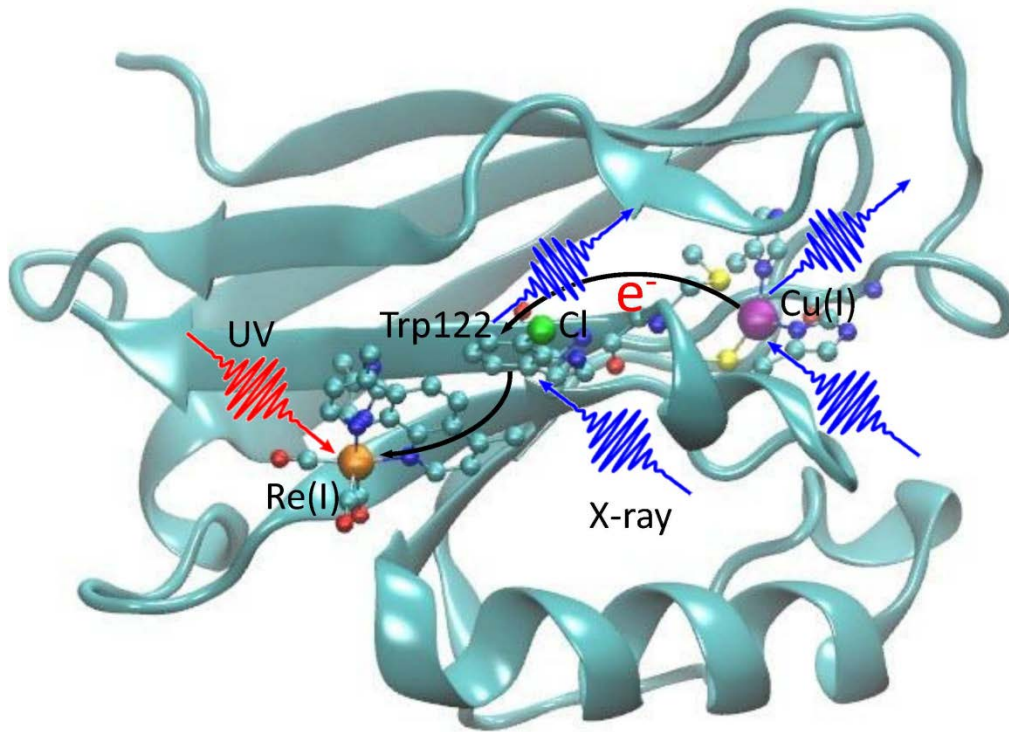
- small protien produced by aerobic bacteria
- In respiration chain, transfers 1 electron from cytochrome c551 to its reductase
- Tryptophan intermediate speeds up electron transfer (ET) from Cu to Re (hopping mechanism)
- photo-excited Re mimics biological e⁻ acceptors

- Our model uses 3 fragments, Re-complex, Trp, Cu-complex
- Chlorine atom added to trp for an X-ray chromophore

Azurin

● Azurin is a small (128 residues for Re-modified azurin) type I blue copper protein (cupredoxin) produced by several aerobic bacteria.

● Azurin transfers one electron between cytochrome c-551 and cytoxidase, which helps *Pseudomonas* oxidase or *Pseudomonas* nitrite reductase to reduce O_2 to H_2O, or NO_2-to NO.

● The Re-modified azurin can be used as a model to study long-range electron transfer in proteins, where the Re complex acts as a trigger for the ET process.

Kolczak, *et al*, in Handbook of Metalloproteins, Vol. 2, p 1170, Wiley, New York, 2001.
Silvestrini, *et al*., Biochem. J., **203**, 445 (1982).
Shih, *et al*., Science, **320** 1760 (2008).

Long-range Electron Transfer Kinetics

2. MLCT singlet converts to triplet state, vibrational relaxes – states A and B

1. UV excitation creates a singlet MLCT state, hole on rhenium

3. Hole migrates to tryptophan, charge-transfer state C

4. Hole migrates to copper, long-range charge transfer state D
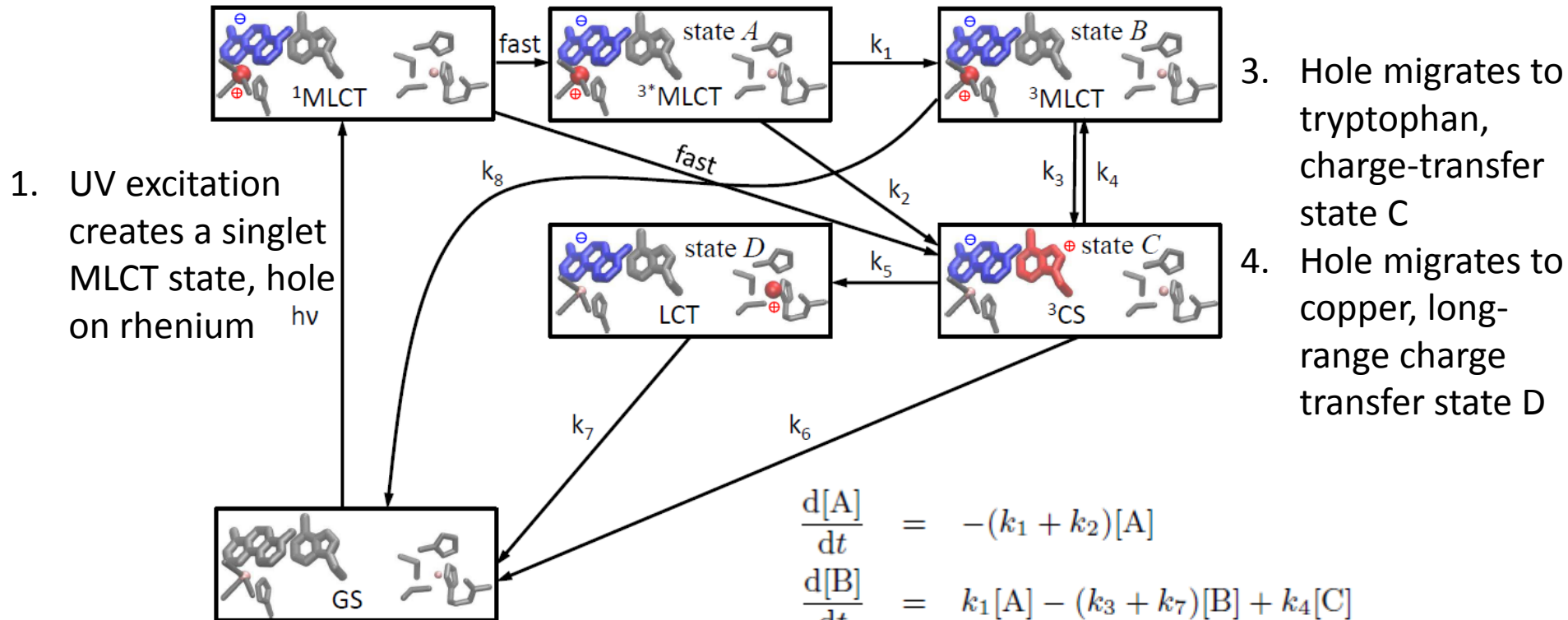
$$\frac{d[A]}{dt} = -(k_1 + k_2)[A]$$

$$\frac{d[B]}{dt} = k_1[A] - (k_3 + k_7)[B] + k_4[C]$$

$$\frac{d[C]}{dt} = k_2[A] + k_3[B] - (k_4 + k_5 + k_8)[C]$$

$$\frac{d[D]}{dt} = k_5[C] - k_6[D].$$
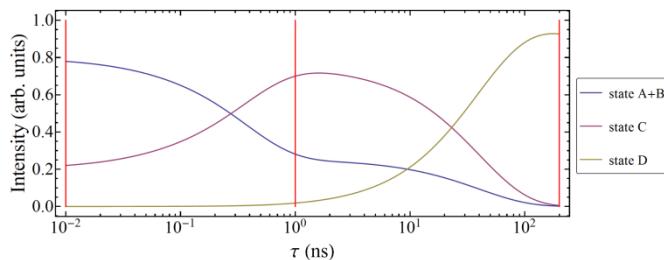
Time-Resolved X-ray Absorption vs. SXRS
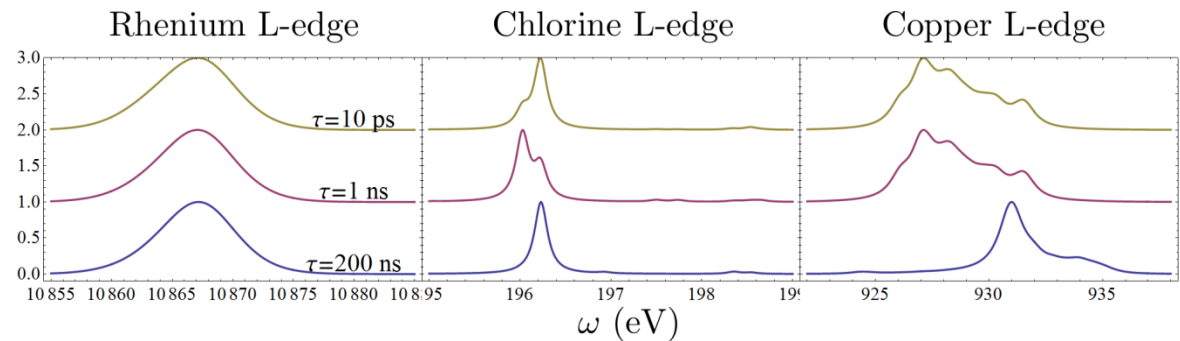
Absorption of a resonant X-ray pulse (FWHM – 10 eV)
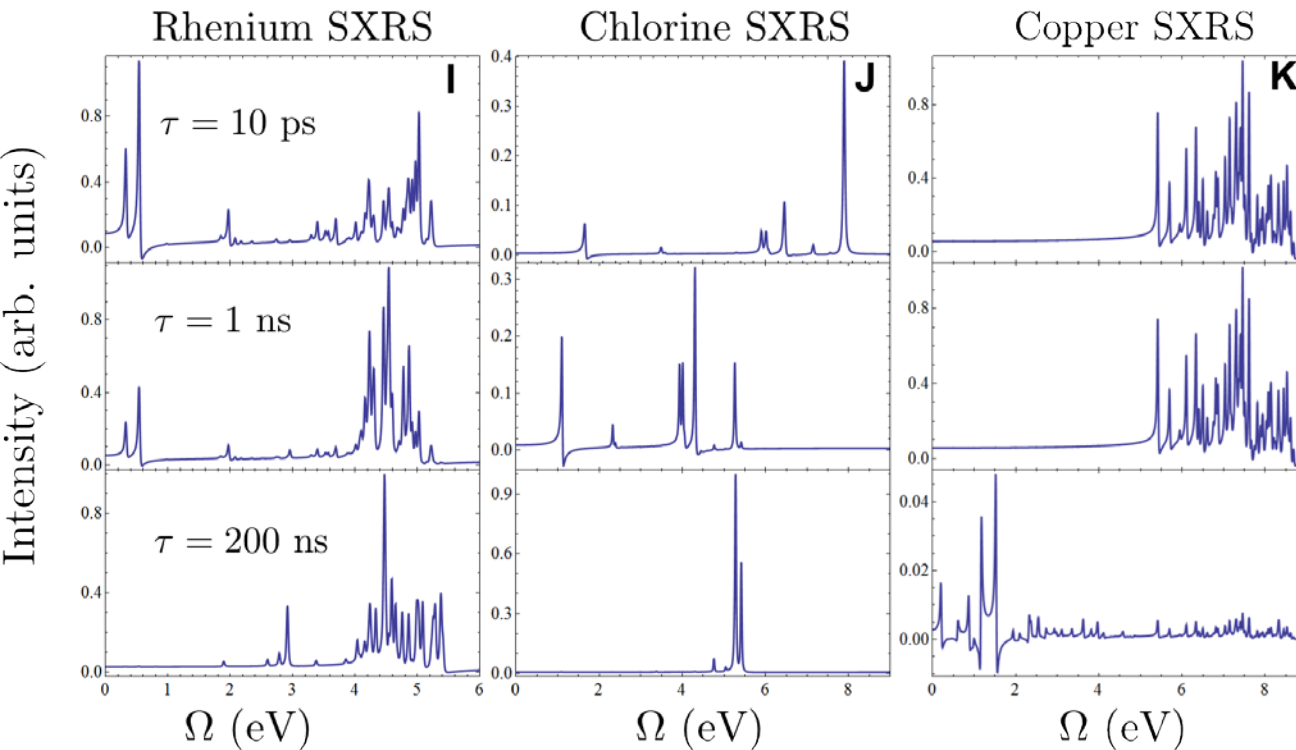
SXRS signals show a greater sensitivity to the ET process.
Presence of hole indicated by new low-frequency peaks

Electron Density Difference Kinetics
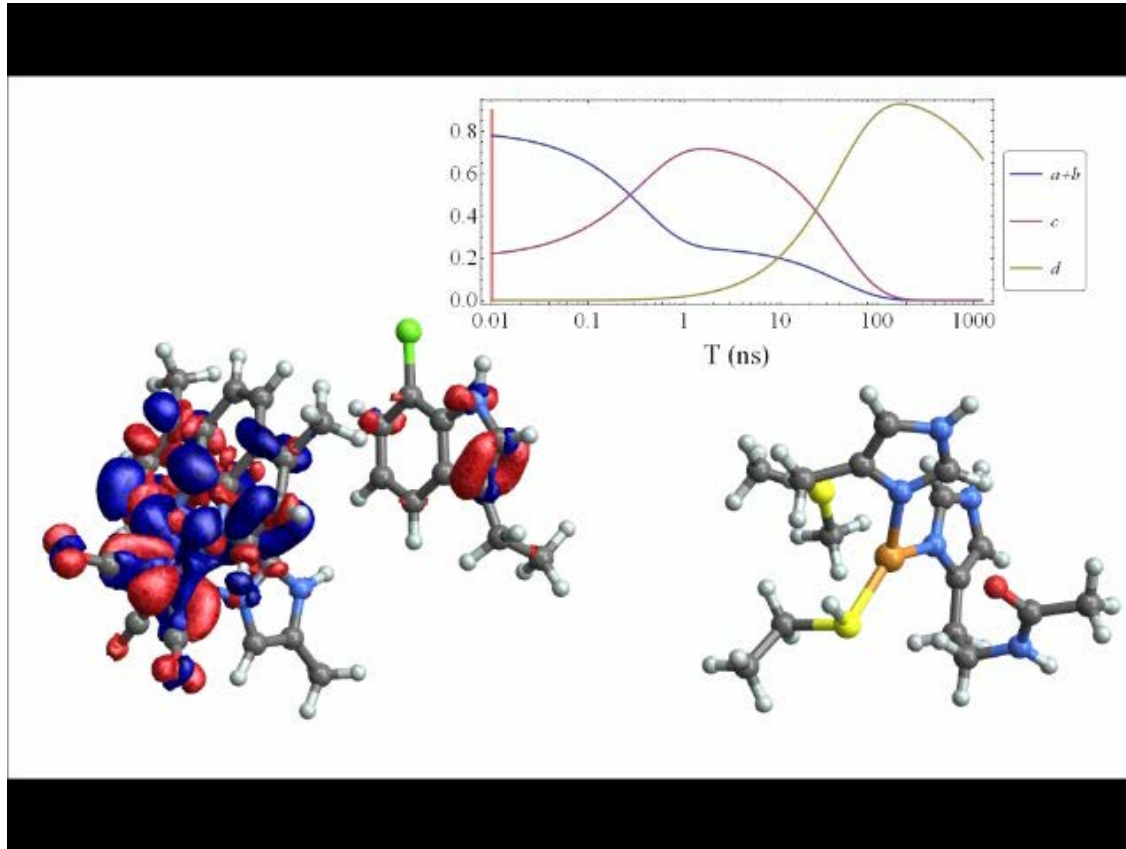
Based upon the kinetic model this movie shows the electronic density difference (excited state – ground state) over the course of the electron transfer. We see the excitation initially created on the Rhenium center, following which the hole migrates first to the tryptophan, then to the copper center.

Stimulated Raman Signals
with Hybrid Broad-and Narrowband pulses

a Time-resolved FSRS

b FSRS pulse timing
- ① Actinic pulse
- ② Raman pulse
- ③ Probe pulse
- Time
- ΔT
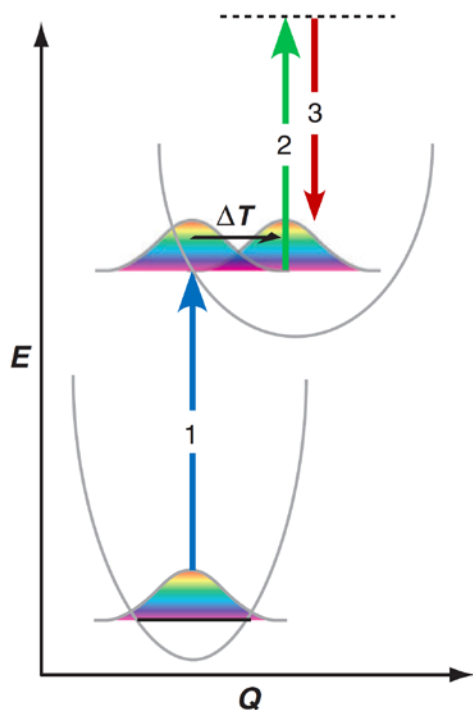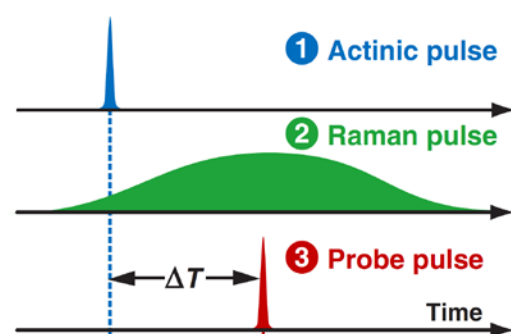
c Energy-level diagram
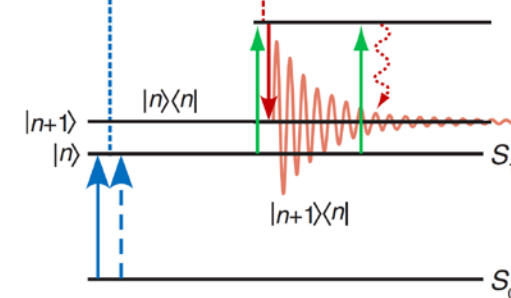
- Ultrashort pulse 1 initiates a chemical reaction in an excited electronic state

- Pulses 2 (narrowband) and 3 (broadband) induce a Raman transition.

- The spectral resolution ($\Delta\omega$) is determined by the monochromator into which the signal is dispersed

- The apparent time resolution (Δt) is determined by the delay time T between broadband pulses k_1 and k_3

- Apparently there is no lower limit to the product $\Delta\omega\Delta t$

- Does the technique offer perfect snapshots of the changing vibrational frequency ω_{ca} **at** time T?

R. Mathies Annual Review of Physical Chemistry 58, 461 (2007),
T. Tahara Yellow protein: The Journal of Physical Chemistry Letters **3**, 2025 (2012),
pNA, pDNA: P. Gilch, Optics Communications 202, 209 (2002),
CO_2: M. Dantus, Journal of Raman Spectroscopy 41, 1194 (2010),
Bacterial endospores: M. Scully Science 316, 265 (2007),
Cell imaging: Sunney Xie Phys. Rev. Lett. 82, 4142 (May 1999),
Multiplex CARS: J.-X. Cheng, J. Phys. Chem. B 106, 8493 (2002)
             M. Müller, J. Phys. Chem. B 106, 3715 (2002)

Photo-induced Isomerization of Rhodopsin

- time-resolved stimulated Raman

- Spectral evolution over the course of a picosecond was observed

- Interpreted as instantaneous change of
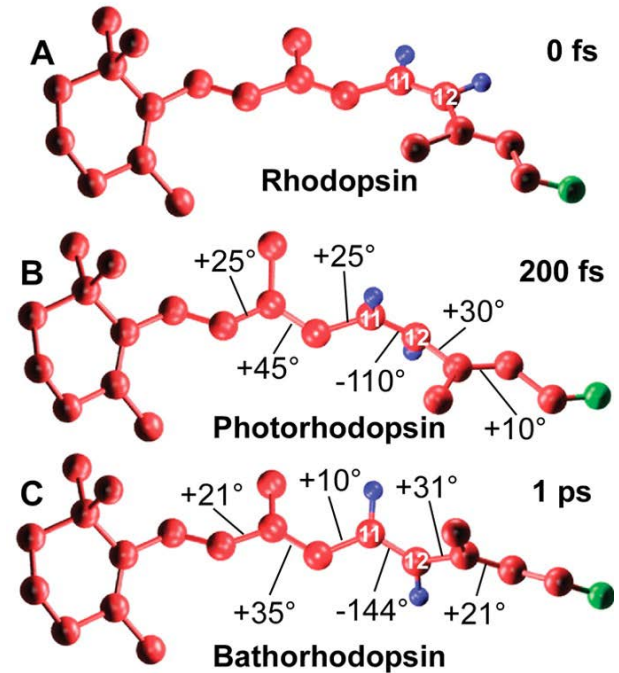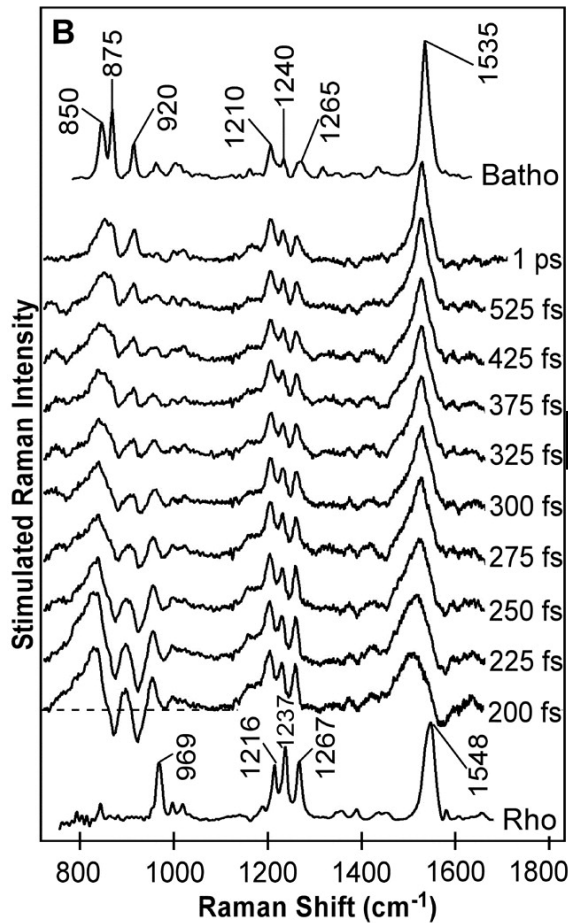
P Kukura et al. Science 2005;310:1006-1009

High Temporal and Spectral Resolution?

LETTERS

Mapping GFP structure evolution during proton transfer with femtosecond Raman spectroscopy

and phytochrome[18] have been successfully studied with femtosecond stimulated Raman spectroscopy (FSRS). This vibrational structural technique[9] uses a femtosecond actinic pump pulse to initiate photochemistry, and a picosecond Raman pump pulse together with a 20-fs Raman probe pulse to stimulate broadband Raman signals within a possible vibrational range of 50–$3,500 \, cm^{-1}$. The time resolution of FSRS is determined by

the cross-correlation between the femtosecond actinic pump and Raman probe pulses, and can be 25 fs or less. The energy resolution is determined by the Raman pump bandwidth and the vibrational-coherence free-induction decay time, and can be as narrow as $5 \, cm^{-1}$.

Nature 462, 200 (2009)

CIRCUMVENTING HEISENBERG

One of the numerous critical advancements in the field of ultrafast spectroscopy over the past two decades involves the apparent circumvention of the uncertainty principle through femtosecond dynamic absorption spectroscopy (14). In this approach to pump-probe transient absorption spectroscopy, the broadband femtosecond probe pulse is dispersed onto a multichannel detector, resulting in measurement of the full pulse spectrum rather than just its intensity. The time resolution of this technique is only fundamentally limited by the durations of the two pulses initiating the macroscopic polarization in the sample that generates the detected signal. The frequency resolution, conversely, is determined by the lifetime of the induced polarization rather than the pulse duration because the detection step is not time resolved. The simultaneous high time and frequency resolution can then be used to observe electronic signatures of ultrafast chemical reaction dynamics with energy resolution much finer than the bandwidth of the femtosecond pulses used in the experiment.

Annu. Rev. Phys. Chem. 58, 461–88 (2007)

$$\Delta\omega\Delta t \approx 500 \text{ fs cm}^{-1}$$
vs.
$$\Delta\omega\Delta t \approx 5000 \text{ fs cm}^{-1}$$
(Fourier uncertainty)
Heisenberg

Comparison of Raman signals

Absorptive lineshape
For FR-SPRS
Dispersive features
For FSRS and TG-ISRS/TR-ISRS

Low time and frequency resolution of FR-SPRS determined by pulse duration <u>only.</u>

Higher resolution of FSRS/TG-ISRS/TR-ISRS determined by combined matter and field parameters.

Strong background for TG-ISRS/TR-ISRS compared to FSRS due to finite time duration of the pump pulse

0   00   300

$\omega - \omega_{20}, \ \mathrm{cm}^{-1}$

Δ-Dispersed Signal

Loop-diagrammatic Ansatz:

$$S_{SRS}(\omega - \omega_3, T) = \mathscr{I} \int_{-\infty}^{\infty} \frac{d\Delta}{2\pi} \mathscr{E}_2^*(\omega) \mathscr{E}_2(\omega + \Delta) \tilde{S}_{SRS}(\omega - \omega_3, T; \Delta)$$

$$\tilde{S}_{SRS}(\omega - \omega_3, T; \Delta) = \frac{2}{\hbar} \int_{-\infty}^{\infty} dt \int_{-\infty}^{t} d\tau_1 \int_{-\infty}^{t} d\tau_3 \int_{-\infty}^{\tau_3} d\tau_5 |\mathscr{E}_3|^2 \mathscr{E}_1^*(\tau_5) \mathscr{E}_1(\tau_1)$$

$$\times \left\langle V_e G^\dagger(\tau_3, \tau_5) \alpha_n G^\dagger(t, \tau_3) \alpha_n G(t, \tau_1) V_e^\dagger \right\rangle e^{i(\omega - \omega_3)(t - \tau_3) - i\Delta(\tau_3 - T)}$$

Broadband infrared and Raman probes of excited-state vibrational molecular dynamics; Simulation protocols based on loop diagrams.
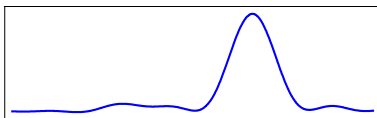
Attosecond Stimulated Raman Spectroscopy (ASRS)

- This technique is analogous to the FSRS femtosecond vibrational Raman protocol

LETTERS

Mapping GFP structure evolution during proton transfer with femtosecond Raman spectroscopy

Chong Fang[1], Renee R. Frontiera[1], Rosalie Tran[1] & Richard A. Mathies[1]
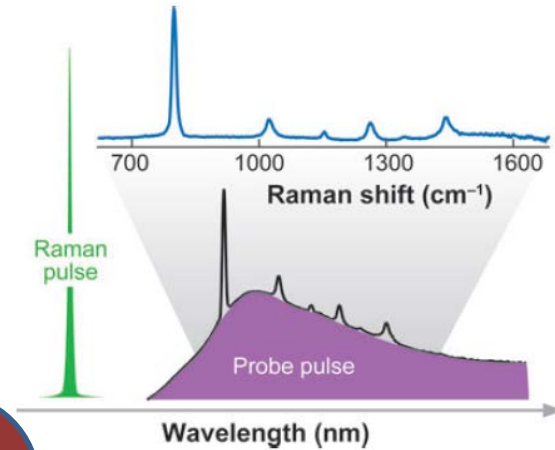
- In the typical application of FSRS, the first pulse initiates some dynamical process that modulates the vibrational frequencies.
- The Raman pump and probe then initiate a Raman process.
- The vibrational frequencies are found in the difference between the peak position and the narrowband Raman pump
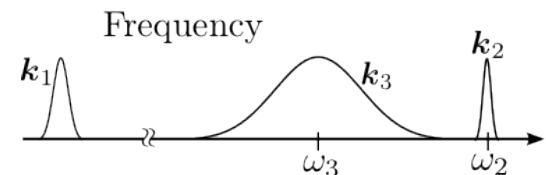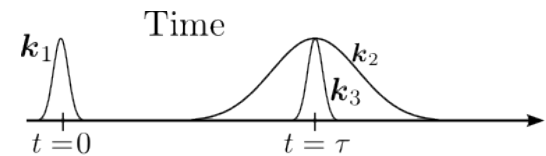
Strong-Field Ionization in Glycine Probed by Attosecond X-Ray Raman Spectroscopy

- **Impulsive ionization from nitrogen 1s orbital creates an electronic wavepacket**

- **The evolution of this wave-packet is then probed by Attosecond Stimulated Raman Spectroscopy (ASRS) at the carbon K-edge**
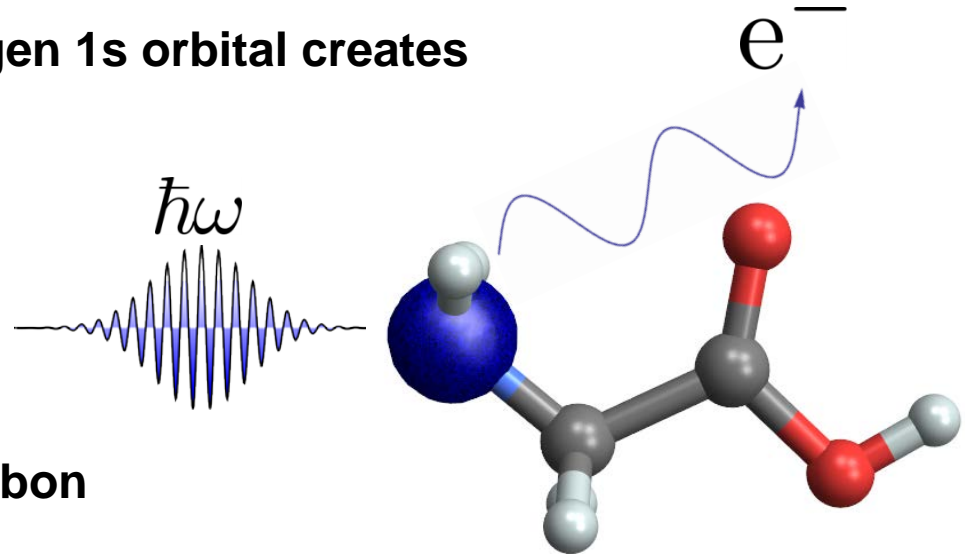
- **Pulse k_1 is resonant with the N1s to continuum transition, and short (<50 as)**
- **Pulse k_2 is long in duration (narrowband) and resonant**
- **Pulse k_3 is broadband and pre-resonant**
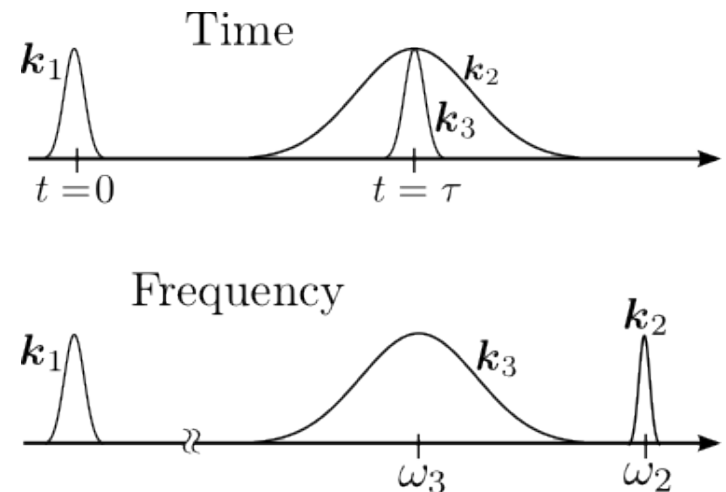
Sudden Ionization

- Assume a pulse shorter than the electron correlation time : a typical response time for spectator electrons to a sudden removal of an electron is ~ 50 as.

- After the core electron is ejected, the molecule will be in a nonstationary state, as the orbitals of the neutral molecule relax in the presence of the core-hole.

- The initial cationic state is described by removing one electron from a single molecular orbital while the other electrons remain in their original self-consistent molecular orbitals—frozen orbital approximation.

- This nonstationary state is expanded in the cation eigenstates,

$$|\Psi_{ns}\rangle = \sum_a C_a |a\rangle$$

$$C_a = \langle a | \Psi_{ns}\rangle$$

A large number of eigenstates are required to describe the ionized state. Several states near 20 eV give rise to collective valence motion.
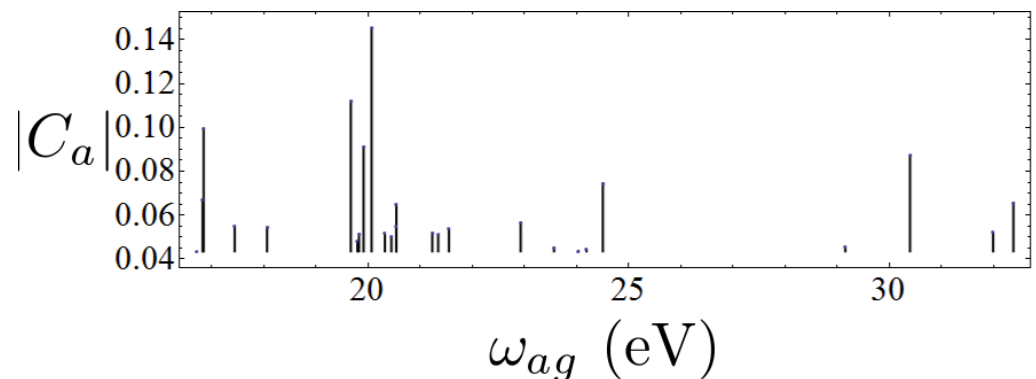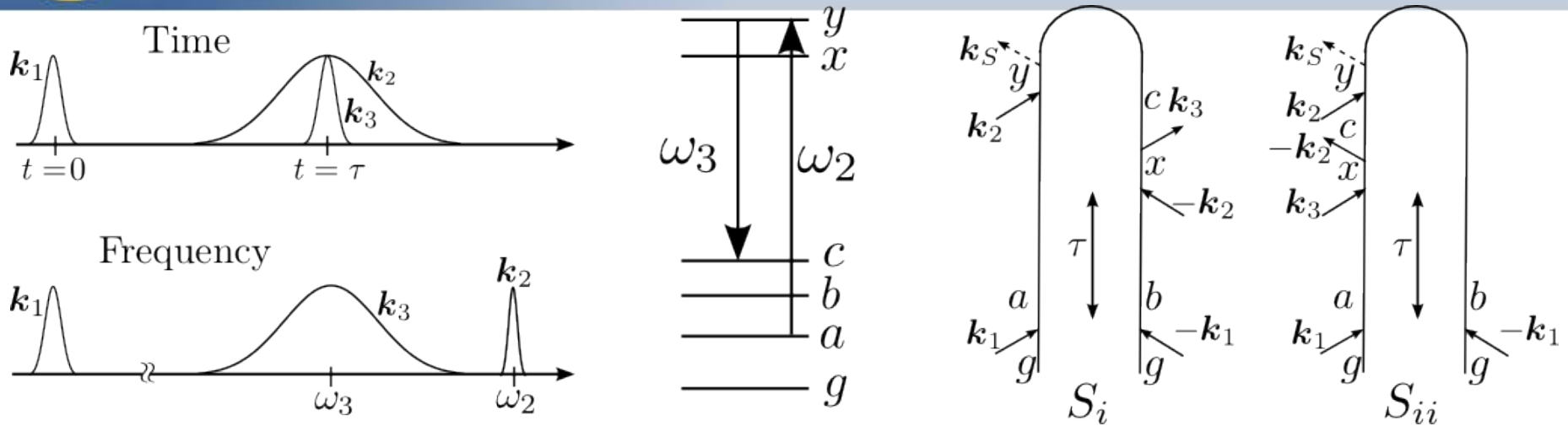
- ASRS uses two probe pulses, k_2 and k_3. k_2 is narrowband (tens of femtoseconds) and on resonance with a core transition, and k_3 is broadband (tens to hundreds of attoseconds), and redshifted from k_2. The signal is given by the frequency-dispersed transmission of the broadband pulse .
- Even though the time delay between the initiation pulse, in this case the ionizing pulse, and the broadband Raman probe is well defined, the resulting signal is not an instantaneous snapshot of the Raman spectrum.
- Rather, the signal is averaged over the lifetime of the final state – there is no free lunch in the tradeoff between temporal and spectral resolution.

Diagram 1 – Stokes Raman transitions

Carbon 1s core-excited states of the cation
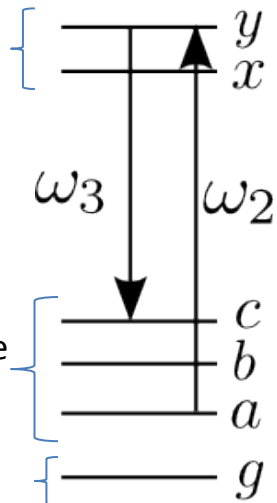
Valence excitations of the cation
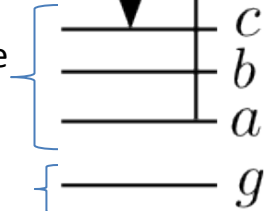
Cationic ground state
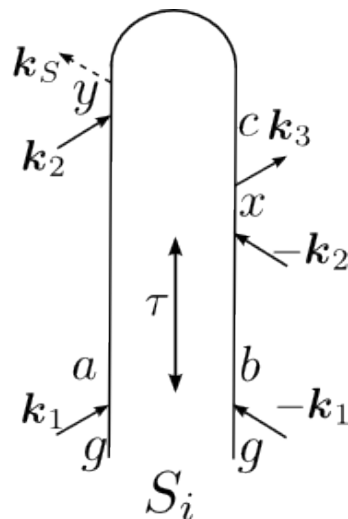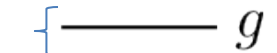
The first diagram corresponds to the conventional Raman process where k_2 excites the system to a core-excited state and k_3 stimulates emission into a valence-excited state. When the initial state is the ground state, the signal is equivalent to the frequency-domain Raman signal – i.e. no time resolution.

$$S(\tau, \omega; \omega_2) = S_i(\omega) + S_{ii}(\omega)$$

$$\rho_{ab}(t) = |\varepsilon_1|^2 C_b{}^* C_a e^{-i\omega_{ab}t - \gamma_{ab}t} \qquad \omega_{\alpha\beta} = \omega_\alpha - \omega_\beta, \; \gamma_{\alpha\beta} = \gamma_\alpha + \gamma_\beta$$

$$S_i(\omega - \omega_2, \tau, \omega_2) = -\Im \sum_{a \neq b, cxy} \frac{1}{\hbar^5} \frac{V_{bx} V_{xc}{}^* V_{cy} V_{ya}{}^* \varepsilon_s{}^*(\omega)\varepsilon_3(\omega - \omega_{ab})|\varepsilon_2|^2 \rho_{ab}(\tau)}{[\omega_2 - \omega_{xb} - i(\gamma_x - \gamma_b)][\omega_2 - \omega_{ya} + i(\gamma_y - \gamma_a)][\omega - (\omega_2 - \omega_{ca}) + i\gamma_{ac}]}$$

The narrowband frequency must be on resonance with a core transition.

Valence excitation frequencies are revealed in the spectrum via $\omega_2 - \omega = \omega_{ca}$

Diagram 2 – Anti-Stokes Raman and Absorption
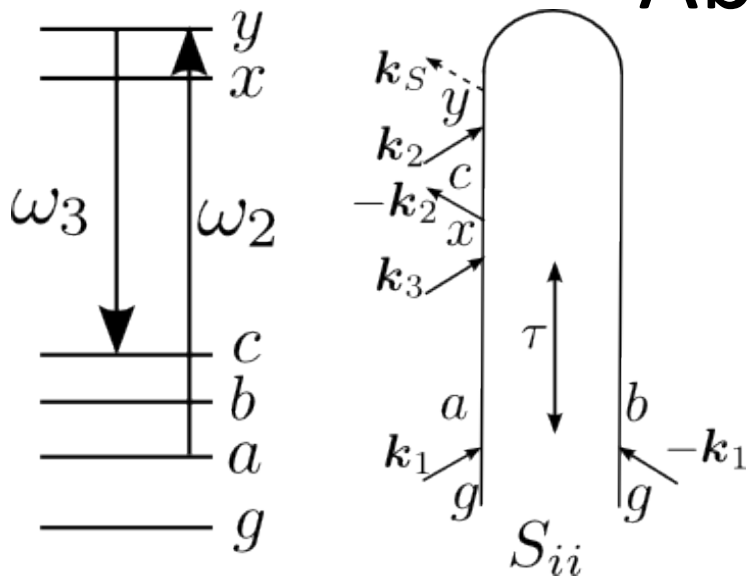
The second diagram is much more complicated and requires the absorption of the broadband pulse followed by emission into the narrowband frequency.

This contribution can be ignored when the molecule is initially in the ground state, but is the dominant contribution when the initial state is an excited state.

This is because the broadband probe, which is redshifted from the ground-state absorption, is resonant with absorption from excited states.

$$S(\tau, \omega; \omega_2) = S_i(\omega) + S_{ii}(\omega)$$

$$\rho_{ab}(t) = |\varepsilon_1|^2 C_b{}^* C_a e^{-i\omega_{ab}t - \gamma_{ab}t}$$

$$\omega_{\alpha\beta} = \omega_\alpha - \omega_\beta, \quad \gamma_{\alpha\beta} = \gamma_\alpha + \gamma_\beta$$

$$S_{ii}(\omega - \omega_2, \tau, \omega_2) = \Im \sum_{a \neq b, cxy} \frac{1}{\hbar^5} \frac{V_{bx} V_{xc}{}^* V_{cy} V_{ya}{}^* \varepsilon_s{}^*(\omega) \varepsilon_3(\omega - \omega_{ab}) |\varepsilon_2|^2 \rho_{ab}(\tau)}{[\omega - \omega_{xb} + i\gamma_{xb}][\omega - \omega_{yb} + i\gamma_{yb}][\omega - (\omega_2 + \omega_{cb}) + i\gamma_{cb}]}$$

Peaks corresponding to excited-state absorption will be seen when $\omega = \omega_{yb}$

Valence excitation frequencies are revealed in the spectrum via $\omega_2 - \omega = -\omega_{cb}$

ASRS signal – Zero Interpulse Delay

$$S_{ASRS}(\omega - \omega_2, \tau = 0, \omega_2 = 277 \text{ eV})$$
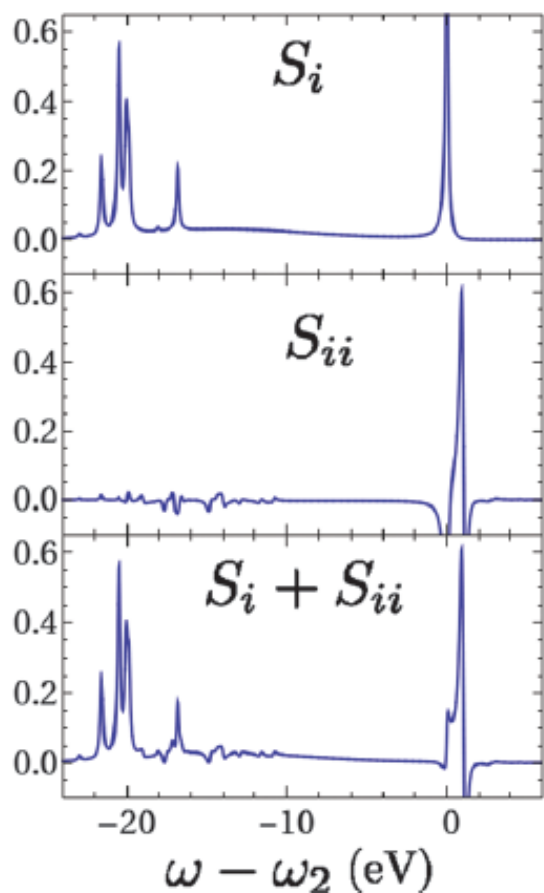
- ASRS signal with the narrowband frequency w2 = 277 eV, just at the blue edge of the carbon K-edge absorption spectrum of the ion.
- Diagram S_i shows a strong Raleigh peak at zero Raman shift, and a series of Raman peaks with shifts around 20 eV.
- Diagram S_{ii} shows a strong absorption peak, a Raleigh peak which cancels the peak from S_i, and several dispersive peaks in the Raman region.

Here we show the XANES from the suddenly ionized state, as well as the narrowband (red) and broadband (blue) pulse envelopes.
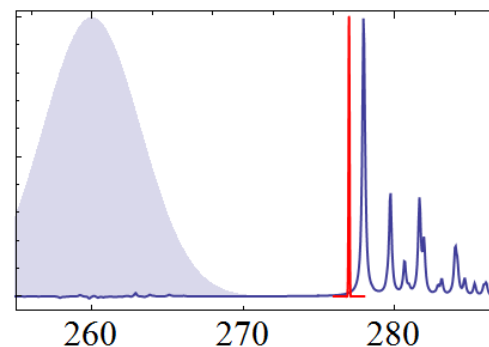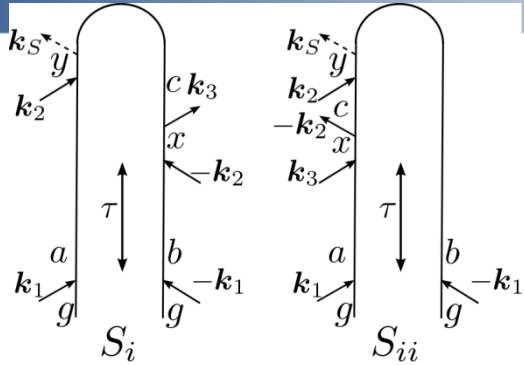
1. **Stokes Raman peaks from the ground-state population ρ_{gg} - diagram S_i**
2. **Absorption peaks from excited-state populations ρ_{gg} - diagram S_{ii}**
3. **Absorption peaks from ground-state population ρ_{gg} - diagrams S_i and S_{ii}**
4. **Absorption peaks from excited-state coherences ρ_{ag} - diagrams S_i and S_{ii}**
5. **Absorption and Raman peaks from excited-state coherences ρ_{ag}**
   i. **Stokes peaks from diagram S_i**
   ii. **Anti-Stokes peaks from diagram S_{ii}**
   iii. **Absorption peaks from diagram S_{ii}**
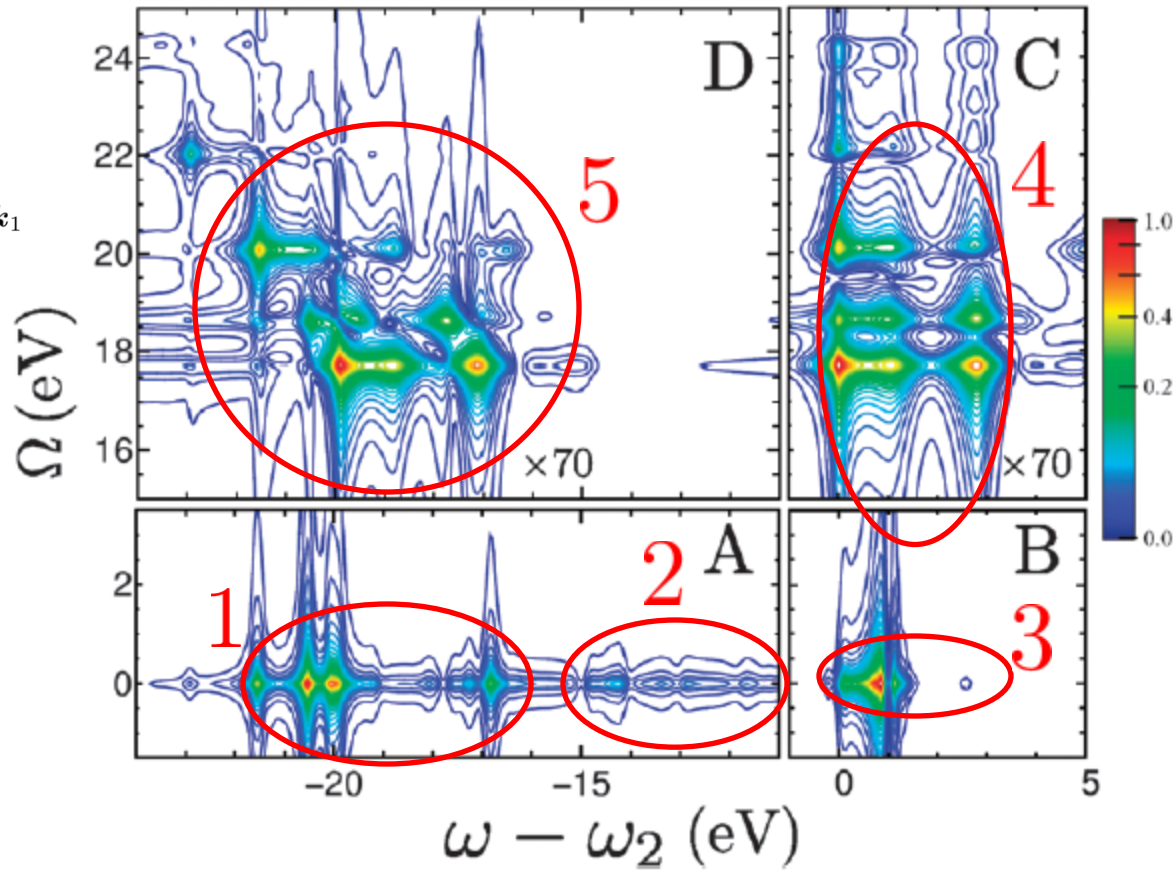
The time-varying contribution to the ASRS signal is obtained by removing the $\Omega=0$ term and back-transforming to the time domain. Oscillations in the amplitude of the carbon K-edge ASRS signal correspond to fluctuations in the electron density in the vicinity of the carbon atoms.
This is collective motion of the many eigenstates that comprise the wave packet

$\Omega = 0$ Removed

τ (fs)

$S_{ASRS}(\omega - \omega_2, \tau, \omega_2 = 277 \text{ eV})$

τ (as)   Density difference   ASRS signal

8.4

110.1

216.8

317.2

424.7

$\omega - \omega_2$ (eV)
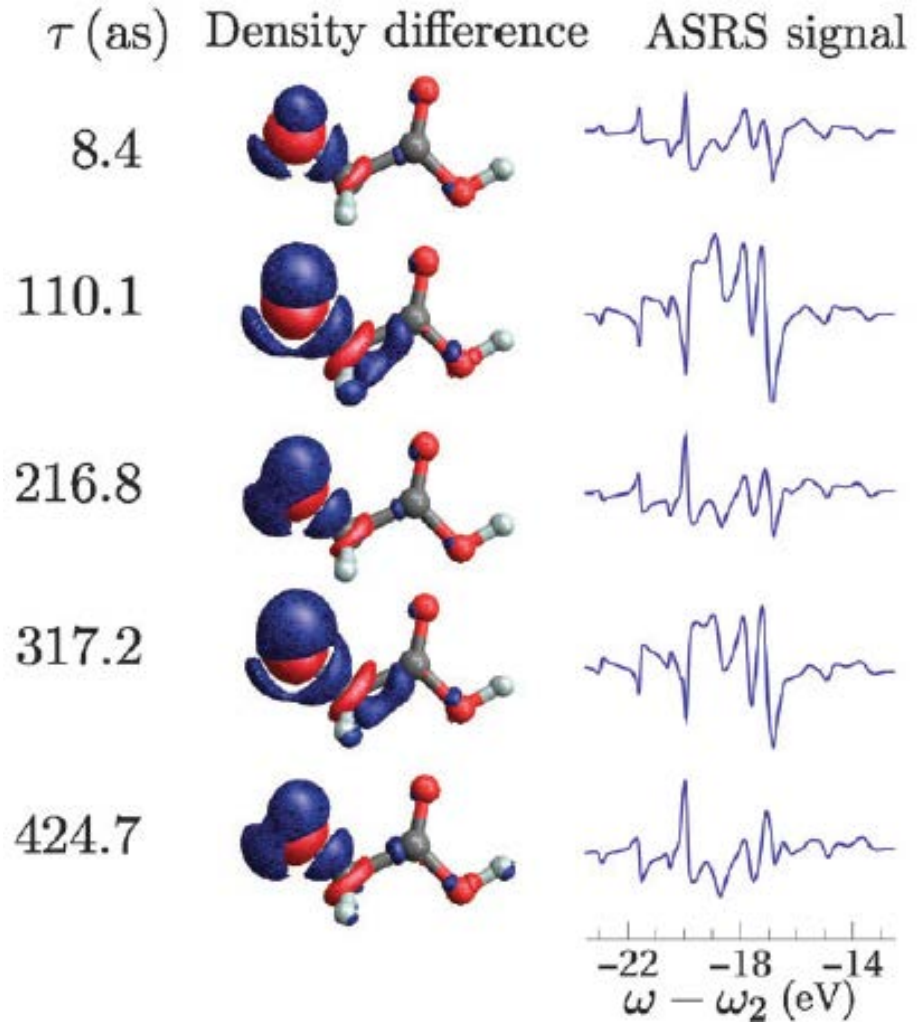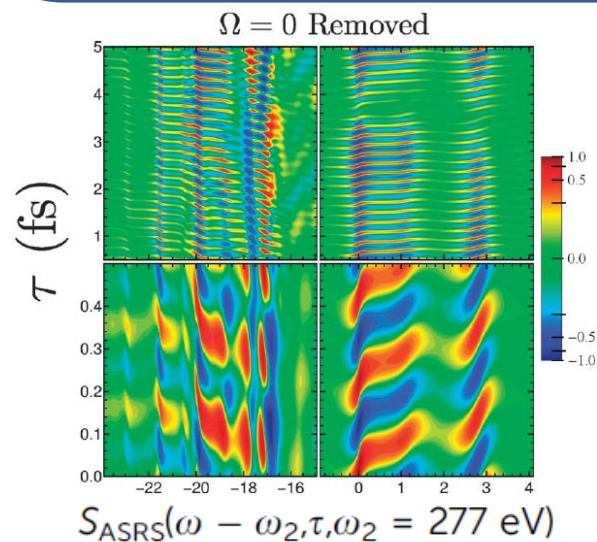
Animation – 5 fs following ionization

3D

$|S(\omega - \omega_2, \Omega, \omega_2)|$

2D ACRS Signal

S_i S_{ii} $S_i + S_{ii}$
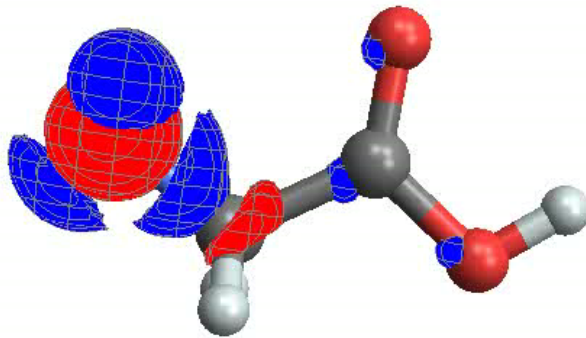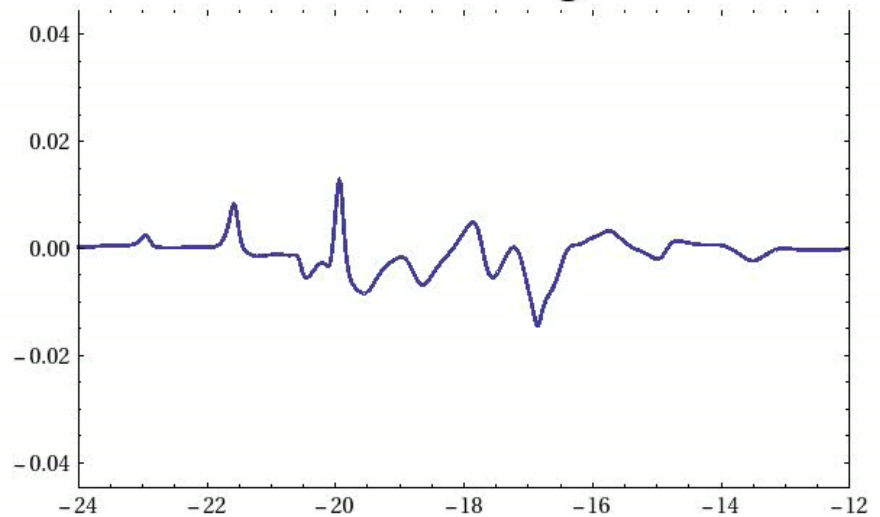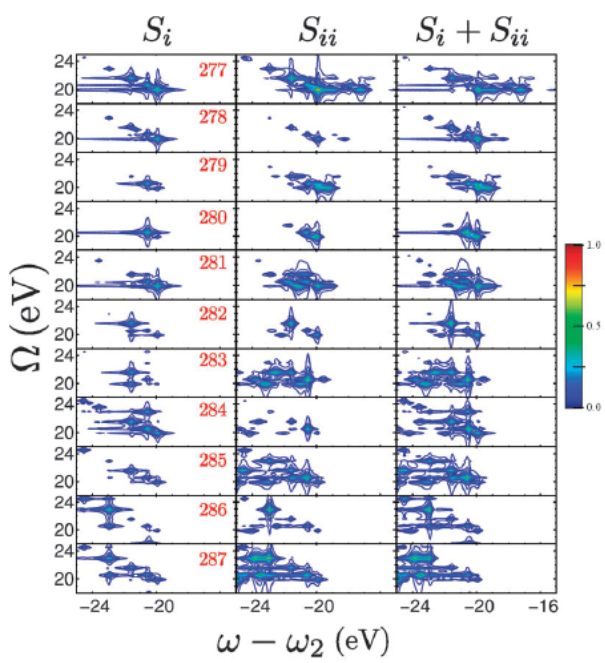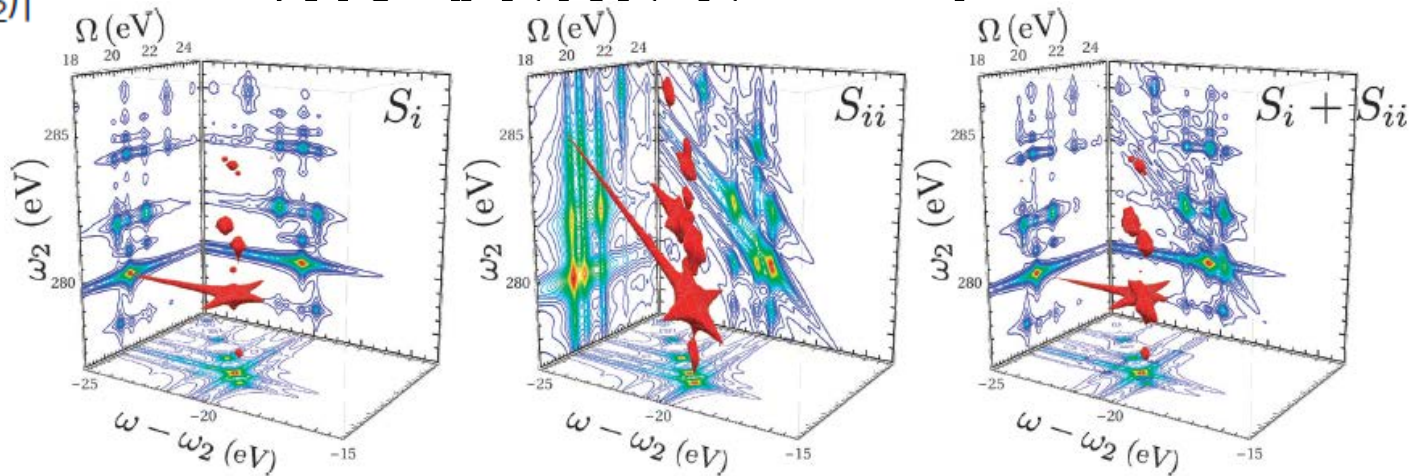
2D constant-ω_2
slices of $|S(\omega - \omega_2, \Omega, \omega_2)|$

➢ Vertical signal pattern for S_i : Raman contribution.
➢ Diagonal signal pattern for S_{ii} : absorption contribution.

Catching Conical Intersection in the Act

Monitoring Transient Electronic Coherences
By Attosecond Stimulated X-Ray Raman Spectroscopy

Markus Kowalewski, Kochise Bennett, Konstantin Dorfman,

Shaul Mukamel
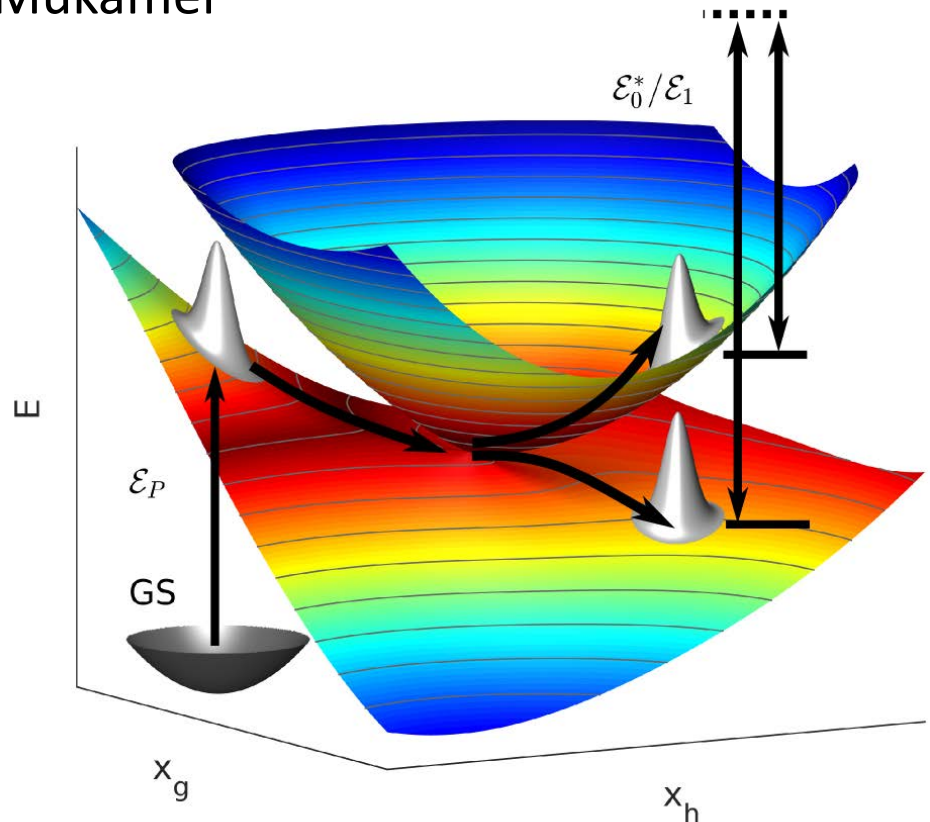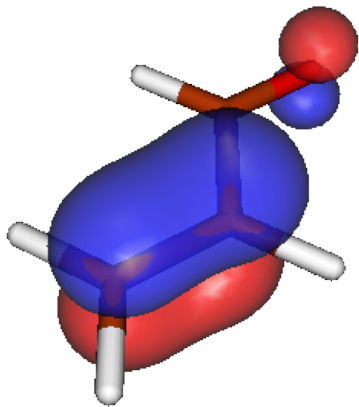
Conical Intersections (CoIns)

- Responsible for fast, radiation less decay

- Very common in polyatomic molecules

- Important in bio-molecules

- Protects DNA from UV-damage

- Not directly probed

- Inferred from fast rates
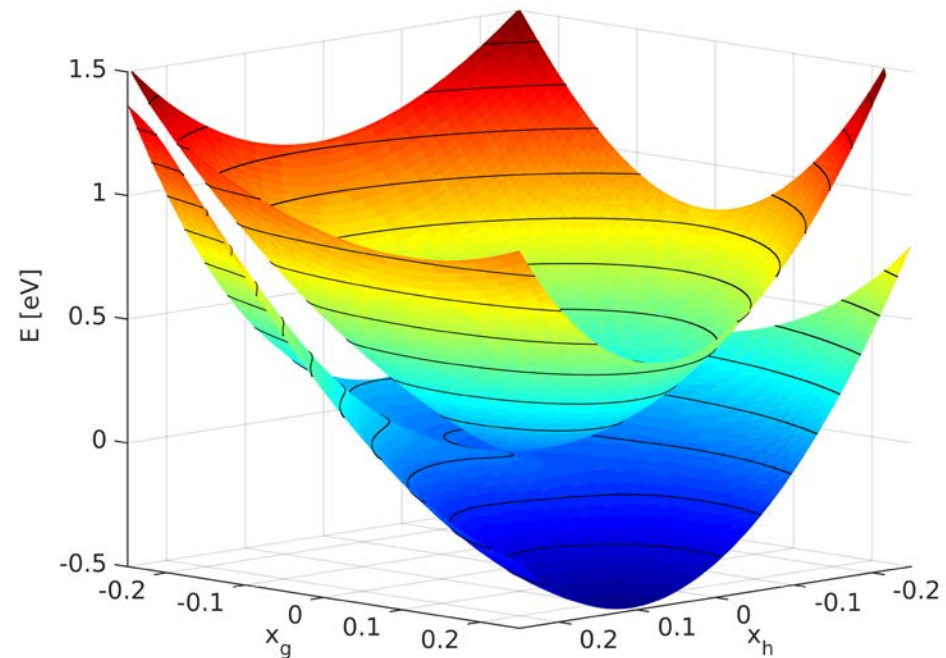
Conical Intersections

- Requires 3 atoms or more

- Point of degeneracy

- Branching space, 2 vib. DOF:

    gradient difference vector (g)

    non-adiabatic coupling vector (h)

- N-2 dim. seam space
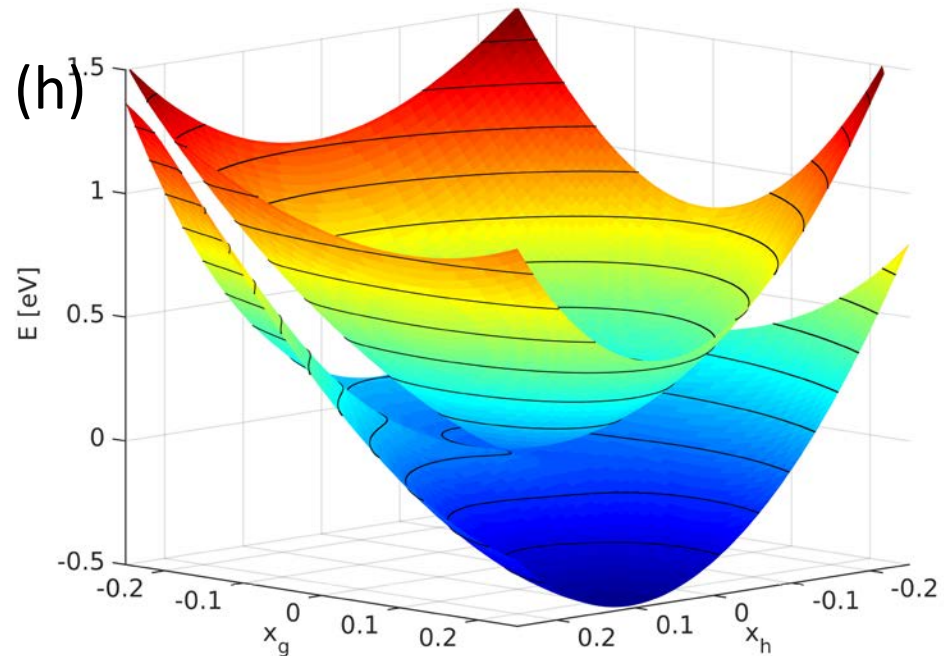
- Conventional Methods are based on Population dynamics

- Infrared/Optical pulses

- Change of vib. Frequencies

- Transient Absorption

- Challenge: rapidly decreasing energy gap

    → huge bandwidth needed

- Solution X-ray pulses (FEL, HHG sources)

Semi-classical Simulation Protocol
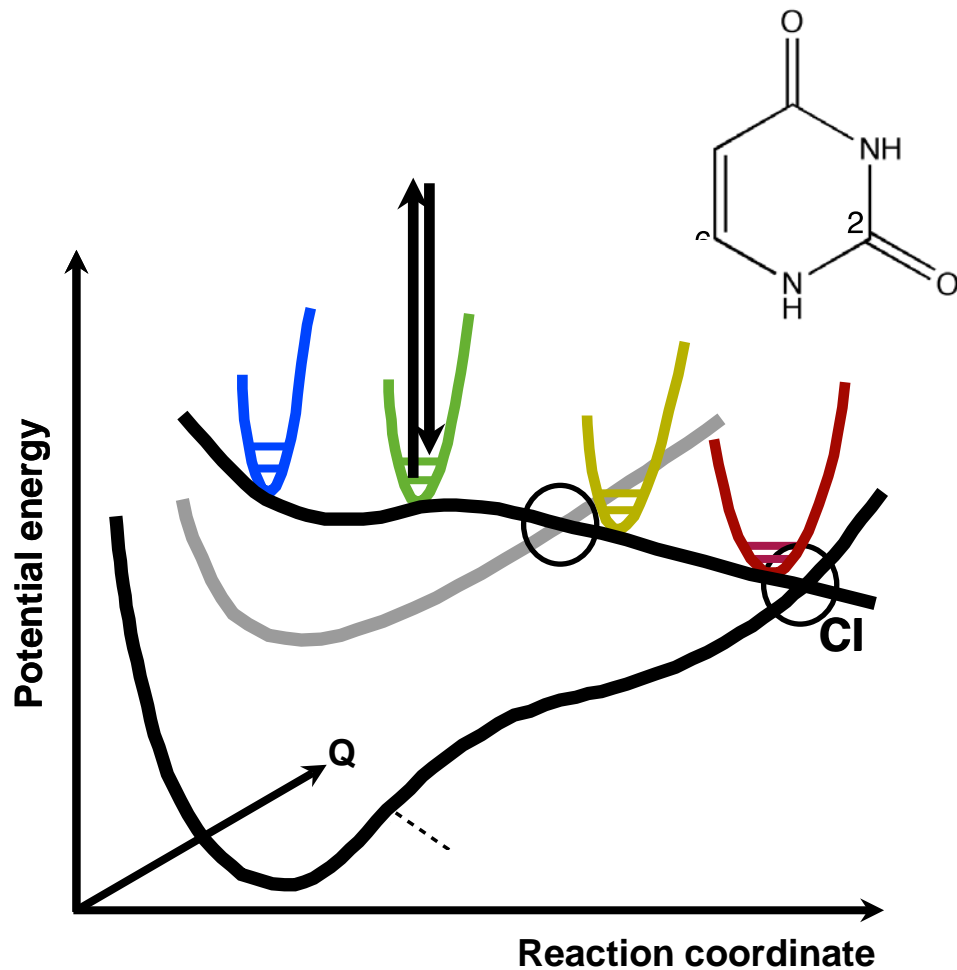
Spontaneous Raman Signal:
focus on high frequency C-H stretch
harmonic approximation (CAS(14/10))
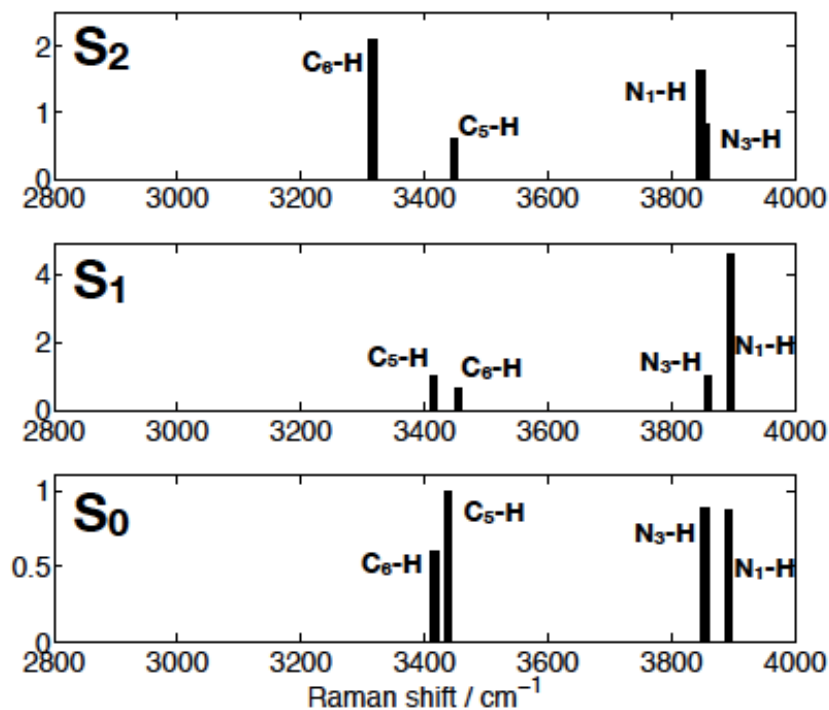
Monitoring Non-Adiabatic Dynamics of the RNA Base Uracil by UV-Pump-IR-Probe Spectroscopy.

Ensemble-Averaged FSRS Signal

C-H stretch modes
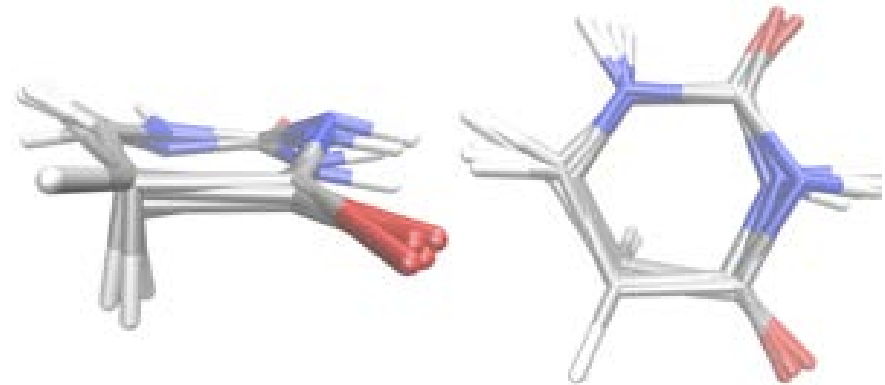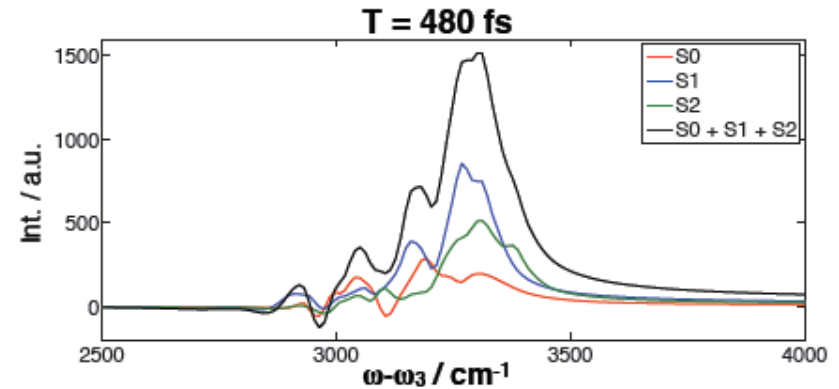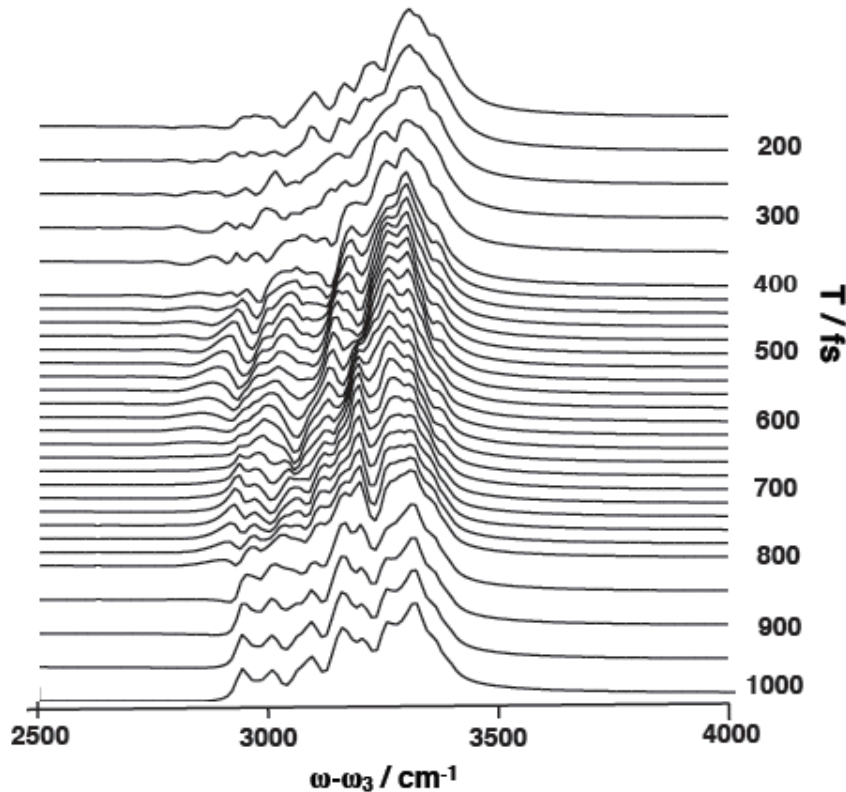
T = 350 - 700 fs: transient dispersive line-shapes

➡rehybridization at CoIn structures induces red-shift of C-H modes

➡instantaneous local probe of ring-planarity

Probing the Conical Intersection Dynamics of the RNA Base Uracil by UV-Pump Stimulated-Raman-Probe Signals;   Ab-Initio Simulations. B. P. Fingerhut, K. E. Dorfman, S. Mukamel, J. Chem. Theory Comput. **10**, 1172 (2014).

Classification of Raman Signals

1. Intensity dependence

$|a\rangle$

1.1 Linear (L)

$|a\rangle$
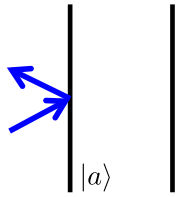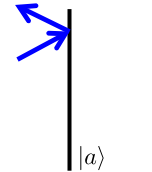
1.2 Quadratic (Q)

2. Pulse shaping

T

E_p
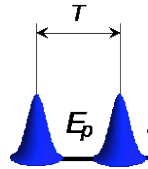
2.1 Broadband (e.g. LB or QB)

E_p E_2 E_3

$\square = 0$ $\square \neq 1$
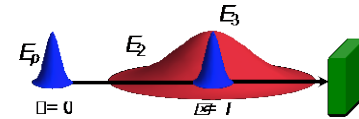
2.2 Hybrid (e.g. LH or QH)

3. Measurement setup

3.1 Frequency dispersed transmission of the probe

e.g. $S_{LB}^{(fd)}, \ S_{LH}^{(fd)}, \ S_{QB}^{(fd)}, \ S_{QH}^{(fd)}$

3.2 Integrated change in the number of photons of the probe

e.g. $S_{LB}^{(N)}, \ S_{LH}^{(N)}, \ S_{QB}^{(N)}, \ S_{QH}^{(N)}$

3.3 Energy change in the probe

e.g. $S_{LB}^{(E)}, \ S_{LH}^{(E)}, \ S_{QB}^{(E)}, \ S_{QH}^{(E)}$

Off-resonant signal; Linear probe
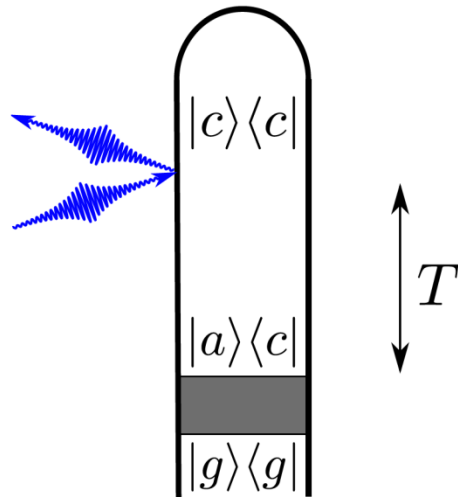
Off-resonant interaction

$$H'(t) = \alpha^{(0)}(t)|\mathcal{E}(t)|^2$$

$\alpha^{(0)}$ Off-resonant polarizability

$|c\rangle\langle c|$

T

$|a\rangle\langle c|$

$|g\rangle\langle g|$

Frequency dispersed transmission of the probe

$$S_L^{(fd)}(\omega, t_0, \tau_0) = \mathcal{I}2i \int_{-\infty}^{\infty} dt e^{i\omega(t-t_0)} \mathcal{E}^*(\omega)\mathcal{E}(t-t_0)\langle\langle I|\alpha_L^{(0)}\mathcal{G}(t-\tau_0)|\rho_i\rangle\rangle$$

Integrated change in the number of photons of the probe

$$S^{(N)}(t_0, \tau_0) = \int_{-\infty}^{\infty} \frac{d\omega}{2\pi} S^{(fd)}(\omega, t_0, \tau_0)$$

Energy change in the probe

$$S^{(E)}(t_0, \tau_0) = \int_{-\infty}^{\infty} \frac{d\omega}{2\pi} \hbar\omega S^{(fd)}(\omega, t_0, \tau_0)$$

Linear broadband (LB) probe

Contributions to the Stokes () and anti-Stokes () sides of the spectrum oscillate with opposite phase.
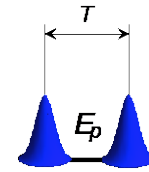
- Field envelopes contain information about Raman frequency shift

- Stokes and anti-Stokes contributions oscillate as a function of T with the π phase shift

Oscillating phase

$$\phi_{ac}(T) = \omega_{ac}T - \phi_{ac}^{\rho}, \ \rho_{ac} = |\rho_{ac}|e^{i\phi_{ac}^{\rho}}$$

Frequency dispersed transmission of the probe

$$S_{LB}^{(fd)}(\omega, T) = -\frac{2}{\hbar}\sum_{a,c}|\mathcal{E}(\omega)||\mathcal{E}(\omega - \omega_{ac})|\alpha_{ca}^{(0)}|\rho_{ac}|\sin\phi_{ac}(T),$$

Integrated change in the number of photons of the probe

$$S_{LB}^{(N)}(T) = 0,$$

Energy change in the probe

$$S_{LB}^{(E)}(T) = -\frac{2}{\hbar}\sum_{a,c}\int_{-\infty}^{\infty}\frac{d\omega}{2\pi}|\mathcal{E}(\omega)||\mathcal{E}(\omega - \omega_{ac})|\alpha_{ca}^{(0)}|\rho_{ac}|\hbar\omega_{ac}\sin\phi_{ac}(T).$$

Linear hybrid (LH) probe
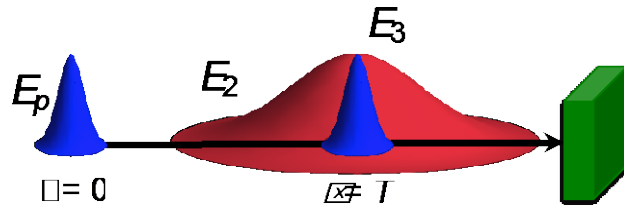
- Raman shift enters explicitly into the signal
- Lorentzian lineshape
- Stokes and anti-Stokes contributions oscillate as a function of T with a π phase shift

Oscillating phase

$$\phi_{ac}^1(T) = (\omega - \omega_1)T - \phi_{ac}^\rho + \phi_\omega - \phi_1 \qquad \tilde{\phi}_{ac}^1(T) = \omega_{ac}T - \phi_{ac}^\rho + \phi_1 - \phi_\omega$$

Frequency dispersed transmission of the probe

$$S_{LH}^{(fd)}(\omega - \omega_1, \omega_1, T) = \frac{2}{\hbar}|\mathcal{E}_0(\omega)||\mathcal{E}_1| \sum_{a,c} \alpha_{ca}^{(0)}|\rho_{ac}|$$

$$\times \left[\frac{\cos \phi_{ac}^1(T)}{\omega - \omega_1 - \omega_{ac}} - 2\pi\delta(\omega - \omega_1 - \omega_{ac})\sin \phi_{ac}^1(T) \right]$$

Integrated change in the number of photons of the probe

$$S_{LH}^{(N)}(\omega_1, T) = 0$$

Energy change in the probe

$$S_{LH}^{(E)}(\omega_1, T) = -\frac{2}{\hbar} \sum_{a,c} |\mathcal{E}_1||\mathcal{E}_0(\omega_1 - \omega_{ac})|\alpha_{ca}^{(0)}|\rho_{ac}|\hbar\omega_{ac}\sin \tilde{\phi}_{ac}^1(T)$$

$S_{LB}^{(fd)}(\omega, T)$

- Broad Spectral peaks, centered at Raman shift, with width of broadband pulse. Peaks oscillate in time between red and blue sides of spectrum.

$S_{LB}^{(E)}(T)$

- Intensity oscillations at Raman frequencies.

$S_{LH}^{(fd)}(\omega - \omega_0, T)$

- Sharp peaks at each transition. The peaks oscillate at their respective frequencies and with phase imparted by the preparation process.

$S_{LH}^{(E)}(\omega_1, T)$

- Broad peaks, centered at $\omega = \omega_0$ where sign reveals Stokes vs. anti-Stokes process.

Energy flow between spectral components in 2D Raman Spectroscopy

Linear (Transient absorption) signal
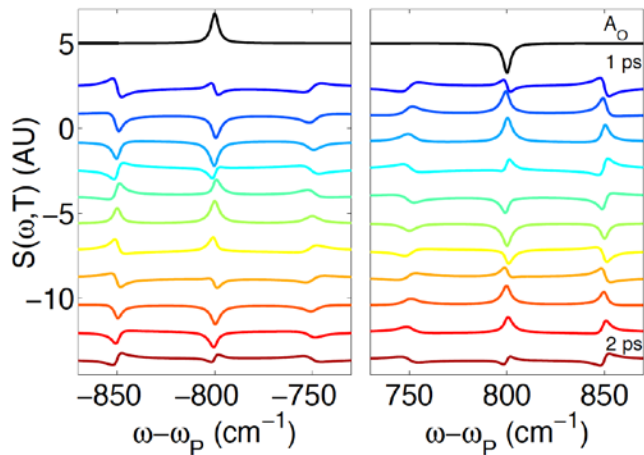
Total energy balance
(oscillations of Stokes – red and anti-Stokes- blue)

$$N_{red}(T) \propto e^{-\gamma_l T} \sin(\omega_l T)$$
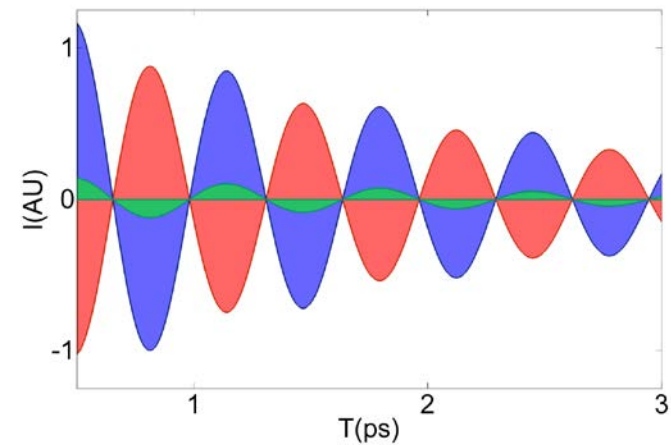
$$N_{blue}(T) \propto -e^{-\gamma_l T} \sin(\omega_l T)$$

Phase information and
energy flow between different
spectral components has
been studied in FSRS signal

G. Batignani, G. Fumero, S. Mukamel, and T. Scopigno, under review

TRUECARS detection scheme

Transient Redistribution of Ultrafast Electronic

Coherences in Attosecond Raman Signals

- → attoseconds, several eV bandwidth

- → sensitive to coherences, background free
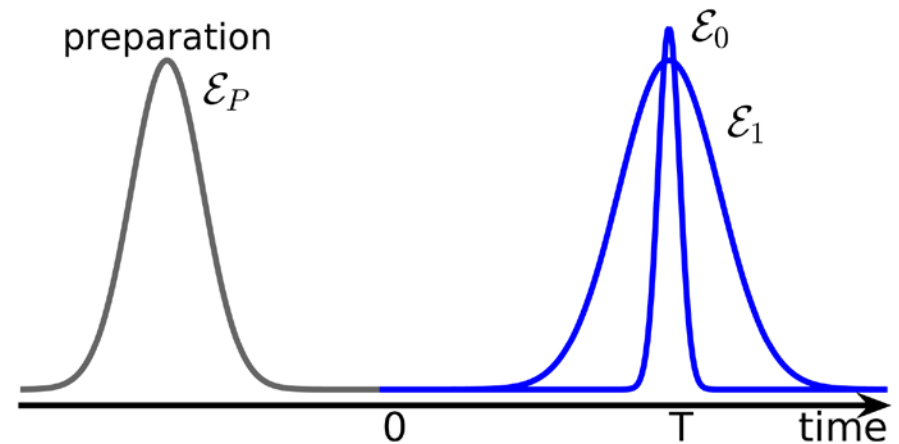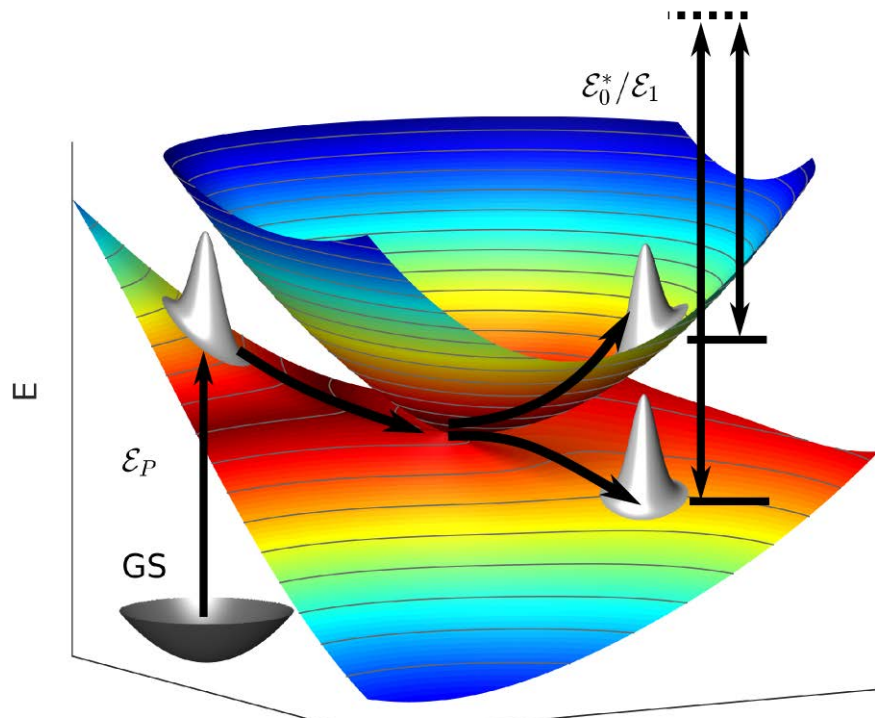
TRUECARS

- A preparation process (gray box) leaves the system in a nonstationary state

- A hybrid pulse with broadband ($\mathcal{E}_0$) and narrowband ($\mathcal{E}_1$) components probes the dynamics

- The frequency-dispersed transmission of the broadband component is plotted versus the delay time $T \equiv t_0 - \tau_0$
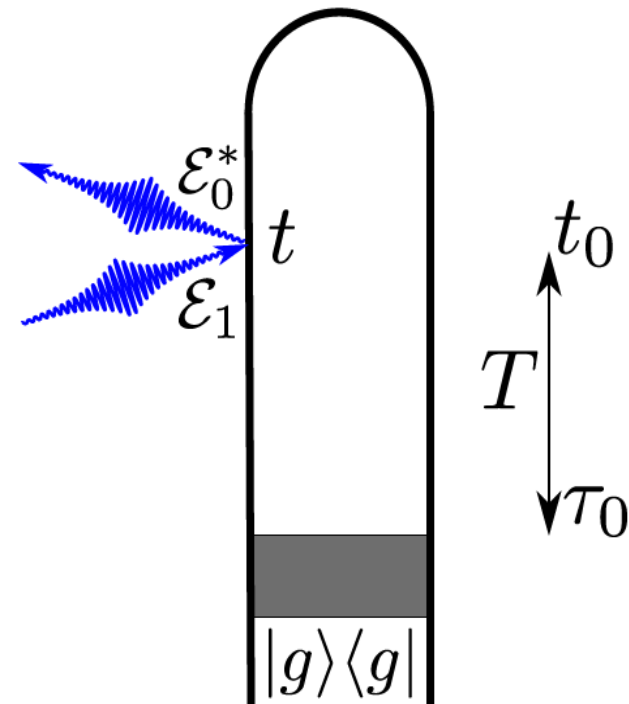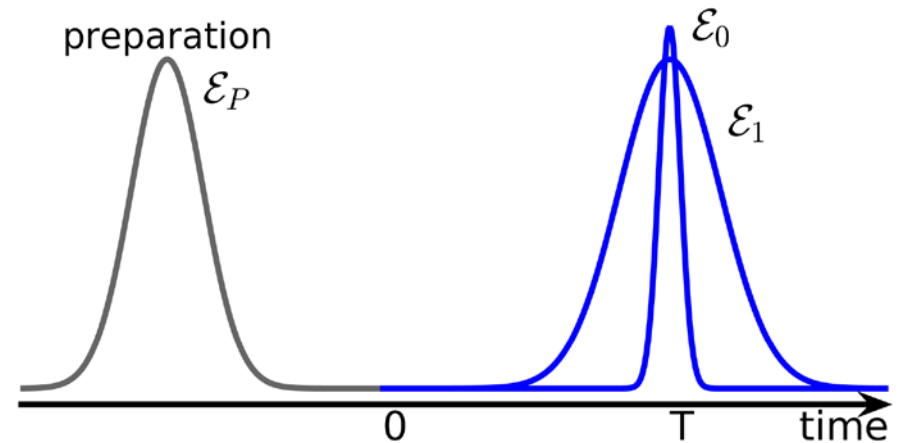
TRUECARS vs SXRS

- TRUECARS is linear (left) and provides background-free measurement of electronic coherence. TCRR depends on relative phase and requires phase-control to observe.
- SRS is quadratic (right) and contains contributions due to populations. The field phases come in pairs and cancel.
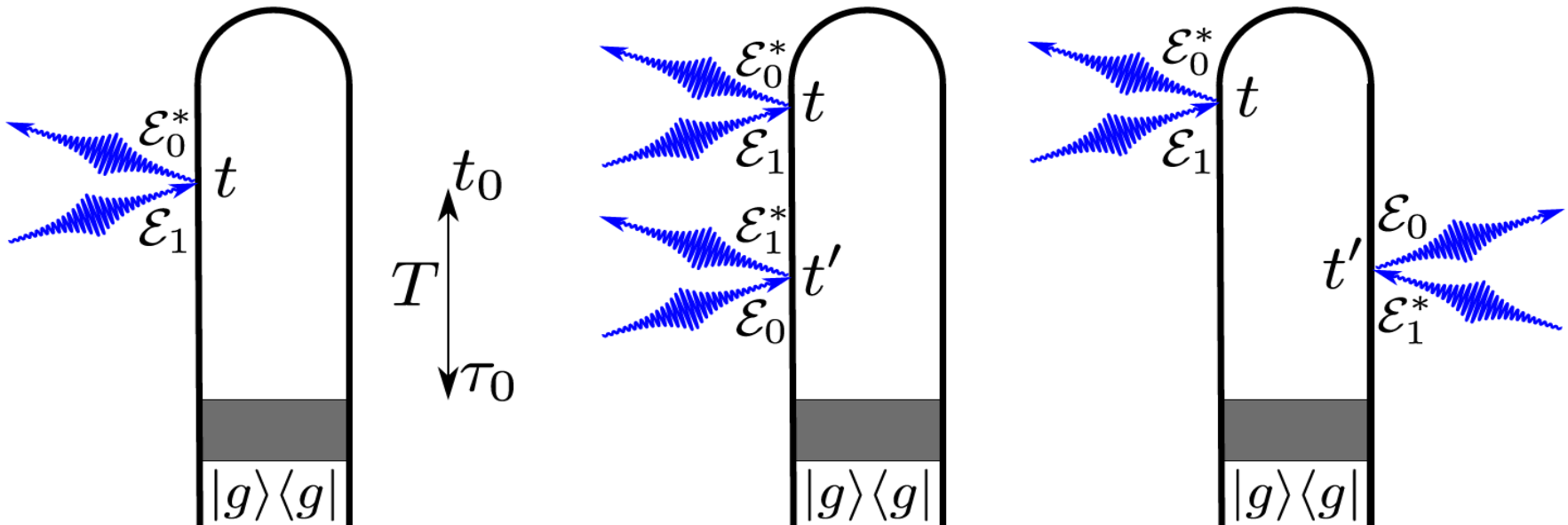
TRUECARS – Similar to CARS

- CARS (right): Electronic coherence generated with a pair of pulses and probed with a second pair after a fixed delay.
- TRUECARS (left): Nonstationary state is prepared and electronic coherence is generated internally through the propagation
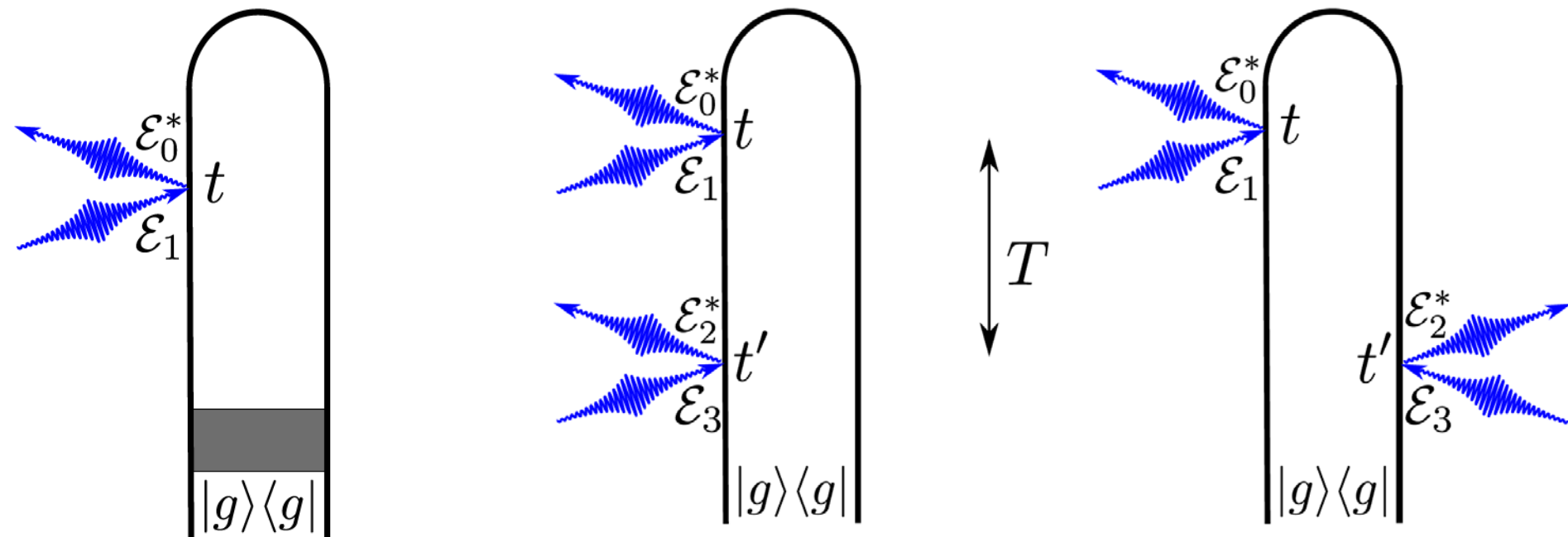
TRUECARS

- Initial state preparation followed by delay and probe with hybrid broadband (as) narrowband (fs) pulse

- Coherences created by laser pulse or system coupling (CoIn)

- Frequency-dispersed photon number change of broadband pulse is detected

- Signal is off-resonant and Linear in probe

- Energy splitting appears as Raman shift between observed and central pulse frequencies

Matter-probe interaction:

$$\hat{H}_{\mathrm{mp}}(t) = \hat{\alpha}|\mathcal{E}_0(t) + \mathcal{E}_1(t)|^2$$

Frequency dispersed photon number change:
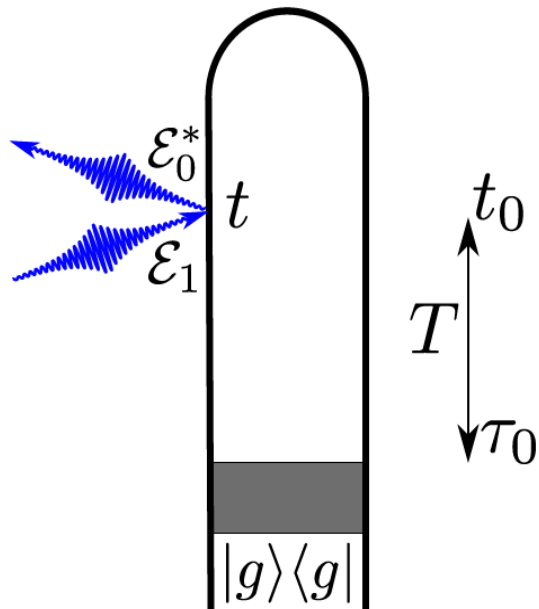
$$S(\omega, T) = 2\Im \int_{-\infty}^{+\infty} \mathrm{d}t\, e^{i\omega(t-T)} \mathcal{E}_0^*(\omega)\mathcal{E}_1(t-T)$$

$$\times \langle \psi(t)|\hat{\alpha}|\psi(t)\rangle$$

$\mathcal{E}_0^*$

$\mathcal{E}_1$

t

t_0

T

τ_0

$|g\rangle\langle g|$

TRUECARS – Spectroscopic information

- Frequency-dispersion of broadband pulse compromises time resolution granted by broadband pulse in the SRS (quadratic) case

- Instead, both temporal and spectral resolution are set by the narrowband pulse and are not independent

- Each transition gives two Raman peaks, positive and negative, that oscillate with a relative π phase

- Signal oscillates in time between Stokes and anti-Stokes

- UV or x-ray probes possible

- → **Clock the CoIn, map the reaction path**

Simple Model System

Model resembles wave packet passing through CoIn/avoided crossing:
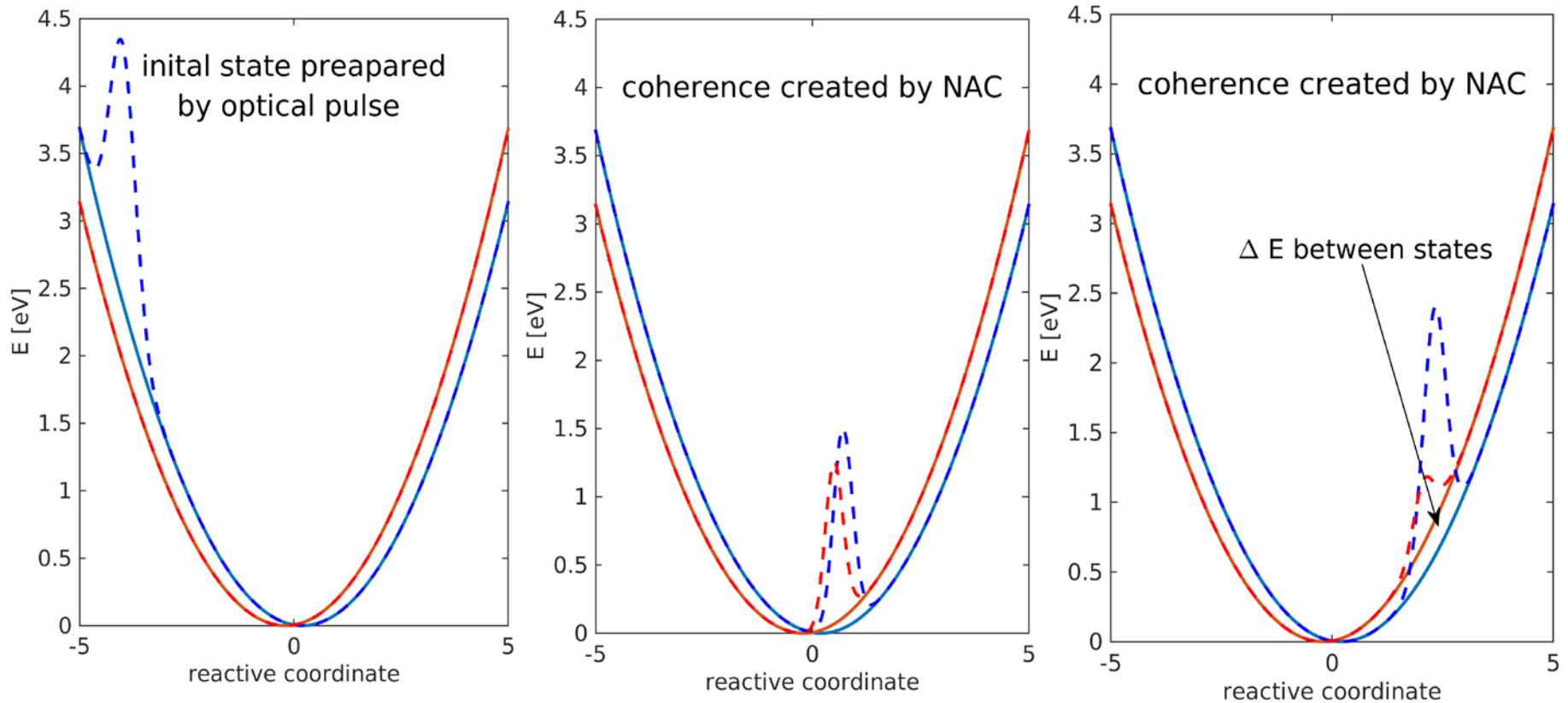
TRUECARS Signal

Spectrum resembles the time-dependent splitting
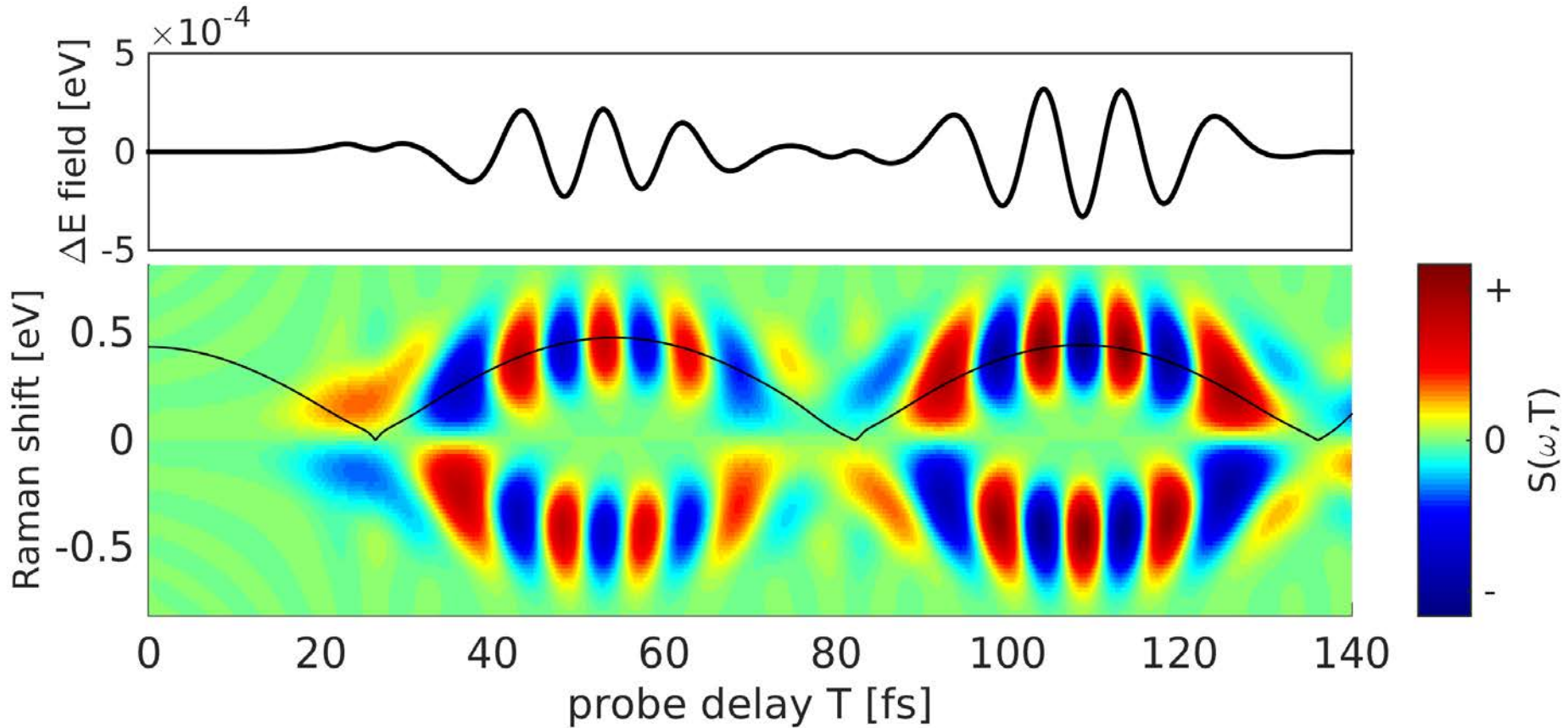
Model System – Conical Intersection

- Two vib. Modes in branching space

- Typical CoIn parameters

- Acrolein S2/S1 CoIn

- Quantum Dynamics

- → Vib .Wave packet

- simulations

$$H = -\mathbb{1}\frac{1}{2m}\sum_{i\in\{h,g\}}\frac{\mathrm{d}^2}{\mathrm{d}x_i^2} + \begin{pmatrix} H_1(x) & H_{12}(x) \\ H_{12}(x) & H_2(x) \end{pmatrix}$$
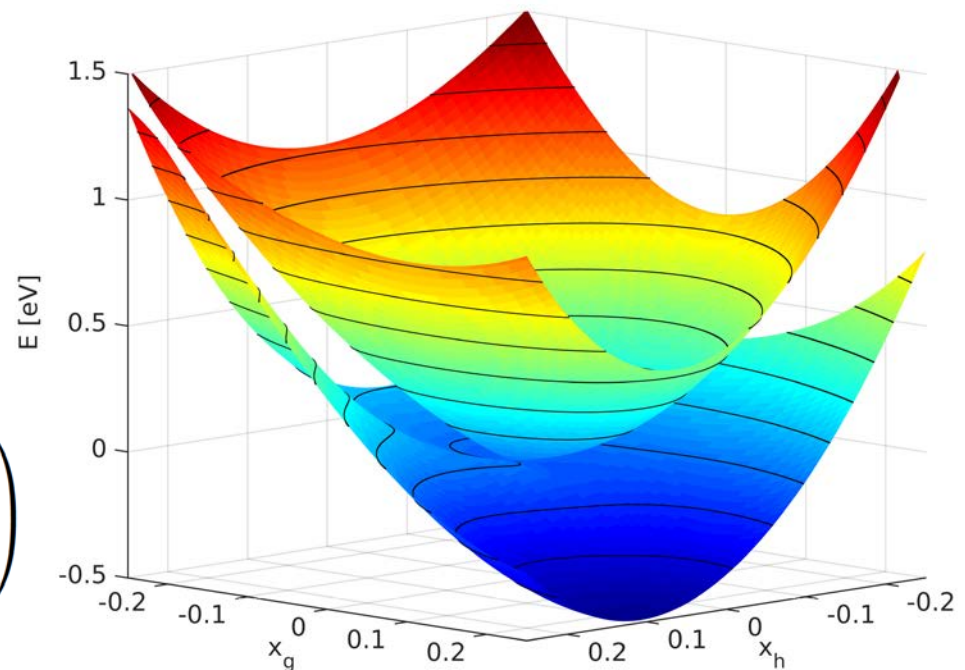
TRUECARS Signal for CoIn Model

- Signal turns on when WP reaches CoIn

- Different gradients

  in S2/S1

- → coherences decay
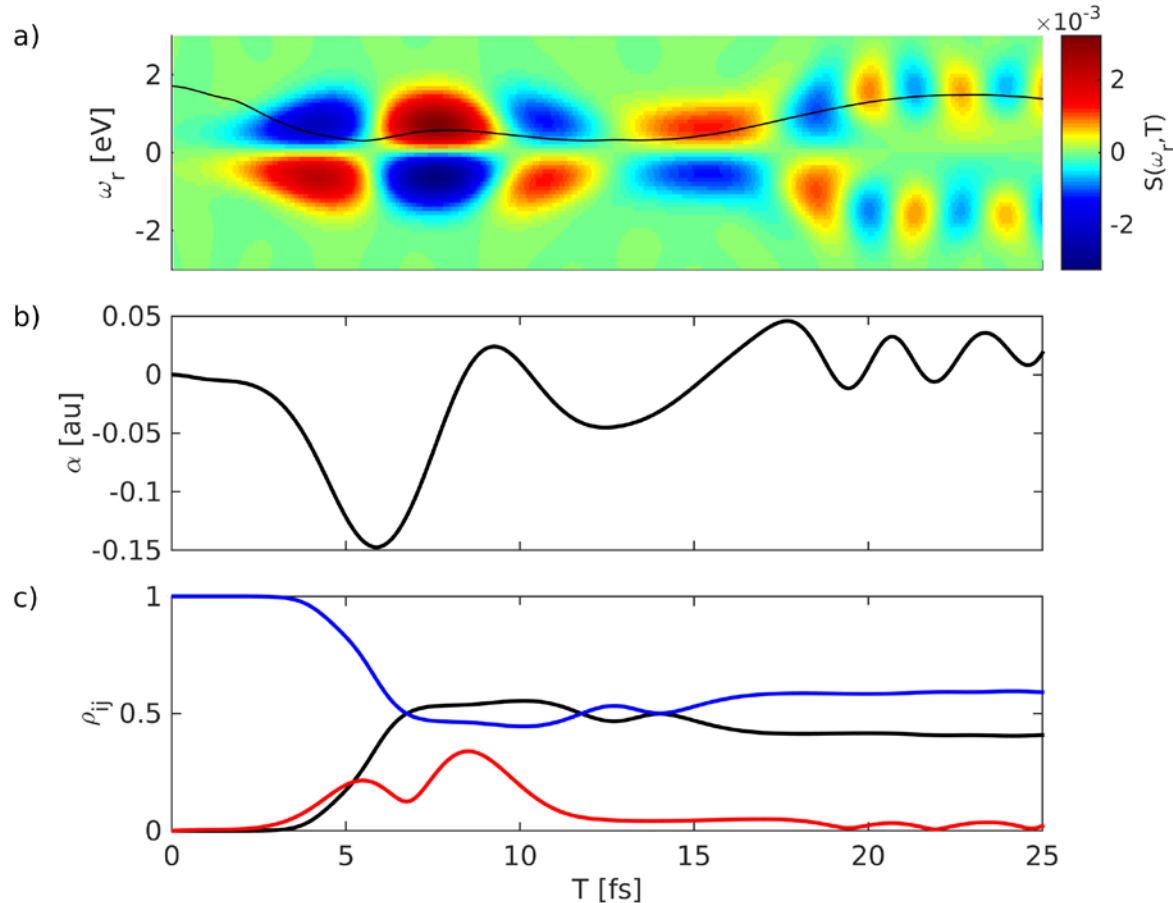
Conclusions

- TRUECARS signal provides background-free measurement of coherences

- Off-resonant technique

- Like CARS but the detected coherence is internally generated by propagation through the CoIn

- Energy splitting of PES directly visible in signal

- Maps reaction path of the molecule

- Determine topology/shape of a CoIn

- UV or X-ray probe pulses

Time, Frequency, and Wave-Vector Resolved Single- and Multi-Dimensional X-Ray Diffraction From Single Molecules

.

The Sample

- Consider a sample composed of N identical particles (atoms, molecules, etc.).

- The spatial electronic density of the total system is then:

$$\hat{\sigma}_T(\mathbf{r}) = \sum_\alpha \delta(\mathbf{r} - \mathbf{r}_\alpha) * \hat{\sigma}(\mathbf{r})$$

- Where α indexes the particles and $\hat{\sigma}(\mathbf{r})$ is the electron density of a single particle.

The Interaction

- We consider an experiment in which the sample is subjected to a broad-band x-ray pulse with which it interacts non-resonantly via the Hamiltonian

$$\hat{H}'(t) = \int d\mathbf{r}\, \hat{\mathbf{A}}^2(\mathbf{r}, t)\hat{\sigma}_T(\mathbf{r}, t)$$

- This describes instantaneous scattering in which the electrons do not have time to respond during the scattering process.

UNIVERSITY *of* CALIFORNIA · IRVINE

- When the system is prepared by a stimulated Raman process, the relevant correlation function for the signal is

$$S(\mathbf{k}_1, T) \propto \langle \hat{\sigma}^\dagger(T, \mathbf{q}_1)\hat{\sigma}(T, \mathbf{q}_1)\hat{\alpha}(0) \rangle$$

$$- \langle \hat{\alpha}^\dagger(0)\hat{\sigma}^\dagger(T, \mathbf{q}_1)\hat{\sigma}(T, \mathbf{q}_1) \rangle$$

$$\alpha = \sum_{c,e} |e\rangle \frac{(\boldsymbol{\epsilon}_R \cdot \boldsymbol{\mu}_{ec})(\boldsymbol{\epsilon}_R \cdot \boldsymbol{\mu}_{cg})}{2\pi} \int_{-\infty}^{\infty} d\omega \frac{\hat{\mathcal{A}}_R^*(\omega)\,\hat{\mathcal{A}}_R(\omega + \omega_{eg})}{\omega - \omega_{ce} + i\Gamma_c} \langle g|$$

- When there is no preparation (the system begins in the ground state) the relevant correlation function for the 2D signal is

$$S(\mathbf{k}_1, T_1, \mathbf{k}_2, T_2) \propto$$

$$\langle \hat{\sigma}^\dagger(T_1, \mathbf{q}_1) \hat{\sigma}^\dagger(T_2 + T_1, \mathbf{q}_2) \hat{\sigma}(T_2 + T_1, \mathbf{q}_2) \hat{\sigma}(T_1, \mathbf{q}_1) \rangle$$

- This signal therefore measures the two-point correlation function of the charge-density.

Time-dependent X-ray diffraction on electronic excited states
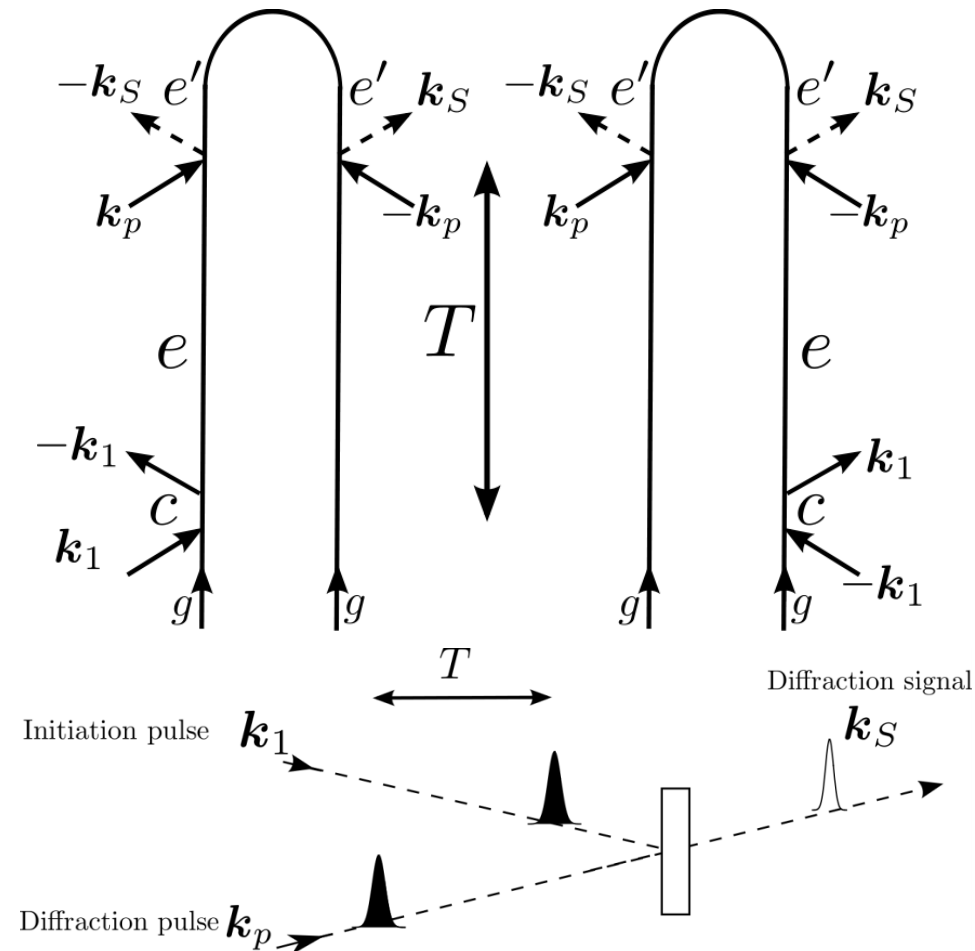
Broadband attosecond X-ray pulses can be used to visualize electronic motion in molecules on very short timescales. In this experiment, dynamics is initiated by an ultrafast pulse at time zero, followed by the diffraction pulse at time T. The signal is the time and frequency gated diffraction pattern. In this example, the initiation pulse is an X-ray Raman process, wherein a core electron is promoted to the valence band before the transient core hole is filled by another valence electron. The resulting molecular state is a coherent superposition of valence excitations.

X-ray diffraction is typically treated classically. By using a QED treatment of the diffraction pulse, inelastic scattering terms, wherein the molecule's state is changed, emerge.

Single-molecule X-ray scattering from cysteine (no preparation)

cysteine: amino acid containing sulfur
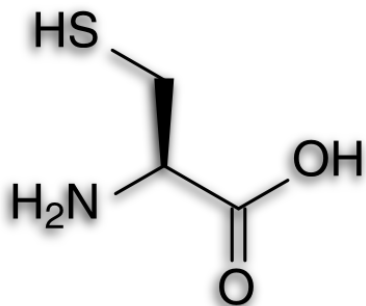
When the detection wavelength (red line) is within the pulse power spectrum (blue shaded region), the signal is dominated by elastic scattering

$$|\mathcal{A}_p(\omega)|^2$$
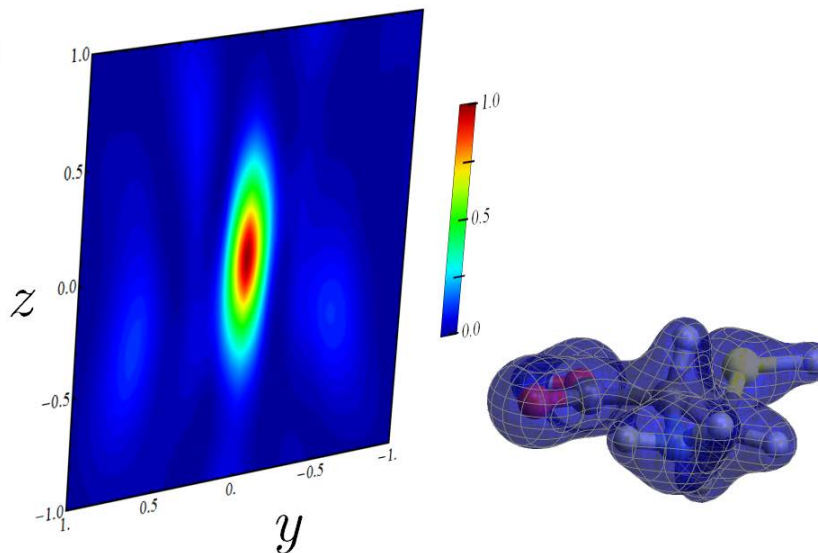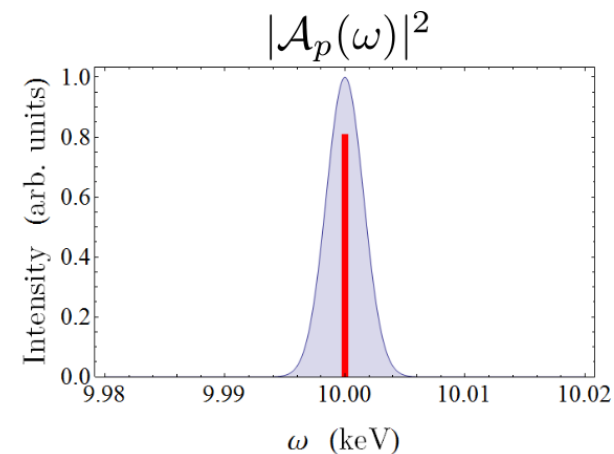
300 attosecond pulse centered at 10 keV.

Oriented molecule

Scattered light is wavevector and frequency resolved.

Ground-state charge density

x

Single-molecule X-ray scattering from cysteine (no preparation) – part 2
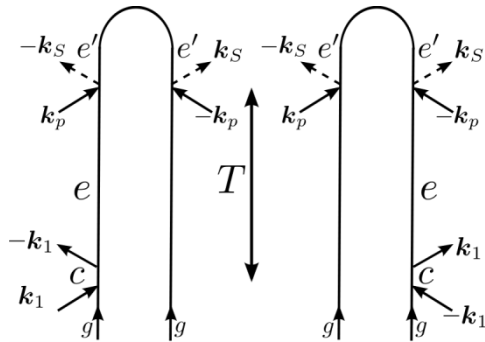
By detecting scattered photons with frequency red-shifted from the pulse power spectrum, we eliminate the elastic and keep only the inelastic Raman-type terms

$$|\mathcal{A}_p(\omega)|^2$$

ω_s
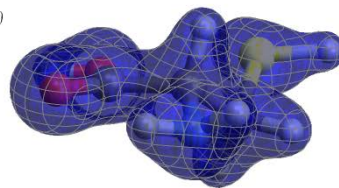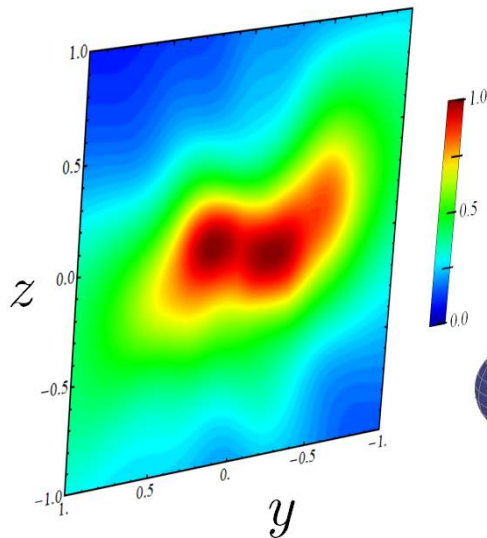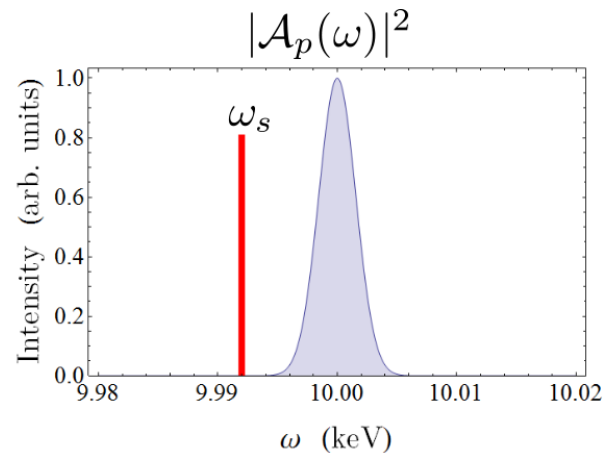
300 attosecond pulse centered at 10 keV.

Oriented molecule

Detected radiation is at 9.992 keV.

Ground-state charge density

x

Stimulated X-ray Raman in Cysteine

cysteine: amino acid containing sulfur
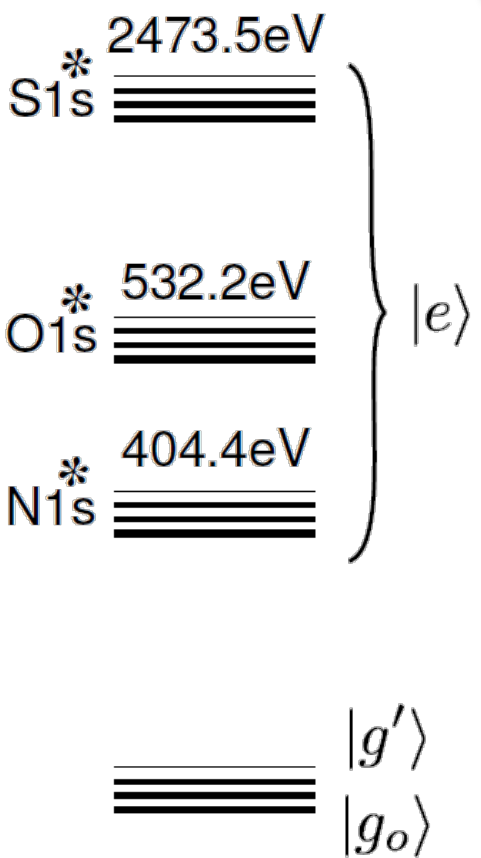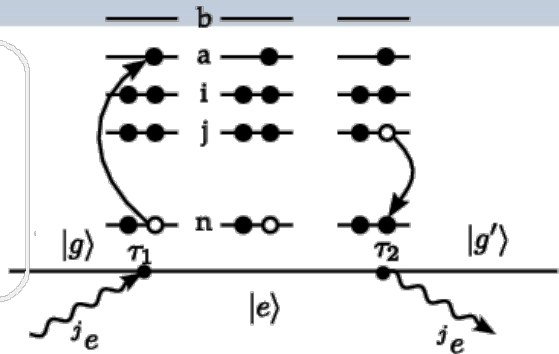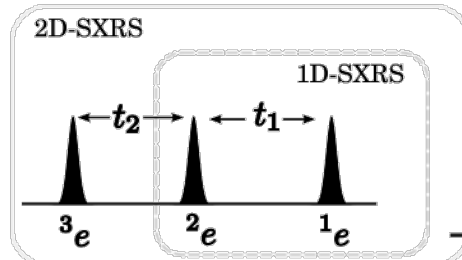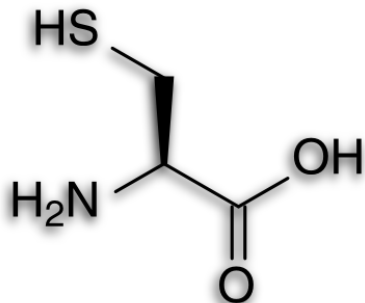
$$\alpha_{j;g'g''} = \int_{\infty}^{\infty} \frac{(V_{g'e} \cdot V_{eg''})\mathcal{E}_j^*(\omega_2)\mathcal{E}_j(\omega_2 + \omega_{g'g''})}{\omega_2 + \omega_j - \omega_{eg'} + i\Gamma_e} \, d\omega_2$$

S1s* 2473.5eV

O1s* 532.2eV $\Big\} |e\rangle$

N1s* 404.4eV

$|g'\rangle$
$|g_o\rangle$

Gaussian pulses
(FWHM: 128as; 14.2eV)
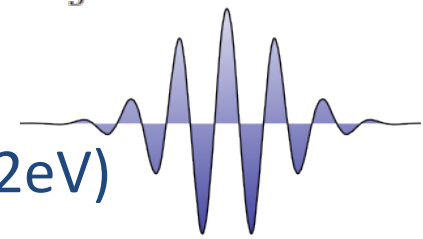
core- and valence-excited states
Devlopment version of NWCHEM
REW-TDDFT; CAM-B3LYP/6-311G**
nuclei fixed

Dr. Yu Zhang
Dr. Niri Govind, PNNL

TD-XRD simulations on Cysteine

$$\sum_{e,e'} e^{-i\omega_{eg}T} \alpha_{eg} A_p(\omega_s + \omega_{e'e}) A_p^*(\omega_s + \omega_{e'g}) \sigma_{ee'}(\boldsymbol{q}) \sigma_{e'g}^*(\boldsymbol{q}) + \text{c.c.}$$

Time-dependent diffraction pattern. Depends upon the resonant Raman polarizability, α, the Fourier transform of the charge density, σ, and the spectral envelope of the diffraction pulse A.
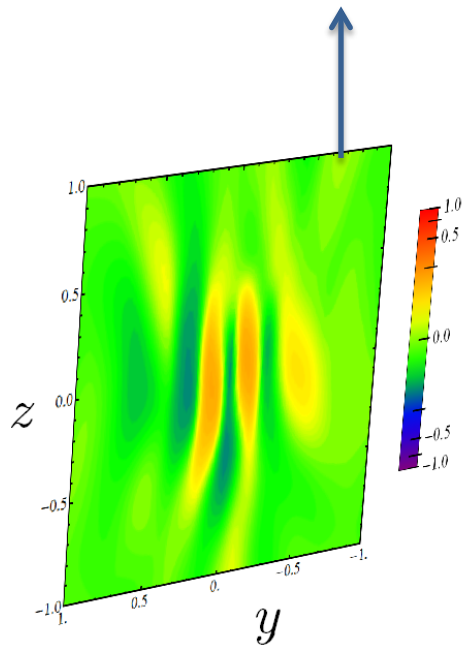
$$\sum_{e} e^{-i\omega_{eg}T} \alpha_{eg} \sigma_{eg}(\boldsymbol{r}) + \text{c.c.}$$

T=0.000 fs
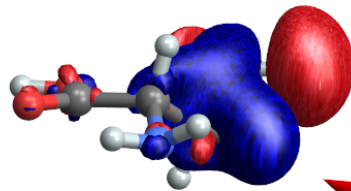
Time-dependent transition density for the X-ray Raman electronic wavepacket.

Diffraction pulse propagates in the X-direction. The signal is recorded on a screen in the forward X-direction.

The central frequencies of the Raman and diffraction pulses are set to 2.47 keV and 10 keV, respectively, with the former corresponding to the sulfur K-edge absorption. Both pulses are taken to have a duration of 100 as, and the detection frequency is set to 10 keV. In this simulation, we assume an oriented molecule.

Due to the fact that the X-ray Raman pulse is resonant with the sulfur K-edge, the transition density of the resulting valence wavepacket is initially localized near the sulfur atom. Since the Raman process occurs on only one side of the density matrix, the diffraction signal depends exclusively on off-diagonal elements of the charge density operator.

Multidimensional scattering of attosecond x-ray pulses detected by photon-coincidence

Jason D Biggs, Kochise Bennett, Yu Zhang and Shaul Mukamel

University of California, Irvine, CA 92697-2025, USA

Abstract

We propose a new photon-coincidence measurement based on the time- and wavevector-resolved detection of photons generated by the scattering of multiple x-ray pulses with variable delays. The technique directly measures multipoint correlation functions of the charge density through superpositions of valence excitations which are created impulsively by the scattering process.

2D Coincidence Detection From A Single-Molecule

- Preparation process followed by two sequential scattering events
- Two time delays provide two dimensions
- Simulations are for the case of no preparation i.e. scattering from the ground state
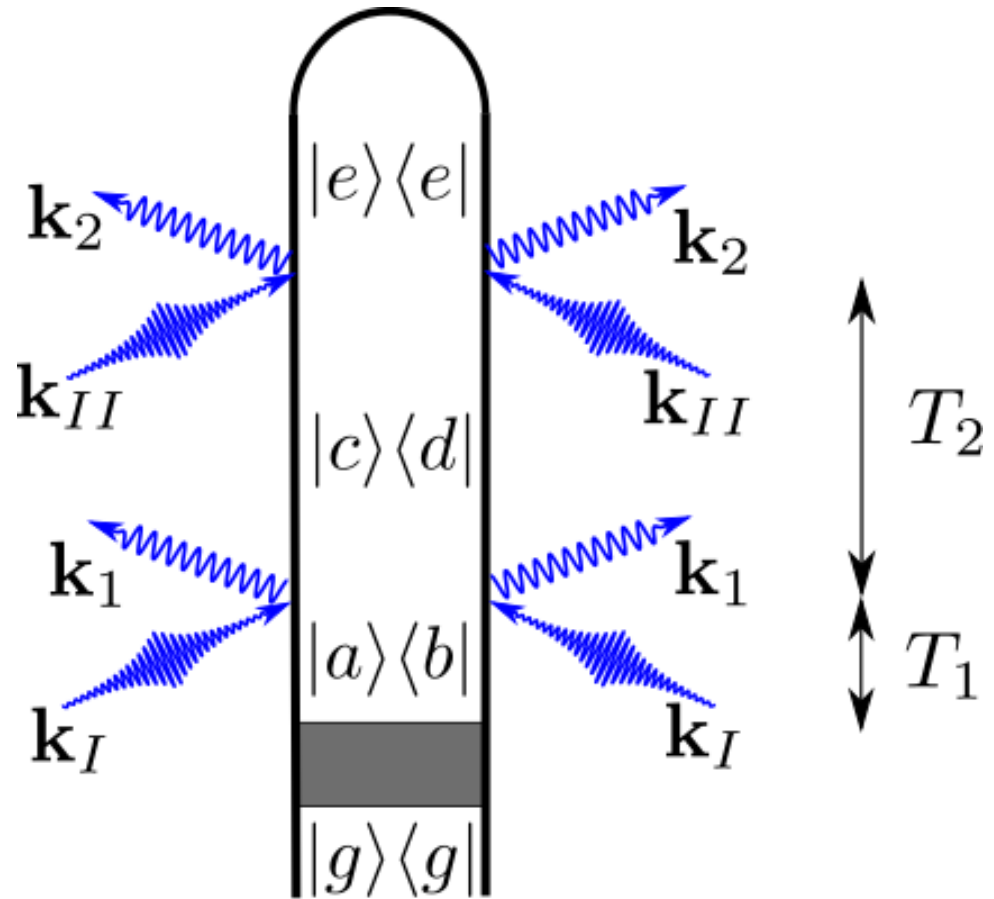
2D Coincidence Detection From the Ground State
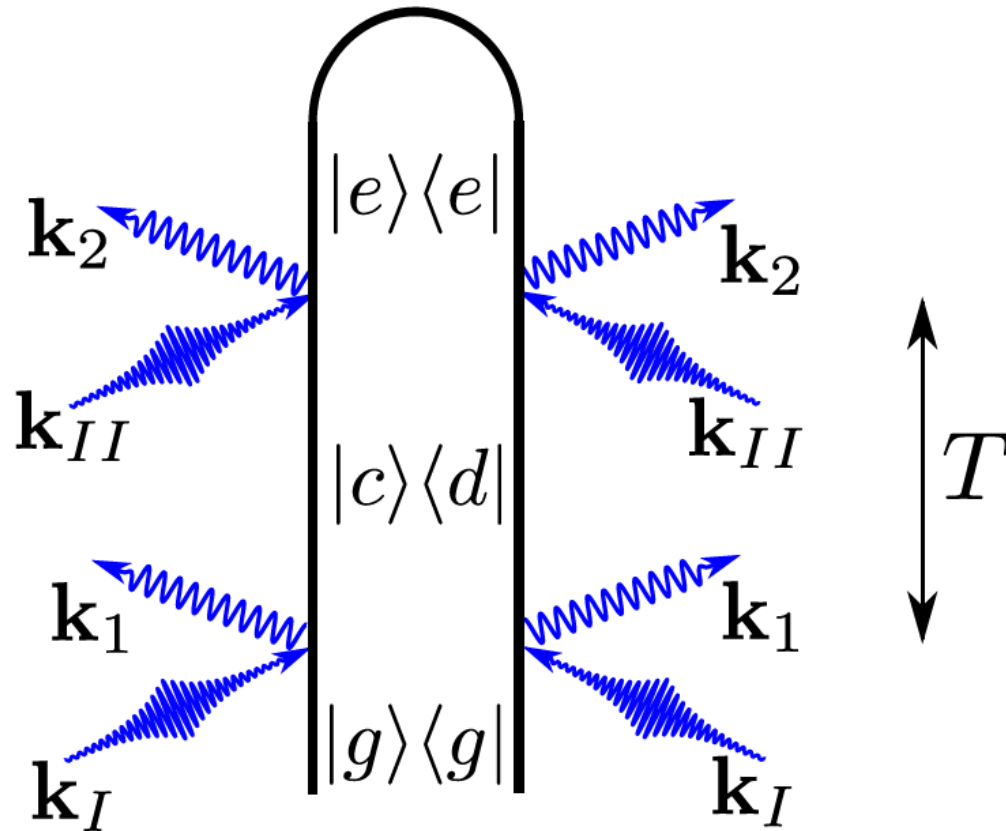
- The simplest case is when there is no preparation and the system is in the ground state prior to the first off-resonant x-ray scattering event.

- In this case, the signal is proportional to a two-point correlation function of the charge density

$$S(\mathbf{k}_1, \mathbf{k}_2, T) \propto$$
$$\langle \hat{\sigma}^\dagger(0, \mathbf{q}_1)\hat{\sigma}^\dagger(T, \mathbf{q}_2)\hat{\sigma}(T, \mathbf{q}_2)\hat{\sigma}(0, \mathbf{q}_1)\rangle$$
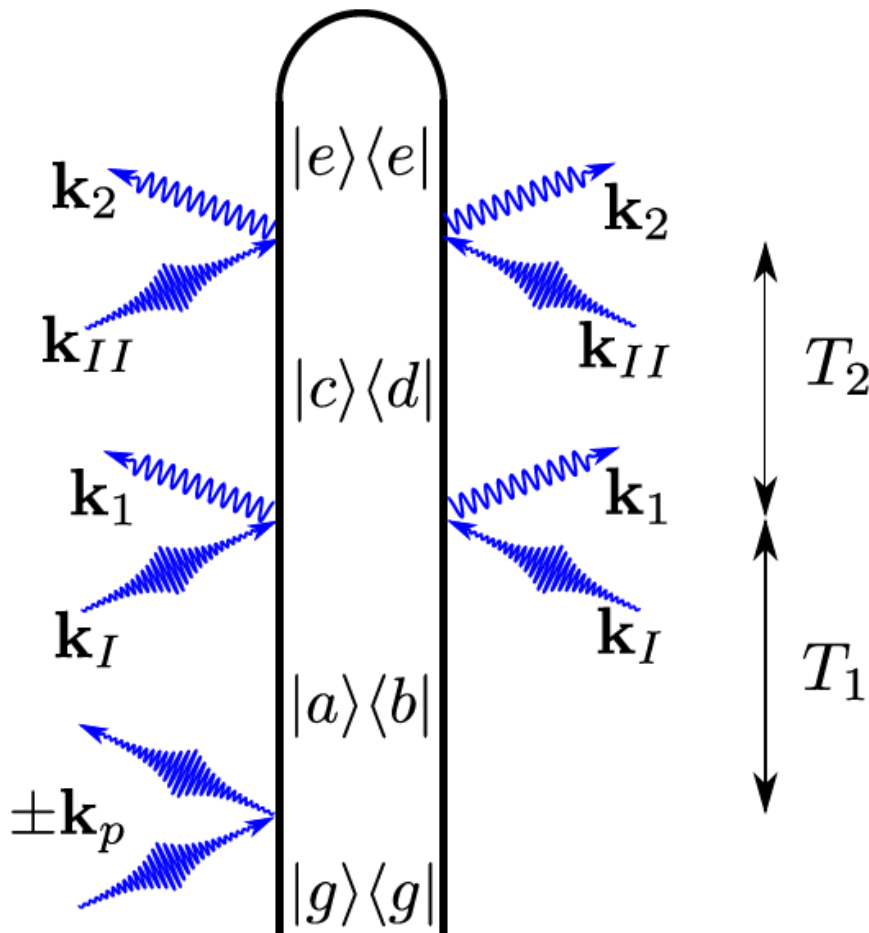
- Another possibility is that the preparation process is a resonant Raman excitation, in which case the signal,

$$S(\mathbf{k}_1, T_1, \mathbf{k}_2, T_2) \propto \langle \hat{\sigma}^\dagger(T_1, \mathbf{q}_1)\hat{\sigma}^\dagger(T_1 + T_2, \mathbf{q}_2)$$
$$\times \hat{\sigma}(T_1 + T_2, \mathbf{q}_2)\hat{\sigma}(T_1, \mathbf{q}_1)\hat{\alpha}(0)\rangle$$
$$- \langle \hat{\alpha}^\dagger(0)\hat{\sigma}^\dagger(T_1, \mathbf{q}_1)\hat{\sigma}^\dagger(T_1 + T_2, \mathbf{q}_2)$$
$$\times \hat{\sigma}(T_1 + T_2, \mathbf{q}_2)\hat{\sigma}(T_1, \mathbf{q}_1)\rangle,$$

  and is related to the two-point charge-density.

- Note that this is one of two diagrams (corresponding to the first term in the signal) and the other diagram simply has the Raman excitation on the bra rather than the ket.
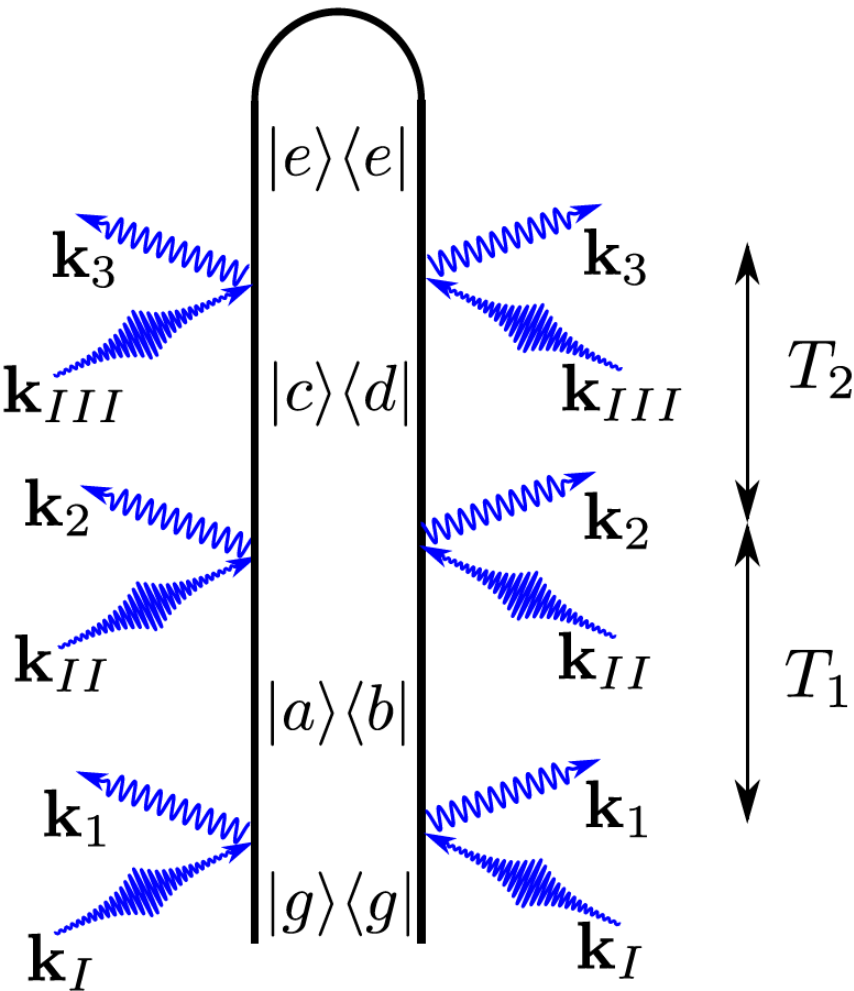
- Another possibility is that the preparation event is itself an off-resonant x-ray scattering process.
- This then corresponds to a three-photon coincidence detection and comes proportional to a three-point correlation function of the unperturbed charge density

$$S(\mathbf{k}_1, \mathbf{k}_2, T_2, \mathbf{k}_3, T_3) \propto \langle \hat{\sigma}^\dagger(0, \mathbf{q}_1)\hat{\sigma}^\dagger(T_1, \mathbf{q}_2)$$
$$\times \hat{\sigma}^\dagger(T_1 + T_2, \mathbf{q}_3)\hat{\sigma}(T_1 + T_2, \mathbf{q}_3)\hat{\sigma}(T_1, \mathbf{q}_2)\hat{\sigma}(0, \mathbf{q}_1)\rangle.$$

$|e\rangle\langle e|$

$\mathbf{k}_3$ $\mathbf{k}_3$

$\mathbf{k}_{III}$ $|c\rangle\langle d|$ $\mathbf{k}_{III}$ T_2

$\mathbf{k}_2$ $\mathbf{k}_2$

$\mathbf{k}_{II}$ $\mathbf{k}_{II}$ T_1

$|a\rangle\langle b|$

$\mathbf{k}_1$ $\mathbf{k}_1$

$|g\rangle\langle g|$

$\mathbf{k}_I$ $\mathbf{k}_I$

Frequency-Resolved 2D Signals

- In the case of a pure state $|\psi_0\rangle = \sum_a c_a |a\rangle$

and the signal can be written as

$$S(\mathbf{k}_1, \mathbf{k}_2, T_1, T_2) = \sum_e \left| T_e(\mathbf{k}_1, \mathbf{k}_2, T_1, T_2) \right|^2$$

$$T_e(\mathbf{k}_1, \mathbf{k}_2, T_1, T_2) = \sum_{ac} c_a \omega_1 \omega_2 \mathcal{A}_I(\omega_1 + \omega_{ca})$$

$$\times \mathcal{A}_{II}(\omega_2 + \omega_{ec}) \sigma_{ca}(\mathbf{q}_{ca}^{(1)}) \sigma_{ec}(\mathbf{q}_{ec}^{(2)}) e^{-i(\omega_{ae} T_1 + \omega_{ce} T_2)}$$

Off-Resonant X-ray Scattering Coincidence From The Ground State – Part 1

Here we use the first scattering event, rather than a resonant X-ray Raman process to generate the electronic wavepacket. As before, we set the detection frequency to the red of the power spectrum to eliminate elastic contributions to the scattering.

$|\mathcal{A}_p(\omega)|^2$

ω_s

ω (keV)

$\hat{k}_I$

k_1

z

y
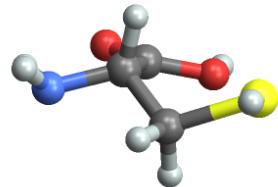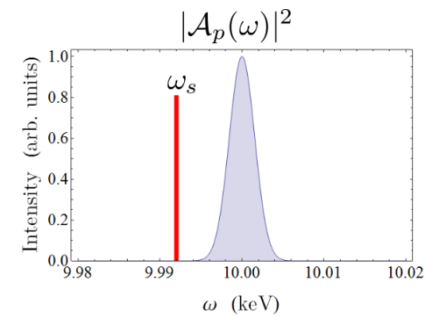
cysteine

Diffraction pulse propagates in the X-direction. The signal is recorded on a screen in the forward X-direction.

The full scattering pattern is collected with high pulse intensity.

We can look at five different points in the k_1 scattering signal. Now we place the detector in one of these positions, and turn the pulse power down low enough that we detect only a single photon. This leaves the molecule in a particular superposition.

cysteine

First we take k_1 to be parallel to the incoming wavevector k_I (i.e. zero scattering angle). This means that the photon has transferred energy (approximately 8 eV) to the molecule, but no momentum.

cysteine

Now we bring in the second pulse (also set to 10 keV) in a direction perpendicular to the first pulse.

cysteine

And we detect the k_2 scattering pattern (this time with the dection frequency set 8 eV to the blue of the pulse center frequency).
These first plots are for an interpulse delay of 0 fs.

We can see that the k_2 scattering pattern is highly dependent on the choice of k_1.

cysteine

We can see that the k_2 scattering pattern is highly dependent on the choice of k_1.

cysteine

We can see that the k_2 scattering pattern is highly dependent on the choice of k_1.

cysteine

We can see that the k_2 scattering pattern is highly dependent on the choice of k_1.

cysteine

Next we show how the k_2 scattering pattern changes with the interpulse delay time.

Next we show how the k_2 scattering pattern changes with the interpulse delay time.

T=500 as

cysteine

Next we show how the k_2 scattering pattern changes with the interpulse delay time.

Next we show how the k_2 scattering pattern changes with the interpulse delay time.

Next we show how the k_2 scattering pattern changes with the interpulse delay time.

cysteine

T=2000 as

Theoretical Formalism of Time-resolved X-ray Spectroscopy

Time-resolved x-ray spectroscopies: Nonlinear response functions and Liouville-space pathways

Satoshi Tanaka,[1,2] Vladimir Chernyak,[1,3] and Shaul Mukamel[1]

[1]Department of Chemistry, University of Rochester, Rochester, New York 14627
[2]College of Integrated Arts and Sciences, Osaka Prefecture University, Sakai 599-8531, Japan
[3]Process Engineering and Modeling, Corning, Inc., Corning, New York 14831

- A systematic description of coherent ultrafast x-ray spectroscopies in terms of nonlinear response functions and susceptibilities is developed. Correlation-function expressions of charge and current densities provide a unified treatment and classification of information content of the various possible techniques and connect them with their optical counterparts. Applications to pump-probe and four-wave mixing measurements are discussed.

X-Ray Four-Wave Mixing Spectroscopy

JOURNAL OF CHEMICAL PHYSICS

X-ray four-wave mixing in molecules

Satoshi Tanaka
*Department of Chemistry, University of Rochester, Rochester, New York 14627
and College of Integrated Arts and Sciences, Osaka Prefecture University, Sakai 599-8531, Japan*

Shaul Mukamel
Department of Chemistry, University of Rochester, Rochester, New York 14627

- An effective core-exciton Hamiltonian is constructed for nitroanilines which includes 1s *core hole* transitions of both nitrogen atoms. The wavevector and frequency dependent third order susceptibility X[(3)] is calculated and used to predict the frequency-domain pump–probe spectra which show both photobleaching and excited state absorption components. Signatures of electron delocalization and differences among the para-, meta-, and ortho-isomers are discussed.

Stimulated X-ray Raman Spectroscopy

Probing valence electronic wave-packet dynamics by all x-ray stimulated Raman spectroscopy: A simulation study

Igor V. Schweigert and Shaul Mukamel[*]

Department of Chemistry, University of California, Irvine, California 92697-2025, USA

- The femtosecond impulsive stimulated x-ray Raman signal from quinolinol is simulated and analyzed using the doorway-window representation of pump-probe spectroscopy. A valence electronic wave packet prepared by the pump, tuned on resonance with a given core hole, is localized in the vicinity of a selected atom and probed by a window localized on a different atom, selected by the probe pulse. All valence electronic states within the pulse bandwidths can be observed with high spatial and temporal resolution by monitoring the variation of the signal with the delay between the pulses. Natural orbital representation of the reduced singleelectron density matrix is used to visualize the dynamics of the valence wave packet, described as a linear combination of determinants made of occupied and unoccupied Kohn-Sham orbitals.

X-ray Double-quantum-coherence (XDQC) Spectroscopy

Double-quantum-coherence attosecond x-ray spectroscopy of spatially separated, spectrally overlapping core-electron transitions

Igor V. Schweigert[*] and Shaul Mukamel[†]

Department of Chemistry, University of California, Irvine, California 92697-2025, USA

(Received 31 July 2008; published 19 November 2008)

- X-ray four-wave mixing signals generated in the k1+k2−k3 phase-matching direction are simulated for N 1s transitions in paranitroaniline and two-ring hydrocarbons disubstituted with an amine and a nitroso groups. The two-dimensional x-ray correlation spectra 2DXCS provide background-free probes of couplings between core-electron transitions even for multiple core shells of the same type. Features attributed to couplings between spatially separated core transitions connected by delocalized valence excitations provide information about molecular geometry and electronic structure unavailable from linear near-edge x-ray absorption XANES.

Multidimensional Attosecond Resonant X-ray Spectroscopy

Multidimensional Attosecond Resonant X-Ray Spectroscopy of Molecules: Lessons from the Optical Regime

Shaul Mukamel, Daniel Healion, Yu Zhang, and Jason D. Biggs

Department of Chemistry, University of California, Irvine, California 92697; email: smukamel@uci.edu

- New free-electron laser and high-harmonic generation X-ray light sources are capable of supplying pulses short and intense enough to perform resonant nonlinear time-resolved experiments in molecules. Valence-electron motions can be triggered impulsively by core excitations and monitored with high temporal and spatial resolution. We discuss possible experiments that employ attosecond X-ray pulses to probe the quantum coherence and correlations of valence electrons and holes, rather than the charge density alone, building on the analogy with existing studies of vibrational motions using femtosecond techniques in the visible regime.

Excitation Energy Transfer Indicated by Stimulated X-ray Raman Spectrosocpy

Watching energy transfer in metalloporphyrin heterodimers using stimulated X-ray Raman spectroscopy

Jason D. Biggs[1], Yu Zhang[1], Daniel Healion, and Shaul Mukamel[2]

Department of Chemistry, University of California, Irvine, CA 92697

- Understanding the excitation energy transfer mechanism in multiporphyrin arrays is key for designing artificial light-harvesting devices and other molecular electronics applications. Simulations of the stimulated X-ray Raman spectroscopy signals of a Zn/Ni porphyrin heterodimer induced by attosecond X-ray pulses show that these signals can directly reveal electron–hole pair motions. These dynamics are visualized by a natural orbital decomposition of the valence electron wavepackets.

UV-pump IR-probe Spectroscopy

Monitoring Nonadiabatic Dynamics of the RNA Base Uracil by UV Pump–IR Probe Spectroscopy

Benjamin P. Fingerhut,* Konstantin E. Dorfman,* and Shaul Mukamel*

Chemistry Department, University of California, Irvine, California 92697-2025, United States

- Resolving the excited-state dynamics of DNA and RNA nucleobases has attracted considerable attention. UV irradiation of the isolated nucleobases leads to the population of an electronic excited state, which is quenched by internal conversion mediated by conical intersections on an ultrafast time scale. We present nonadiabatic onthe- fly molecular dynamics simulations of the UV pump–IR probe signal of the pyrimidine nucleobase uracil using a novel semiclassical protocol that takes into account the path integral over the excited-state vibrational dynamics and properly describes the joint temporal and spectral resolution of the technique. Simulations of vibrational motions of carbonyl fingerprint modes in the electronically excited states reveal clear signatures of different relaxation pathways on a time scale of hundreds of femtoseconds, which arise from an ultrafast branching in the excited state. We show that the inherent temporal and spectral resolution of the technique is not purely instrumental but also depends on the vibrational fluctuation time scale.

Catching Conical Intersections in the Act: Monitoring Transient Electronic Coherences by Attosecond Stimulated X-Ray Raman Signals

M. Kowalewski*, K. Bennett*, and S. Mukamel

Abstract:

Many important molecular processes take place via conical intersections (CoIns). We propose a coherent technique that can detect the passage through a CoIn with high temporal and spectral sensitivity.
The two novel aspects are the detection of electronic coherences (rather than state populations) and the use of X-ray (rather than optical) pulses.
A composite femtosecond/attosecond X-ray pulse detects the electronic coherences that are generated as the system approaches the CoIn.

● Work in progress.
* These authors contributed equally to this manuscript

Former and Current Nonlinear X-ray Spectroscopy Team Members

- Satoshi Tanaka
- Vladimir Chernyak
- Luke Campell
- Sergei Volkov
- Oleg Berman
- Rajan K. Pandey
- Igor V. Schweigert
- Haitao Wang

- Daniel M. Healion
- Jason D. Biggs
- Yu Zhang
- Kochise Bennett
- Konstantin E. Dorfman
- Weijie Hua
- Markus Kowalewski